QUANTITATIVE IMAGING OF THE LIVER WITH ^{18}F-FDG PET/CT IN PATIENTS WITH HEPATIC STEATOSIS

GEORGIA KERAMIDA

A thesis submitted in partial fulfilment, of the requirements of the University of Brighton and the University of Sussex for the degree of Doctor of Philosophy.

June 2016

Declaration of Authorship

I, Georgia Keramida, declare that the research contained in this thesis, unless otherwise formally indicated within the text, is the original work of the author. The thesis has not been previously submitted to this or any other university for a degree, and does not incorporate any material already submitted for a degree.

Signed:

Dated: 03rd of June 2016

Acknowledgements

As is the convention, I would like to thank a number of people for supporting me over the last 4 years, both professionally and personally, as it would have been impossible to complete this course without them.

Firstly I should thank my supervisor Professor A. M. Peters for the great support from the first day of my fellowship in Clinical Imaging Sciences Centre throughout the difficulties of setting up the research project and analysing the results and finalising the project.

I would like to thank my second supervisor Dr Sumita Verma for her contribution to my project.

I would like to thank the Academic director of the Clinical Imaging Science centre, Professor Mara Cercignani, who was my sponsor and who supported me hugely all the way through.

Next, I would like to thank the team of radiographers who have been hugely active and contributed to my research project and, specifically, James Hunter, Janice Bush, Doug Hawkes, Sarah Savidge and Georgina Haywood.

I would particularly like to thank the PET/CT secretary from the Royal Sussex County Hospital, in the Nuclear Medicine Department, Davina Towse, for her contribution to patient recruitment.

I would like to thank the physicists Mark Aplin, Mathew Lee, Alex Dunford, and John Lutkin for their help with Patlak-Rutland analysis.

Lastly, I would like to thank Professor Gary Cook and Muhammad Siddique from Kings College London for their help with the texture analysis of my project.

Contents

List of Acronyms

AA	Ascending aorta
ANCOVA	Analysis of covariance
ASH	Alcoholic steatohepatitis
BMI	Body mass index
BSA	Body surface area
CT	Computed tomography
CTD	Computed tomography density
CV	Coefficient of variation
DA	Descending aorta
DICOM	Digital Imaging and Communications in Medicine
EANM	European Association of Nuclear Medicine
FDG	Fluorodeoxyglucose
FDG-6-P	Fluorodeoxyglucose-6-phosphate
GFR	Glomerular filtration rate
GLCM	Grey level co-occurrence matrices
GLDM	Grey level difference methods
GLRLM	Grey level run length matrices
GLSZM	Grey level size zone matrices
HCC	Hepatocellular carcinoma
^{1}H-MRS	Proton Magnetic resonance spectroscopy
HU	Hounsfield units
LBM	Lean body mass
LC	Lumped constant
LFC	Liver fat content
MBq	Mega Becquerel
MRE	Magnetic resonance elastography
MR_{GLU}	Metabolic glucose utilization rate
MRI	Magnetic resonance Imaging
MRS	Magnetic resonance spectroscopy
NAFLD	Non alcoholic fatty liver disease
NASH	Non alcoholic steatohepatitis

NGTM	Neighbourhood grey tone difference matrices
NRMSD	Normalised root mean standard deviation
nSUV	Normalised Standardised uptake value
PDFF	Proton density fat fraction
PET	Positron emission tomography
ROI	Region of interest
SD	Standard deviation
SE(M)	Standard error (of mean)
SPECT	Single photon emission computed tomography
SUV	Standardised uptake value
SUV_{ave}	Average standardised uptake value average
SUV_{LV}	Standardised uptake value left ventricular cavity
SUV_{max}	Maximum standardised uptake value
SUV_{peak}	Peak standardised uptake value
SUV_{w}	Standardised uptake value based on weight
TE	Transient elastography
TLG	Total lesion glycolysis
VOI	Volume of interest

Publications arising from this thesis

Keramida G, Potts J, Bush J, Dizdarevic S, Peters AM. Hepatic steatosis is associated with increased hepatic FDG uptake. *Eur J Radiol* 2014; 83: 751-5.

Keramida G, Potts J, Bush J, Verma S, Dizdarevic S, Peters AM. Accumulation of ^{18}F-FDG in the liver in hepatic steatosis. *Am J Roentgenol* 2014; 203: 643-8.

Keramida G, Dizdarevic S, Bush J, Peters AM. Quantification of tumour ^{18}F-FDG uptake: normalise to blood glucose or scale to liver uptake? *Eur Radiol* 2015; 25: 2701-8.

Keramida G, Hunter J, Dizdarevic S, Peters AM. The appropriate whole body index on which to base standard uptake value in 2-deoxy-2-[^{18}F]fluoro-d-glucose PET. *Br J Radiol* 2015 Aug;88(1052):20140520. doi: 10.1259/bjr.20140520. Epub 2015 Jun 17.

Keramida G, Peters AM. Fallacy of quantifying lymphoma activity by scaling to the liver in 2-deoxy-2-[^{18}F]fluoro-d-glucose PET (Deauville criteria). *J Clin Oncol* 2015; 33 (34): 4120-1.

Keramida G, Hunter J, Dizdarevic S, Peters AM. Heterogeneity of intrahepatic fat distribution determined by ^{18}F-FDG PET and CT. *Ann Nucl Med* 2016 Apr; 30 (3): 200-6.

Keramida G, Dunford A, Siddique M, Cook GJ, Peters AM. Relationships of body habitus and SUV indices with signal-to-noise ratio of hepatic ^{18}F-FDG PET. *Eur J Radiol* 2016 May;85(5):1012-5 .

ABSTRACT

Background and Aims: Hepatic steatosis (≥10% fat within the liver) affects ~75% of obese and ~15% of non-obese adults. It leads to steatohepatitis (SH) in ~10% of patients. SH may then lead to cirrhosis. The primary aim of the thesis was to image the liver with FDG PET/CT to determine if glucose utilisation rate (MRglu) is increased in steatosis. Texture analysis of FDG PET/CT was also explored as a means of detecting steatosis and SH. Previous PET studies of steatosis quantified hepatic FDG uptake as the standardised uptake value (SUV).

Methods: All patients were referred for routine PET/CT. ROI were placed over the liver on whole body scans for measurement of CT density, which is inversely proportional to hepatic fat content, and SUV. SUV may be expressed as the 'hottest' pixel (SUV_{max}) or as the average of all pixels in the ROI (SUV_{ave}). Dynamic imaging from 0-30 min post-injection was also done in 60 patients and hepatic FDG clearance and MRglu were measured using Patlak-Rutland analysis. Texture analysis of PET and CT scans was explored as possible means of identifying SH at an early stage.

Results: SUV was overestimated in obese individuals when calculated using weight but not when using estimated lean body mass. SUV_{max}, but not SUV_{ave}, was increased in steatosis because SUV_{ave} is reduced in fatty liver as a result of 'signal dilution' by the fat. SUV_{max}/SUV_{ave} is therefore a marker of steatosis. Hepatic FDG clearance and MRglu were increased in steatosis, irrespective of BMI, but not in obese patients who did not have steatosis. Results of texture analysis were promising but inconclusive.

Conclusions and future work: SUV has major shortcomings as a surrogate for FDG clearance but in general indicates increased MRglu in steatosis. Dynamic studies confirm that MRglu is increased in steatosis. SUV_{max}/SUV_{ave} is a marker of steatosis.

Future work should aim to a) use dynamic FDG imaging to diagnose hepatic inflammation, and b) explore texture analysis to detect transition from steatosis to SH.

Chapter 1: Introduction to hepatic steatosis

1. 1. INTRODUCTION

In Europe, liver disease affects approximately 6% of the population (Bohte et al 2011). It is the fifth most common general cause of death both in Europe and the USA. In the UK, liver disease is the only major cause of death that is increasing. Liver-related mortality is largely the result of cirrhosis and primary liver cancer, both representing end-stage liver pathology. Viral hepatitis B and C, alcohol consumption and non-alcoholic fatty liver disease (NAFLD) are the leading causes of end stage liver disease in Europe (Bohte et al 2011). It is estimated that 170,000 and 47,000 Europeans die of cirrhosis and primary liver cancer each year, respectively (Vernon et al 2011). The main indications for liver transplantation in Europe are cirrhosis and liver cancer. In viral hepatitis Band C, fibrosis and even early cirrhosis can reverse after successful antiviral treatment (Tsoulfas et al 2009, El-Serag et al 2004).

1.2. HEPATIC STEATOSIS

1.2.1. Epidemiology

Fatty infiltration of the liver (hepatic steatosis) is very common and in most cases benign (Anstee et al 2011). It is defined as a liver fat content of 10% or more and is estimated to be present in approximately 75% of obese Caucasian adults and approximately 15% of non-obese Caucasian adults. There are several causes, including excess alcohol consumption and other toxins, including chemotherapeutic agents. The type of steatosis that is increasing most rapidly, however, is NAFLD, which is seen commonly in patients who are obese, have metabolic syndrome or type-

2 diabetes mellitus, but who do not drink to excess (i.e. less than 21 units per week for men and 14 units per week for women) (Williams et al, 2011). The prevalence of NAFLD in type-2 diabetes is estimated to be 43-70% (Boyce et al 2010). NAFLD encompasses not only simple fatty liver but also the more serious condition of non-alcoholic steatohepatitis (NASH), which slowly progresses from hepatic inflammation to fibrosis (Figs 1.1 and 1.2). As NASH eventually leads to cirrhosis, NAFLD is becoming an increasingly important cause of chronic liver disease in the western world (Mehta et al 2010) and a major healthcare issue (Rinella et al 2015).

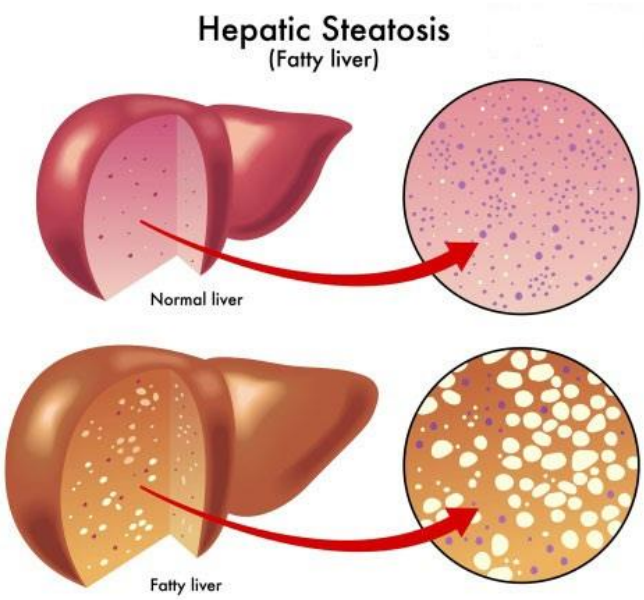

Fig 1.1. (taken form www.liverdoctor.com)

Over the last decades the contribution of NAFLD to the total burden of chronic liver disease has increased. This increase is largely explained by the growing prevalence of obesity, insulin resistance and type-2 diabetes, with which NAFLD is strongly

associated (Paschos et al 2009, Boyce et al 2010). Liver fibrosis is the result of a continuous cycle of injury and healing in response to injury. If untreated, it may progress to cirrhosis, liver dysfunction, portal hypertension and hepatocellular carcinoma (HCC) (Agopian et al 2012).

NAFLD is the hepatic manifestation of metabolic syndrome (Nugent et al 2007), which is defined by the presence of 3 or more of the following criteria (Table 1): elevated waist circumference, high fasting glucose, hypertension, increased triglycerides and decreased high density lipoprotein concentration (Miette et al 2011). Predictors of NASH include hypertension, increased alanine aminotransferase (Dixon et al 2006) and insulin resistance, which is the strongest (Bugianesi et al 2002). As only a fraction of patients with simple steatosis progress to the more severe NASH, other metabolic, environmental and genetic factors must participate in the pathogenesis of NASH (Miette et al 2011). Increased liver fat content in patients with NAFLD is associated with increased rates of the metabolic syndrome, independent of NASH (Miette et al 2011).

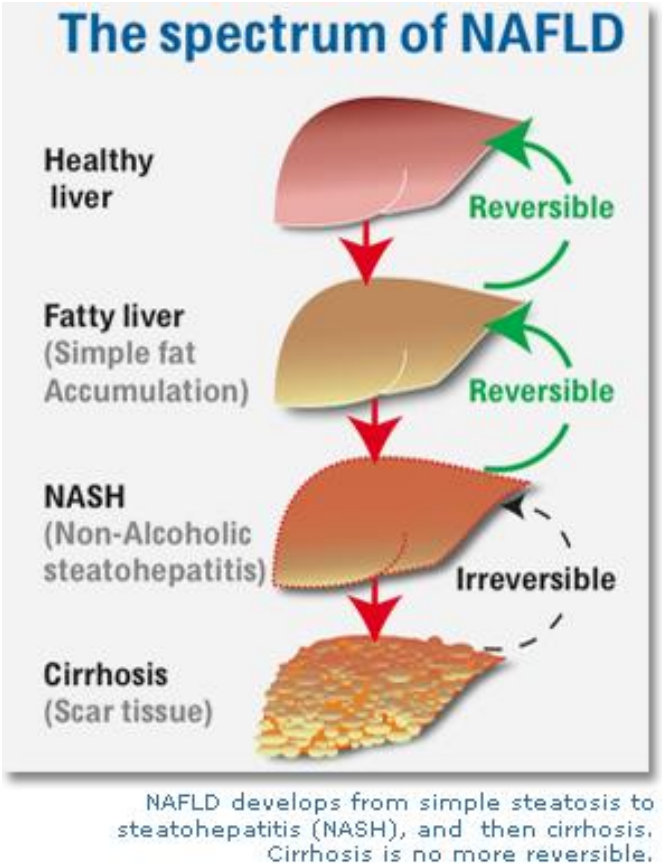

Fig 1.2. (taken from www.vitamindwiki.com**)**

1.2.2. Histology

In hepatic steatosis, fat is deposited in the liver as fat droplets within the hepatocytes (Ma et al 2009). The size of the droplets varies so that some hepatocytes may have a large amount of fat whilst others only have a minimal amount. This gives rise to heterogeneity of fat distribution in the liver in hepatic steatosis both at a microscopic as well as macroscopic level (Kleiner et al 2005). The progression of steatosis to steatohepatitis is associated with hepatic inflammation, the histology of which is described below.

Table 1.1. Criteria for Clinical Diagnosis of the Metabolic Syndrome from (modified from Alberti et al. 2009, Adult treatment panel III 2002).

Measure	Abnormal value
Elevated waist circumference	>102 cm in men >88 cm in women
Elevated triglycerides(drug treatment for elevated triglycerides is an alternate indicator)	≥150 mg/dL (1.7 mmol/L)
Reduced HDL-cholesterol (drug treatment forreduced HDL-cholesterol an alternate indicator)	In Males: < 40 mg /dL (1.0 mmol/L) In Females : < 50 mg/dl (1.3 mmol/L)
Elevated blood pressure (antihypertensive drug treatment in a patient with history of hypertension in a alternate indicator)	Systolic ≥ 130 and/or diastolic≥85mmHg
Elevated fasting glucose (drug treatment is alternate indicator	≥ 100 mg/dL

1.2.3. Association between NAFLD and cardiovascular disease

NAFLD is associated with an increased risk of mortality from cardiovascular disease (Angulo et al 2002, Li 2012). Such an association is not surprising as both have similar risk factors. However, the risk of cardiovascular disease is increased when NAFLD is also present (Arulanandam et al 2015). Cardiovascular disease is the most common cause of death in NAFLD patients, as both cardiovascular morbidity and NASH in particular may persist even after liver transplantation (Vanwagner et al 2012). Although the mortality risk from liver disease in patients with NASH is 13%, the mortality risks in the presence of concurrent cardiovascular disease and malignancy are 25% and 28%, respectively (Adams et al 2005). NAFLD is also associated with an increased risk of HCC (Angulo et al 2002).

1.3. ASH and NASH

1.3.1. Subtypes

There are two main forms of steatohepatitis. In the first, heavy drinking leads to fatty infiltration followed by alcoholic steatohepatitis (ASH), whilst in the second, inflammation is induced by fatty infiltration in the absence of heavy drinking (non-alcoholic steatohepatits - NASH) defined as less than 21 units per week for men and 14 units per week for women (Chalasani et al 2012).

NASH and ASH result in cirrhosis in 11% of patients over a period of approximately 10 years (Angulo et al 2010). A further complication of NASH is HCC. Recent data suggest that NASH-related cirrhosis accounts for approximately 20% of liver transplants, which represents a 500% relative increase in frequency over the last 10 years (Agopian et al 2012). It is predicted that in a few years, more transplants will be performed for NASH than for alcoholic liver disease.

Other forms of liver inflammation, from which ASH and NASH need to be distinguished, are severe alcoholic hepatitis, which is an acute, life-threatening condition that presents as jaundice in a heavy drinker, chemotherapy-induced inflammation (eg tamoxifen, methotrexate, retrovirals), storage disorders (e.g. hemochromatosis, Wilson disease), the various forms of viral hepatitis, e.g. hepatitis C and less often hepatitis B, and toxins such as carbon tetrachloride and arsenic (Musso et al 2011, French et al 1989, Hamer et al 2006).

The development of liver abnormalities in these conditions depends on the cause (Ma et al 2009). For example, in alcoholic fatty liver disease, the stages are similar

to those of NAFLD, and progress from alcoholic steatosis through steatohepatitis and fibrosis to cirrhosis, whereas in viral infections, the progression to fibrosis or cirrhosis is attributed to chronic active hepatitis (Purohit et al 2004, El-Zayadi et al 2008). Although the progression of fatty liver disease depends on the cause, early stages are usually reversible with changes in lifestyle (Ma et al 2009). Liver cirrhosis, whether due to NAFLD or another cause, may develop into HCC, although less commonly in NASH-related cirrhosis than in cirrhosis resulting from hepatitis C or chronic alcohol abuse (Ma et al 2009, Adams et al 2005, Hui et al 2003).

1.3.2. Histology

The histologic features of hepatic steatosis depend on its cause and stage (Ma et al 2009). In the initial stage (simple fatty liver), there are numerous large lipid vacuoles that displace the nuclei of hepatocytes toward the cell periphery (Ma et al 2009, Lee et al 1995, Nagore et al 1988). In the intermediate stage (steatohepatitis), there is ballooning degeneration of hepatocytes accompanied by lobular inflammation (that may be lymphocytic or neutrophilic) and pericellular (sinusoidal) fibrosis in the perivenular or central regions of lobules (Lee et al 1995, Falchuk et al 1980). Perinuclear Mallory collagen, or Mallory hyaline, which is eosinophilic material composed of aggregates of intermediate (cytokeratin) filaments, may be present in a perinuclear location (Lee et al 1995, Falchuk et al 1980).

NASH is typically characterized by predominantly lymphocytic inflammation in the lobules, with less Mallory hyaline (Mallory bodies, also known as alcoholic hyaline), in contrast to fatty liver disease due to a toxic cause, especially ASH, which has more of a neutrophilic inflammation (Ma et al 2009). The end stage (steatohepatitis with cirrhosis) is associated with fibrosis surrounding proliferating liver nodules, in which fat-laden hepatocytes become less frequently visible (Brunt et al 1999).

1.3.3. Diagnosis

Prior to the development of fibrosis, it is not possible to diagnose steatohepatitis other than by liver biopsy. Even in cirrhosis, liver function tests may be normal, and it is therefore not surprising that steatohepatitis cannot be diagnosed by biochemistry.

Liver biopsy is the standard test for making a definite diagnosis of both alcoholic liver disease and NASH, and for evaluating the inflammatory activity and stage of fibrosis. Biopsy can be performed percutaneously under sonographic guidance or via the jugular vein under CT guidance. The latter approach is generally preferred in severe liver disease because conventional percutaneous biopsy is contraindicated as a result of moderate to severe ascites and risk of bleeding from severe coagulopathy. Disease severity can be interpreted qualitatively or semi-quantitatively based on validated staging systems (Atwell et al, 2010).

The drawbacks of liver biopsy are as follows. Firstly, a small tissue sample of 2-3 cm in length is biopsied, representing approximately 1/50,000 of the total liver (Guido et al 2004, Bravo et al 2001). Due to the heterogeneous distribution of liver fibrosis and

steatosis, such a small sample is prone to sampling error (Soloway et al 1971, Bedossa et al 2003, Ratziu et al 2005). Secondly, liver biopsy is invasive with a severe complication rate of 0.57% and mortality rate of approximately 0.01% (Bravo et al 2005, Soloway et al 1971, Bedossa et al 2003, Ratziu et al 2005, Cadranel et al 2000). Thirdly, there is wide inter- and intra-observer variation in interpretation (Soloway et al 1971, Bedossa et al 2003, Cadranel et al 2000).

The limitations of liver biopsy have initiated the search for non-invasive alternatives for the evaluation of liver fibrosis and steatosis. Ideally, such methods should be easy to perform, reliable and inexpensive, and have a low inter- and intra-observer variability (Bohte et al 2011) so that they can be used to monitor patients over time and evaluate treatment response.

A non-invasive technique called transient elastography (*Fibroscan*) has been developed that measures liver stiffness and elasticity. It is a semi-quantitative measure of liver fibrosis and so useful only for detecting relatively late, moderate-to-severe liver fibrosis (Sandrin et al 2003) rather than early NASH. It cannot detect hepatic inflammation before the onset of fibrosis and moreover is less sensitive in obese patients and patients with ascites (Tsochatzis et al 2011). Diagnosis by non-invasive imaging techniques is described below under imaging methods.

1.4. IMAGING TECHNIQUES

1.4.1. X-rays and CT

Conventional radiography and computed tomography (CT) use X-rays, which are at the low energy range on the electromagnetic spectrum. Radiographic images are based on absorption of externally generated X-rays as they pass through tissues of the

body. The anatomical resolution of normal versus abnormal structures depends on differential absorption (Armstrong et al 2004). CT is also based on X-ray transmission through the body but differs from conventional radiography in that it uses a more sensitive X-ray detection system and the acquired data undergo manipulation in a computer. The X-ray tube (source) and detectors rotate around the patient so that tomographic (3-dimensional images) are generated. Small differences in X-ray absorption are transformed into an image. The attenuation (absorption) of X-rays (CT density) is expressed as Hounsfield units (HU) after Godfrey Hounsfield who invented CT. The CT density of water is set at zero, while the density of air is minus 1000 HU and of bone is plus 1000 HU. Relevant to this thesis, fat has a CT density of less than zero.

1.4.2. Ultrasonography

Ultrasound examinations use very high frequency sound directed into the body from a transducer placed in contact with the skin (Armstrong et al 2004). As the sound travels through the body, it is reflected by tissue interfaces to produce echoes that are detected by the transducer and converted into an electrical signal (Armstrong et al 2004). Ultrasonography is poor for quantification of tissue composition.

1.4.3. MRI

Magnetic resonance (MRI) is based upon the interaction between an applied magnetic field and a nucleus that possesses spin. Nuclear spin, or nuclear spin angular momentum, is an intrinsic property of an atom. All elements in the Periodic Table except argon and cerium have at least one naturally occurring isotope that possesses spin (Brown et al 2003). In principle, therefore, nearly every element can be subjected

to MR, as the basic concepts of resonance, absorption and relaxation are common to all of them (Brown et al 2003, Dale et al 2015).

1.4.4. Magnetic resonance spectroscopy (MRS)

MRS measures the molecular composition of tissue. The signals originating from protons in different molecular structures within an image voxel are displayed as a spectrum. The molecular structures are resolved from each other by differences in their precession frequency (Bohte et al 2011). The signal intensity and widths of the peaks of the spectrum give additional information regarding the relative quantities of the chemical components. Different nuclei can be used for liver fat quantification with MRS, e.g. protons (^{1}H) (Longo et al 1995), phosphorous (^{31}P) (Angus et al 1990, Sevastianova et al 2010) or carbon (^{13}C) (Petersen et al 1996).

^{1}H-MRS has the advantage that it is easier to perform, more widely available and provides a higher signal-to-noise ratio. The difference between ^{1}H-MRS and MRI is that the former does not contain information on the spatial origin of the signal; i.e. doesn't give an image. Therefore, a voxel for ^{1}H-MRS has to be placed in the location of interest on a separately acquired anatomical MR image.

^{1}H-MRS is considered to be very accurate and is non-invasively measures liver fat, even small amounts such as 0.5% (Bohte et al 2011, Hughes et al 2009, Ma et al 2009). Its disadvantages include the complexity of data analysis and the need for a skilled operator for interpretation.

1.4.5. Nuclear Medicine

An element that is radioactive has an unstable nucleus. When the nucleus emits a neutron or proton (nuclear disintegration), it becomes a new element. Disintegration results in the emission of electromagnetic radiation (photons) of a specific energy that is measured in KeV. Most radioactive elements that are used in routine imaging emit gamma photons of a single energy. The photons are detected in a transparent crystal of sodium iodide that is housed in the detector. If the photon is absorbed in the crystal, its energy is converted into a flash of light, or scintillation, which is then recorded by a photomultiplier that contains a light-sensitive photo-electric cell. In a gamma camera, the scintillations are detected by an array of photomultiplier tubes that identify the location of the scintillations within the crystal. The 'lens' of a gamma camera is called a collimator, which is a lead disc perforated with many long and narrow parallel holes that permit the transit of photons travelling perpendicular to the camera face. The crystal is in the form of a large thin disc placed immediately behind the collimator so that the scintillations take place in specific locations within the disc. Like light cameras, gamma cameras generate 2-dimensional images. However by rotating the camera around the subject and obtaining an image every 6^{o} of rotation, 3-dimensional images can be re-constructed (single photon emission computerized tomography - SPECT) (Dizdarevic and Peters 2014).

1.4.6. Positron emission tomography (PET)

1.4.6.1. Principles of PET

Positron emission tomography is a non-invasive technique that has similar principles to SPECT and is based on the detection of positron emission. Many radionuclides emit positrons from the nucleus when it is unstable. A positron is positively charged

and has the same mass as an electron. Following emission from the nucleus, a positron is immediately attracted to a negatively charged electron. The two particles then collide and undergo mutual annihilation. Following annihilation, the masses of the two particles are converted into two gamma photons each of 511 KeV energy that leave the atom at exactly 180^{o} to each other. Called co-incident photons, they are simultaneously detected by a ring of detectors encircling the patient. The direction emission of the two photons is random and their simultaneous detection allows the construction of a tomographic image.

Gamma cameras and PET cameras give images of relatively poor anatomical resolution. Modern detectors have therefore been developed that contain CT or MR scanners so that the functional image given by the gamma radiation can be registered on to an anatomical image of high resolution. This is called 'hybrid' imaging (Dizdarevic and Peters 2014).

1.4.6.2. PET radiopharmaceuticals.

The original tracers used in PET were C-11, N-13 and O-15. Many PET radiopharmaceuticals are now available the most widely used of which clinically is F-18-fluorodeoxyglucose (FDG), which is a chemical analogue of glucose. It is transported into cells using the same transport enzymes as glucose, but unlike glucose, is 'metabolically trapped' in cells that do not possess glucose-6-phosphatase because it is not recognised by pyruvate kinase and cannot therefore be further metabolised. FDG is 'recognised' as foreign by renal tubular cells and is not reabsorbed from the glomerular filtrate. Instead it is excreted in the urine

(Krishnamurthy et al 2009) - about 20% of the injected dose within 1 h (Mejia et al 1991).

1.4.6.3. Pharmacokinetics of FDG

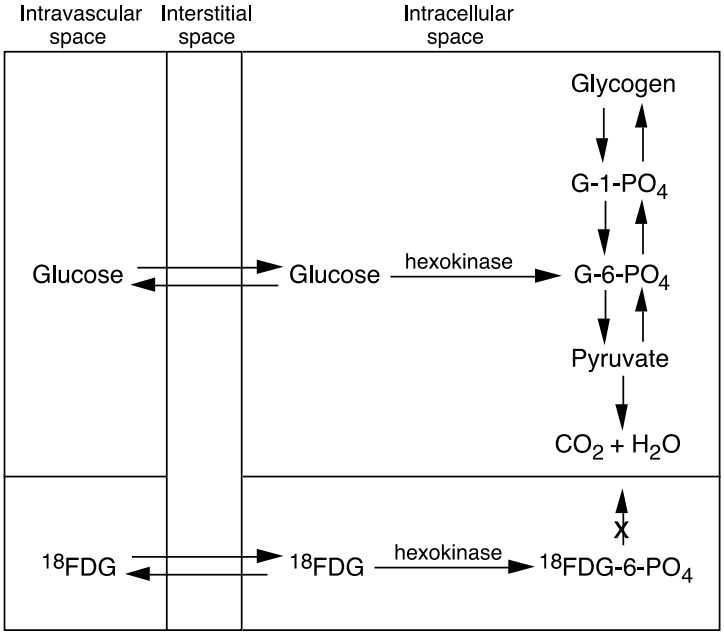

Fig 1.3. Mechanism of glucose and FDG exchange across cells. Through the enzyme hexokinase, both molecules are converted into their 6-phosphate forms. Unlike glucose, FDG does not undergo any further metabolic processing. In cells lacking glucose-6-phosphatase, FDG is therefore trapped, enabling imaging. Glucose, in contrast, is converted into glycogen or utilised with generation of $CO_2 + H_2O$. Modified from Nuclear Hepatology, a textbook of Hepatobiliary Diseases; 2nd edition, Springer, Berlin (Krishnamurthy & Krishnamurthy 2009).

After intravenous injection, FDG enters the extracellular fluid space including that of the central nervous system (i.e. it crosses the blood/brain barrier). Tissues with high hexokinase activity show higher FDG uptake than those with low activity. Hexokinase content of organs is ranked as follows: brain > heart > kidney > lung > liver (Long et al 1952). Intracellular retention depends upon tissue metabolic pathways. Tissues with high glucose-6-phosphatase enzyme activity (liver and kidney), which de-phosphorylates FDG, return FDG to the blood. As they function to

maintain the blood glucose level during fasting, hepatocytes are rich in glucose-6-phosphatase.

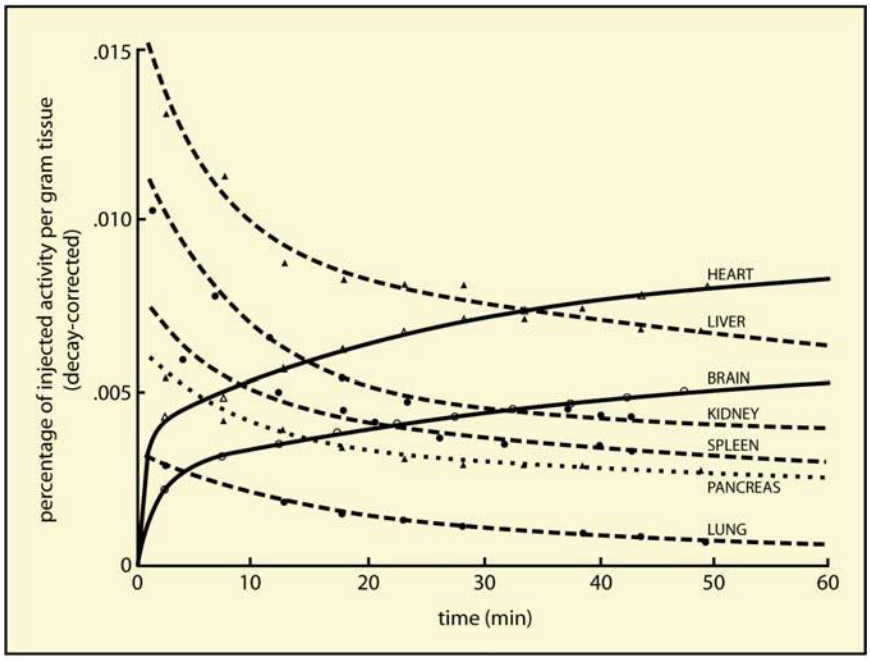

^{18}FDG uptake by human organs.
(Mejia, Alvaro A., et al. JNM 1991; 32: 699-706)

Fig 1.4. Time-activity profiles of FDG in various tissues. Brain and heart show continuous uptake for 1 h, whereas other organs show net clearance.

Prerequisite for taking correct information from the PET scan is the increased uptake of isotope from malignant and inflammatory reactive/active populations of cells. Here it should be noted that the uptake of FDG is influenced by a large number of factors, the principal of which is the histologic type, degree of aggressiveness, viability of malignant cells, the presence of hypoxia and local vascularisation. Although FDG is used as a tracer for glucose, their transport into tissue and phosphorylation occur at different rates so a correction factor is necessary to convert FDG accumulation to glucose accumulation. This correction factor is called the ‘lumped constant and it is the composite of 6 constants that relate FDG variables to corresponding glucose

variables. A lumped constant of one is often assumed in FDG quantitative studies. It is almost one for liver (Iozzo et al 2003) and slightly less than one for brain (Hasselbalch et al 2001, Graham et al 2002).

The main application of FDG PET is in tumour imaging and to a lesser extent imaging inflammation. Routine FDG PET/CT comprises about 85% cancer, 5% neurology, 5% cardiology and 5% inflammation (see below).

1.4.6.4. Quantification of tissue FDG uptake as standardised uptake value

The conventional clinical method for quantification of tissue FDG uptake is the standardised uptake value (SUV), which is defined as

$$\text{SUV} = \frac{\text{tissue activity/ml}}{\text{administered dose of FDG}} \times \text{body weight} \qquad (1.1)$$

SUV varies according to time post-injection, which in routine clinical work is usually 60 min.

There are 2 variants of SUV: SUV_{max}, which is the SUV from a voxel with the highest signal in the ROI, and SUV_{ave}, which is the average SUV in the ROI.

The term, body weight, appears in the above equation to account for the effective volume of distribution of FDG throughout the body. However, when it is based on weight, liver SUV correlates with weight because adipose tissue in general takes up minimal FDG. SUV in a heavy obese person is therefore overestimated (Sugawara et al 1999). It has been suggested that lean body mass (LBM) may be more appropriate,

since SUV based on LBM, unlike SUV based on weight, shows no correlation with body weight (Sugawara et al 1999). However, there is, as yet, no agreement as to whether weight or LBM should be used to calculate SUV, so weight remains in common use.

1.5. IMAGING THE LIVER

1.5.1. Tc-99m-sulphur colloid and nanocolloid

Radiocolloid is taken by all organs of the reticuloendothelial system: liver, spleen and bone marrow. The liver takes up the majority; about 85%. In liver disease, including acute and chronic hepatic inflammation, there is a shift in radiocolloid uptake to the spleen and bone marrow. In cirrhosis of moderate severity, radiocolloid uptake by the liver decreases to 65–70% while splenic and bone marrow uptakes increase. In advanced cirrhosis, liver uptake may be as low as 30–35%% (Krishnamurthy et al 2009). Radiocolloid imaging is therefore non-specific but has been used to diagnose alcoholic hepatitis (Kudo et al 1989).

1.5.2. Tc-99m-HIDA

HIDA is an organic anion and cleared from blood into hepatocytes from where it is excreted into bile. Like colloid imaging, HIDA imaging is non-specific as marker of hepatic function and has no significant role in imaging NAFLD or alcoholic hepatitis.

1.6. IMAGING AND QUANTIFYING NAFLD

Hepatic steatosis can be imaged and quantified using several imaging techniques, including ultrasonography (US), computed tomography (CT), magnetic resonance imaging (MRI) and proton magnetic resonance spectroscopy (^{1}H-MRS) (Bohte et al

2011). For evaluation of liver fibrosis, imaging methods include ultrasound based transient elastography and magnetic resonance elastography (Oudry et al 2009).

.

1.6.1. Ultrasonography

US is widely used to diagnose and evaluate hepatic steatosis as it is safe, non-invasive, cheap and free of ionising radiation. The criteria for steatosis assessment include liver echogenicity, echo-texture, visibility of the diaphragm and large vessel beam attenuation. However, evaluation of hepatic steatosis is qualitative rather than quantitative and the technique cannot give an insight of subtle changes throughout the time course of the condition (Armstrong et al 2004).

1.6.2. Computed tomography

Fat has a lower CT density than water and can therefore be detected and quantified in the liver by CT. However CT is associated with radiation exposure and CT density measurement is limited by the presence of cirrhosis or of glycogen, iron or amyloid, which interfere with the results and may be misleading. Various threshold values of CT density below which hepatic steatosis can be diagnosed have been reported but in this thesis I have used a value of 40 HU (Boyce et al 2010, Zeb et al 2012). Forty HU corresponds to liver fat content of 10% (Ricci et al 1997, chapter 6 this thesis).

1.6.3. Magnetic resonance imaging and magnetic resonance spectroscopy

MRI and proton MRS (^{1}H-MRS) are the most accurate non-invasive imaging methods so far, for liver steatosis quantification compared to CT and US according to recent meta analysis. The mean sensitivities were 73.3–90.5% (US), 46.1–72.0% (CT), 82.0–97.4% (MRI) and 72.7–88.5% (^{1}H-MRS). Mean specificity ranges were 69.6–

85.2% (US), 88.1–94.6% (CT), 76.1–95.3% (MRI) and 92.0–95.7% (^{1}H-MRS) (Bohte et al 2011). MRS also provides a quantitative biomarker of liver fat content called proton density fat fraction (Libaque et al 2013) but it is time-consuming to perform, not widely available and limited in sample size (Runge et al 2014, Krssak et al 2010).

1.6.4. Imaging hepatic steatosis with FDG PET

It is important to quantify tumour FDG uptake in clinical practice, especially to assess response to treatment. A recommended method is expression of the tumour SUV as a ratio with liver SUV; in other words to use the liver as a reference region (Khadhani et al 2005, Kumar et al 2004, Van Kouwen et al 2005). This approach is used extensively in FDG PET/CT of lymphoma and is the recommended method in the Deauville criteria (Barrington et al 2014). Recent interest has been shown in FDG PET/CT of hepatic steatosis because the presence of excess fat may invalidate the liver as a reference region for this purpose. Several studies have therefore examined the relation between liver FDG uptake, quantified as the SUV, and hepatic CT density as a marker of liver fat but they have come up with conflicting results (Bural et al 2010, Abikhzer et al 2011, Lin et al 2011, Abele et al 2010). Uncertainty remains, therefore, as to whether or not hepatic steatosis is associated with increased or decreased FDG accumulation (Lin et al 2011, Abele et al 2010). A likely explanation for this uncertainty is that the previous studies, which used SUV to quantify FDG uptake, did not take into account a) the effect of blood glucose concentration on intrahepatic FDG kinetics (see below) (Choi et al 1994); b) the invalidity of using body weight to calculate SUV, which, when based on weight, is overestimated in

obese individuals (Sugawara et al 1999); and c) potential 'dilution' of the hepatic FDG signal by hepatic fat (see later in this thesis).

1.7. IMAGING INFLAMMATION

Inflammation can be imaged by several techniques, most effectively by conventional nuclear medicine and PET/CT.

1.7.1. Gallium-67

Ga-67 was the first radionuclide to be used for imaging inflammation. Following i.v. injection, Ga-67 binds to transferrin in blood (Tsan et al 1985). The metal-protein complex then diffuses across capillary endothelium. Capillary permeability is increased in inflammation, thereby promoting accumulation of the radiotracer. Within the interstitial space, the complex is retained through binding to transferrin receptors that are expressed in inflammation. Ga-67 remains useful for imaging certain forms of chronic inflammation such as sarcoidosis, but otherwise has been largely replaced by labelled leucocytes and PET/CT (Aulbert et al 1976, Lomas et al 1972).

1.7.2. Radiolabelled leucocytes

Leucocytes can be isolated from venous blood and radiolabelled *ex vivo*. Following re-injection they target inflammatory lesions, which, as a result, become radioactive and can be imaged with a gamma camera. Leukocytes can be labelled with either In-111-labelled chelates or Tc-99m-HMPAO (Thakur et al 1977, Lantto et al 1991, Datz et al 1994). They migrate into inflammation and are ultimately phagocytosed by macrophages. In-111 then undergoes irreversible intracellular binding and is retained but Tc-99m is less stable and tends to elute from both leucocytes and macrophages

following leucocyte engulfment. Imaging is routinely performed at 4 and 24 h following injection. Currently the main clinical indications for leucocyte scanning are musculoskeletal sepsis, infected prosthetic joints, unexplained fever, suspected abdominal or vascular sepsis and inflammatory bowel disease.

1.7.3. FDG

A general technique for imaging inflammation that is becoming increasingly important in clinical practice is FDG PET. Like cancer cells, inflammatory cells are metabolically active and so take up increased amounts of FDG, which is subsequently phosphorylated to FDG-6-phosphate. However, following intracellular uptake, FDG cannot be further metabolised nor de-phosphorylated and so the FDG becomes metabolically trapped. Inflammatory cells have no glucose-6-phosphatase. Following migration into tissues, they are metabolically active and, like cancer cells, take up increased amounts of FDG. PET therefore has been used to image inflammation, especially vasculitis (Vaidyanathan et al 2015), sarcoidosis (Tezuka et al 2015), atheroma (Rudd et al 2010), and infected joint prostheses (Kwee et al 2013). PET/CT is now considered the best technique for the imaging evaluation of pyrexia of unknown origin ((Blockmans et al 2001). This results from its ability to detect both metabolically active inflammatory cells and cancer cells. However, PET/CT has not been used to image hepatic inflammation because, as with other radiopharmaceuticals that have been developed for imaging inflammation, FDG is taken up by the liver physiologically.

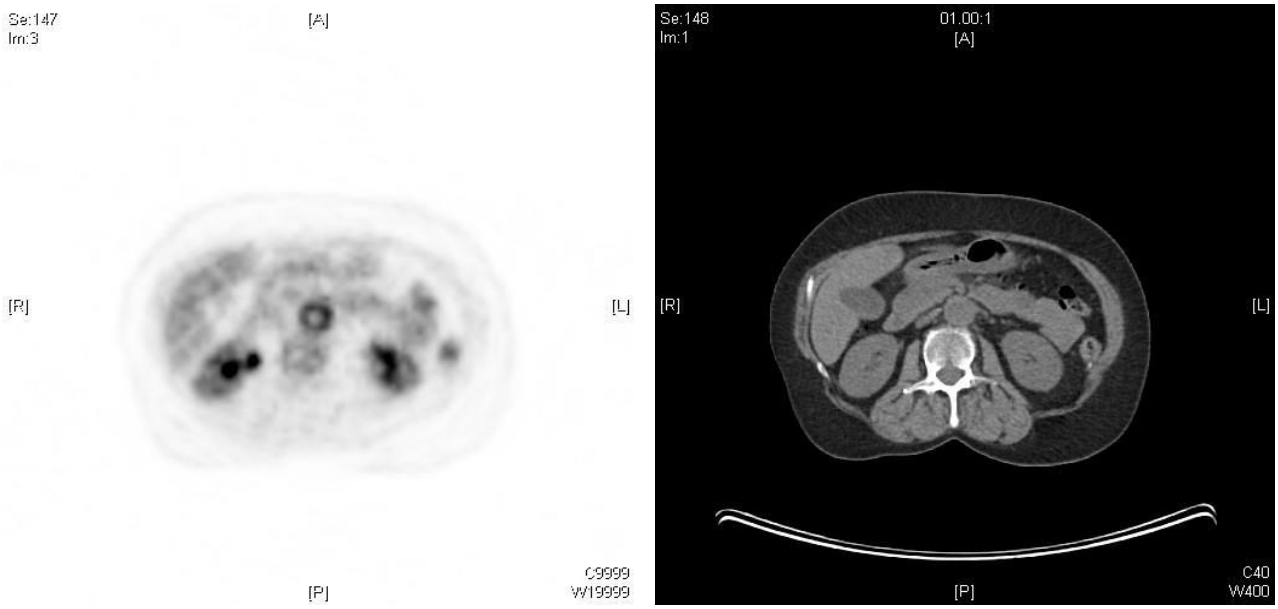

A

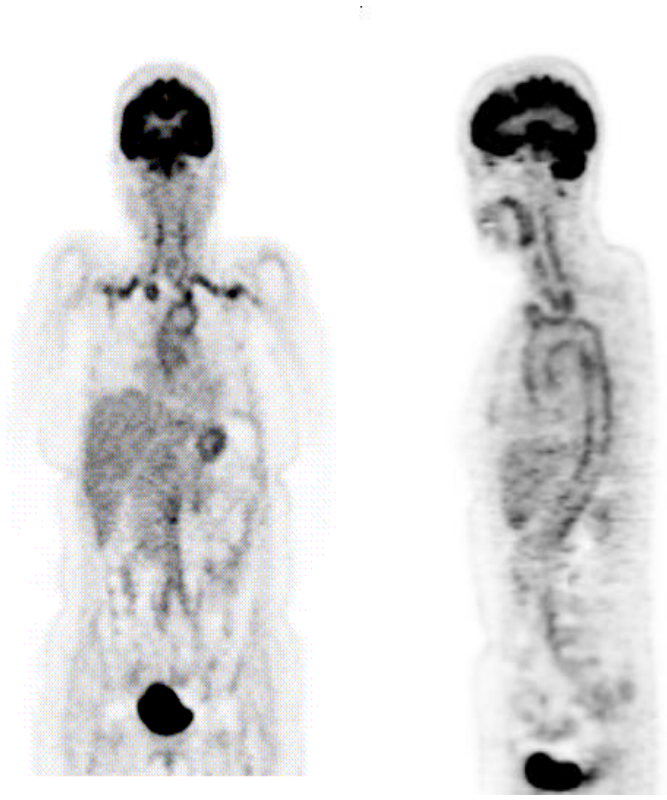

B

Fig 1.5. FDG PET in vasculitis. A: transaxial sections of PET and CT scans showing increased uptake throughout the circumference of the abdominal aorta. B: coronal (left) and sagittal (right) sections showing increased uptake throughout the aorta, and in iliac, subclavian and carotid arteries.

1.8. IMAGING LIVER INFLAMMATION

Diagnosis of diffuse hepatic inflammation using radionuclide imaging techniques is very difficult and until recently had not been attempted apart from imaging intrahepatic sepsis. This difficulty arises from non-specific hepatic uptake of virtually all radiolabelled agents used for imaging inflammation. Indium-111-labelled neutrophils, for example, are physiologically initially pooled and then destroyed in the liver over 24 h, thereby making it difficult to identify any signal from inflammation. The liver is also a physiological target for Ga-67 citrate and FDG, as well as novel biological agents (e.g. *Leukoscan*) designed to target specific molecules expressed by activated leucocytes. Diagnosing diffuse liver inflammation has become more important in the wake of the obesity epidemic and increasing prevalence of NASH, especially to diagnose NASH in its reversible intermediate stage before the onset of liver fibrosis.

1.8.1. In-111-labelled leucocytes

Radiolabeled leucocytes are used primarily for the detection and localization of abscesses and delineation of sites of diffuse or focal infection. In hepatology, labelled leucocytes can be used for the diagnosis of focal septic liver disease, such as liver abscess, empyema or acute cholecystitis (Fink-Bennett et al 1991). Labelled leucocytes have not been used, however, to diagnose diffuse liver inflammation because they are physiologically destroyed in the liver at the end of their lifespan (Saverymuttu et al 1986) and give a signal that cannot be separated from the signal arising from labelled leucocytes migrating into inflammation. Potts et al (PhD thesis, 2014) recognised that this physiological function is impaired in severe liver disease. They made use of the principle that the time courses of uptake of labelled leucocytes

into inflammation and physiological uptake in the liver are different. Physiological pooling of labelled leucocytes in the liver takes place soon after injection, whereas uptake into inflammation takes longer. By comparing images at 30 min and 24 h post-injection, they successfully imaged acute alcoholic hepatitis, a severe inflammatory disease of the liver seen in heavy drinkers (see below). Imaging at 24 h gave a signal disproportionately larger than the signal at 30 min. This was assumed to be the result of migration of labelled cells into intrahepatic inflammation because physiological destruction of labelled leukocytes in the liver, which has a similar time course to uptake into inflammation (Saverymuttu et al 1986), is, like pooling, impaired. Ga-67 could potentially be used in the same way, presuming that its physiological uptake in severe liver inflammation is also impaired.

1.8.2. PET/CT.

PET/CT has not previously been used to image hepatic inflammation because, as with other radiopharmaceuticals that have been developed for imaging inflammation, FDG is taken up by the liver physiologically.

1.9. INTRAHEPATIC KINETICS OF FDG

Intrahepatic FDG kinetics are summarised in the model shown in Fig 1.6. FDG and glucose rapidly enter the hepatic interstitial space and the hepatocyte so their uptake rates in the hepatocyte are largely determined by liver blood flow, represented by K_1. Both are then free to diffuse rapidly back into blood via k_2. This rapid exchange process means that following bolus intravenous injection, the liver FDG concentration closely follows the blood FDG concentration. As FDG enters all the tissues of the body, the blood FDG concentration falls and the liver FDG concentration closely

follows it, indeed so closely that the liver can effectively be used as a blood pool region in dynamic FDG PET, as has been recommended in small experimental animals in which blood pool regions, like the aorta, are too small to accurately monitor.

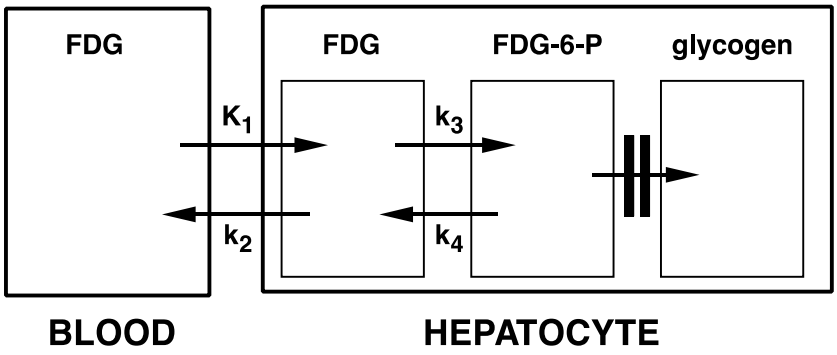

Fig 1.6. Model of hepatic FDG kinetics. K_1 is the delivery rate of FDG to the liver and represents hepatic blood flow; k_2 is the diffusion rate of free FDG back into blood; k_3 represents hexokinase which phosphorylates FDG to FDG-6-phosphate and k_4 represents glucose-6-phosphatase, which converts FDG-6-phosphate back to free FDG.

Inside cells in general, glucose and FDG are phosphorylated by hexokinase (k_3) to glucose-6-phosphate and FDG-6-phosphate, respectively. Glucose-6-phosphate is then metabolised to water and carbon dioxide or incorporated into glycogen to an extent that depends on whether the subject is fasting or post-prandial. FDG-6-phosphate, in contrast, is not recognised by the enzymes of the glyconeogenic or glycolytic pathways and not further metabolised. In all tissues, except the liver and kidney, FDG is therefore metabolically trapped. In the liver and kidney, however, FDG-6-phosphate is dephosphorylated by glucose-6-phosphatase (k_4) and returns to the blood via k_2 as free FDG. In the liver, phosphorylation (k_3) and de-

phosphorylation (k_4) rates are much lower than K_1 and k_2. Values of these transport constants obtained by Choi et al 1994, Iozzo et al 2003, Borra et al 2008 and Munk et al 2001 are summarised in Table 8.1.

Choi et al (1994) performed dynamic imaging for 60 min in healthy subjects before and after a glucose load. Blood and hepatic FDG concentrations fell in parallel during the course of the dynamic imaging both before and after glucose administration (Fig 1.7). Because of competition between FDG and glucose for uptake into the tissues of the body in general, which means that blood FDG concentration increases at high blood glucose levels, hepatic and blood FDG concentrations were both higher 60 min following glucose administration compared to euglycaemic values. The liver-to-blood FDG concentration ratio was also slightly increased as a result of insulin-induced up-regulation of hexokinase (k_3) and increased production of FDG-6-phosphate. Thus, insulin functions to move glucose in the direction of blood to hepatic glycogen and therefore stimulates k_3 and inhibits k_4.

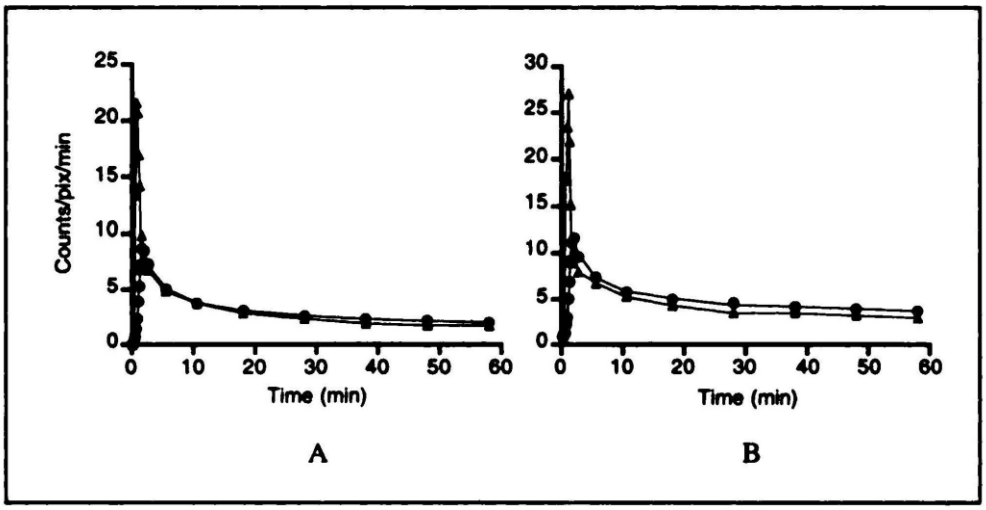

Fig 1.7. Effect of acute hyperglycaemia on the liver-to-blood FDG concentration ratio in normal subjects. In baseline studies, liver and blood FDG concentrations closely follow each other with low concentration ratio (A). The concentration ratio increases in hyperglycaemia as a result of up-regulation of k_3, but the curves still closely follow each other (B). (From Choi et al 1994).

These studies, however, have generated contradictory results, some showing a positive relation between SUV and steatosis (Bural et al 2010), others a negative relation (Abikzer et al 2011) and, some, no relation (Lin et al 2011). A further study found higher hepatic FDG uptake in patients with metabolic syndrome compared with those without (Kamikura et al 2010).

1.10. TEXTURE ANALYSIS

Texture analysis is based on quantification of grey level intensities in voxels and the statistics of their distribution in images. It quantifies the variations of voxel values in images. These values have units of counts in nuclear medicine and PET, and of Hounsfield units in CT. Texture analysis can also be applied to MRI and ultrasonography, as well as photographs. At least 80 parameters have described,

although some, for example entropy and energy, are essentially the inverse of each other.

Parameters of texture can be categorised as follows.

Measures of central tendency include mean, median, mode, percentiles and quartiles of voxel values.

Measures of variability include range, interquartile range, variance, standard deviation, coefficient of variation, kurtosis and skewness of voxel values. Kurtosis and skewness are illustrated in Fig 1.8.

Measures of texture include first order energy and entropy. Inhomogeneous images have high energy, while homogeneous images have low energy. Entropy is essentially the inverse of energy.

Grey level co-occurrence matrices (GLCM) describe the frequency of various combinations of grey level values within a region and include angular second moment, autocorrelation, cluster prominence, cluster shade, contrast, correlation, dissimilarity, energy, entropy, homogeneity and maximum probability.

Grey level run length matrices (GLRLM) calculate the number of texels, describing the coarseness of the region or image. Texels or run lengths are consequent pixels with the same intensity. GLRLM parameters include short run emphasis, long run emphasis, low grey level run emphasis, high grey level run emphasis, short run low

level emphasis, short run high grey level emphasis, long run high grey level emphasis, grey level non uniformity, run percentage, intensity variability and run length variability.

Grey level size zone matrices (GLSZM) describes the size of clusters of voxels within a region and include short and long zone emphasis, intensity non-uniformity, zone length non-uniformity, zone percentage, high intensity zone emphasis, short zone low intensity emphasis, short zone high intensity, long zone low intensity, long zone high intensity, intensity variability, size zone variability and run percentage.

Grey level difference methods (GLDM) describe the intensity differences between vectors and include mean, entropy, variance and constant.

Fractal based features. Fractal dimension describes the texture of a fractal. The fractal dimension correlates with image roughness. A small value of the fractal dimension represents fine texture, while a large fractal dimension corresponds to a coarse texture. The fractal dimension includes mean, standard deviation, lacunarity and Hurst exponent.

Neighbourhood grey tone difference matrices (NGTM) describe local intensity differences between each voxel and its direct 26 neighbours and include coarseness, contrast, busyness, complexity and texture strength.

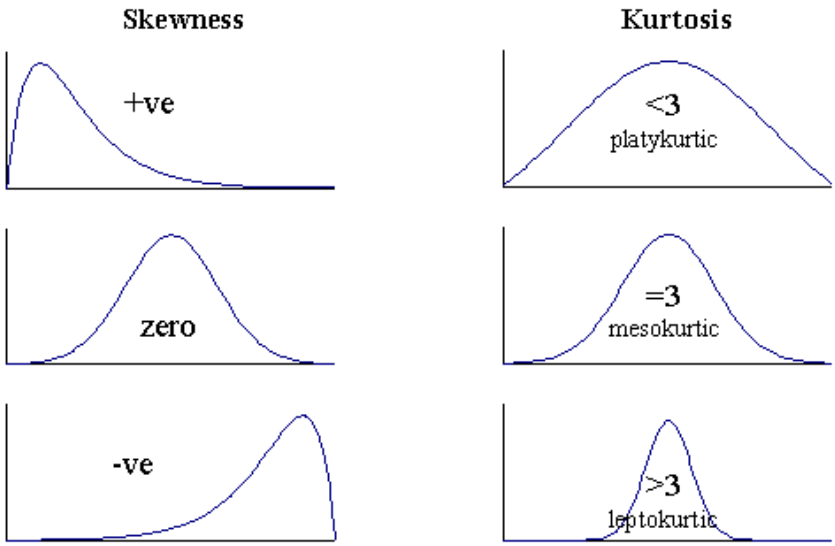

Fig 1.8. Skewness and kurtosis of voxel values in an image. Skewness is an indicator used in distribution analysis as a sign of asymmetry and deviation form a normal distribution. If skewness is negative the data are spread out more to the left of the mean. If skewness is positive the data are spread out more to the right. The skewness of the normal distribution is zero. Kurtosis is a sign of flattening or "peakedness" of a distribution and is a measure of how outlier prone a distribution is. The kurtosis of a normal distribution is 3. Distributions that are more outlier-prone have kurtosis of less than 3 while distributions of less than 3 are less outlier–prone.

There are many publications showing how texture analysis can contribute to improved diagnosis and prognostication in cancer. Some work has also been performed in the liver to identify fibrosis (House et al 2015), but there are no publications to my knowledge that have attempted to use texture analysis to improve the accuracy of imaging methods to quantify hepatic steatosis and detect hepatic inflammation prior to the development of fibrosis.

1.11. AIMS OF THESIS

My original aim was to develop PET CT for the imaging and diagnosis of hepatic inflammation, especially NASH and alcoholic hepatitis. First, however, my aim was to better understand the kinetics of FDG in hepatic steatosis, especially in view of the contradictory results that have been published to date. It was necessary for me to

understand the intrahepatic kinetics of FDG in steatosis before I could proceed with my original aim. I have been unable to prospectively recruit patients with alcoholic hepatitis. I have however performed texture analysis on patients with and without hepatic steatosis and patients with steatohepatitis with the aim of seeing if the last mentioned group have texture features that would allow an early diagnosis of NASH.

Chapter 2: General methods

2.1. Patients

All patients studied in this thesis were referred for routine FDG PET/CT at the Clinical Imaging Sciences Centre (CISC) of Brighton and Sussex Medical School. Almost all the patients attending CISC are investigated for cancer, and a small minority (~5%) for inflammatory or neurological disease.

In chapters 3, 5, 6 and 7, I initially included a random consecutive group of 156 patients irrespective of blood glucose over a two-year period (2011-2012). To increase the numbers of patients with low or high blood glucose levels, I included 148 further patients imaged over a period from 2007-2012 who had blood glucose levels > 6 mmol/l (n =113) or < 4 mmol/l (n = 35) to give a total of 304 patients, of whom 15 and 101 patients had known diagnoses of types 1 and 2 diabetes mellitus, respectively.

In chapter 4, 100 separate patients were retrospectively studied.

For chapters 8, 9, 11 and 12, 60 patients were recruited prospectively to undergo dynamic imaging in addition to their routine FDG PET/CT.

For chapter 10, 24 separate patients were retrospectively studied.

2.2. Whole body metrics

Body mass index (BMI) was estimated as weight divided by square of height.

Body surface area (BSA) was estimated from height and weight using the equation of Haycock et al (1978).

$$BSA = 0.0243 \times weight(kg)^{0.538} \times height(cm)^{0.396} \quad (2.1)$$

Lean body mass (LBM) was estimated from height and weight using the equations of Boer (1984).

$$\text{Men:} \quad LBM(kg) = [0.407 \times weight(kg)] + [0.267 \times height(cm)] - 19.2 \quad (2.2)$$

$$\text{Women:} \quad LBM(kg) = [0.252 \times weight(kg)] + [0.473.height(cm)] - 48.3 \quad (2.3)$$

Whole body % fat was calculated as 100 – ([LBM x 100]/weight)%.

2.3. Ethics

All patients attending our PET CT Unit are asked to give informed consent for use of any of their clinical data for clinical research. All patients retrospectively studied as part of this thesis had done so. In addition, for dynamic imaging, ethical approval was obtained from a research ethics committee because although no additional radiation exposure was given, dynamic imaging is not part of our routine protocol.

2.4. PET/CT acquisition

2.4.1. Whole body imaging

Departmental protocol dictated that patients fasted for at least 6 hours prior to their appointment. The blood glucose level was measured using a glucometer (ACCU-

CHEK Performa; Inform II strips; Roche, Burgess Hill, Sussex, UK). All the glucometers were checked for quality control and synchronised daily every morning before patient use. The quality control process allows users to monitor the "variables" of blood glucose testing in order to consistently obtain reliable test results.

FDG was injected intravenously via the ante cubital fossa or hand. Patients were required to relax, semi recumbent, in a warm, quiet area during the uptake period. Imaging was performed 60 min post-injection of 400 MBq (+/- 10%). A Siemens Biograph 64-slice PET scanner, with immediate non-enhanced CT scanning(120 Kvp/50 mA - Care dose 4D; slice 5 mm; pitch 0.8; rotational speed 0.5/sec convolution kernel B19f PET, very smooth), was used to cover the area from the orbital margin to the lesser trochanters. Arms were up, as arms down may result in artificial elevation of the liver FDG signal due to beam-hardening effects. 3D emission data were then acquired at 3 min per bed position (PET reconstruction: 4 iterations; subset 8; Gaussian pre-filter; FWHM 5 mm; matrix size 168x168; zoom 1) with the patient breathing freely.

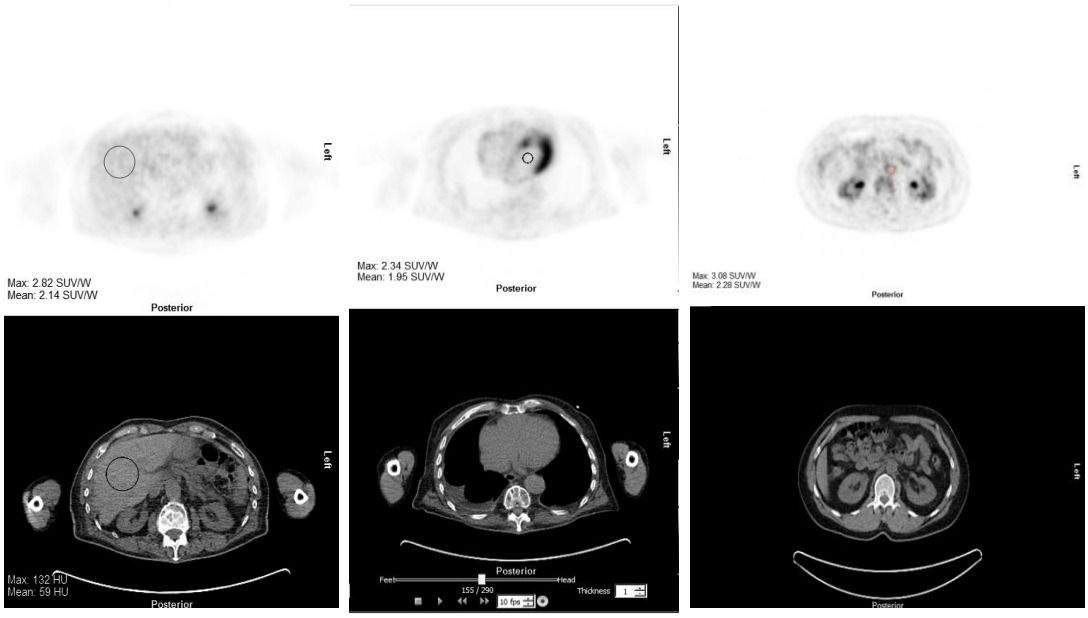

Fig 2.1. Regions of interest placed over the liver (left panel), myocardial blood pool (middle panel) and abdominal aorta (right panel).

2.4.2. Dynamic imaging (see chapter 8)

2.4.3. Image analysis

For each patient, an ROI of 3 cm diameter was drawn over the right lobe of the liver. Identical ROIs were drawn on the PET and CT scans of the liver, avoiding any focal lesions in either scan (Fig 2.1). An ROI was also drawn over the left ventricular cavity (LV), carefully avoiding the myocardial walls, to record blood pool activity (Fig 2.1). SUV was calculated as the tissue concentration of FDG in an ROI divided by the activity injected per kg body weight (equation 1.1). The maximum SUV, which is from the voxel in the ROI with the highest count rate (SUV_{max}) and average SUV (SUV_{ave}) were recorded for the liver. SUV (SUV_{LV}) was recorded for the left ventricular cavity, both SUV_{max} and SUV_{ave}. CT density of the liver was measured in Hounsfield units (HU) in the same ROI as for liver SUV.

2.4.4. Statistical analysis

Normal distributions of data were confirmed using the Shapiro-Wilks test, so parametric statistics were used throughout this thesis. Significance of differences between patient groups (e.g. steatosis versus non-steatosis) was tested using Student's unpaired *t*-test. Relations between variables were quantified using Pearson's regression analysis of continuous data.

In addition for my retrospective studies based on 304 patients, patients were categorised into 6 sub-groups based on blood glucose within the following ranges (patient numbers in brackets): <4 (59), 4-4.9 (76), 5-5.9 (38), 6-7.9 (38), 8-9.9 (58) and 10+ (35) mmol/l. Patients were also subdivided into those with hepatic steatosis (CT density $\leq$ 40 HU; n = 71) and those without (> 40 HU; n = 233) [19,20]. The significance of the differences based on all 6 blood glucose categories between patients with and without steatosis was calculated using ANCOVA.

A p value of < 0.05 was taken to indicate statistical significance.

Chapter 3: Correlates of CT density

3.1. INTRODUCTION

As outlined in the Introduction, there have been several previous publications examining the relationship between hepatic SUV and CT density. The purpose of these studies in general was to find out if the liver could be used as a reference region for quantification of FDG uptake in tumours when its fat content is increased (hepatic steatosis). These studies varied in their use of SUV_{max} and SUV_{ave} as semi-quantitative markers of hepatic FDG uptake, and calculated SUV using body weight. purpose of this chapter is to compare the relationships of CT density with SUV indices in my own large retrospective database of 304 FDG PET/CT studies and also to examine the relationships of CT density with blood glucose and body weight.

3.2. METHODS

The patient database comprised 304 patients, as outlined in chapter 2.
PET/CT acquisition and blood glucose measurement was as described in chapter 2.

ROI were placed over the right lobe of the liver and SUV_{max} and SUV_{ave} measured from equation 1.1 using weight. It was not possible to calculate SUV from lean body mass or body surface area, as height was not routinely recorded in the period during which these patients had their PET/CT studies. Data were analysed continuously using Pearson linear regression analysis.

3.3. RESULTS

3.3.1. Relationships between CT density and blood glucose and weight

CT density correlated significantly with both blood glucose and with body weight (Figs 3.1 and 3.2, respectively; Table 3.1).

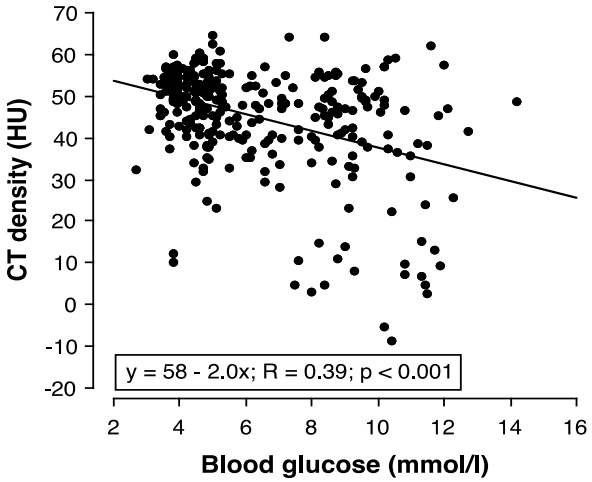

Fig 3.1. Relationship between CT density and blood glucose. Linear regression line and equation are shown. Patients with high blood glucose tend to have low hepatic CT density; i.e. fatty liver.

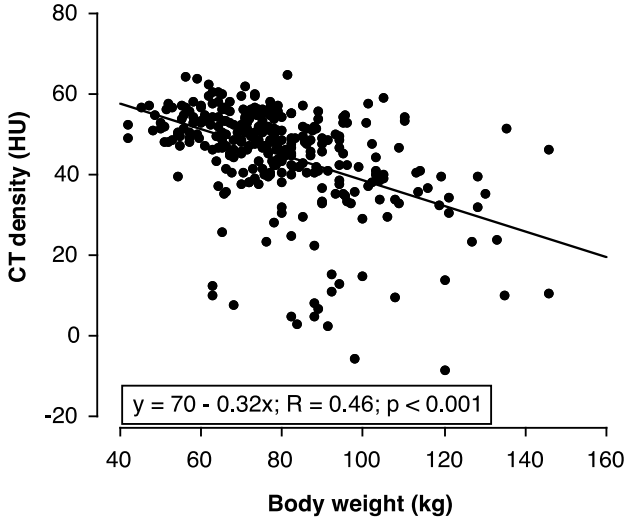

Fig 3.2. Relationship between CT density and body weight. Linear regression line and equation are shown. Note that heavy patients tend to have fatty liver.

3.3.2. Relationships between CT density and liver SUV indices

Liver SUV_{ave} showed no significant correlation with CT density (r = -0.1) (Fig 3.3; Table 3.1). In contrast, liver SUV_{max} correlated inversely and moderately strongly with CT density (r = -0.33; p < 0.001; Fig 3.4). The ratio of SUV_{max} and SUV_{ave} correlated significantly with CT density (r = -0.35; p < 0.001; Fig 3.5).

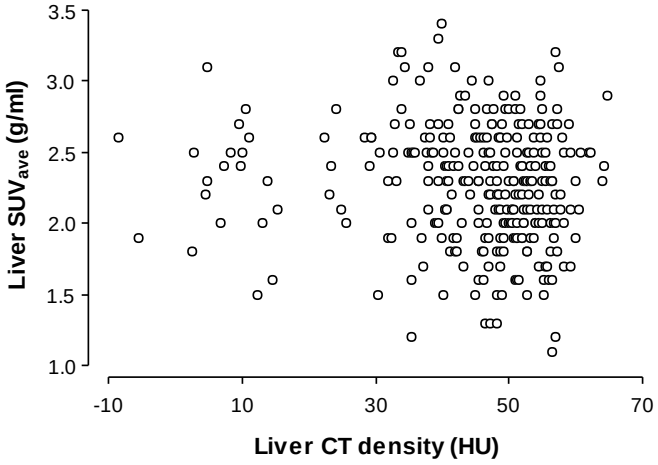

Figure 3.3. Relationship between CT density and SUV_{ave}. Regression line and equation are shown. SUV_{ave} shows no correlation with CT density.

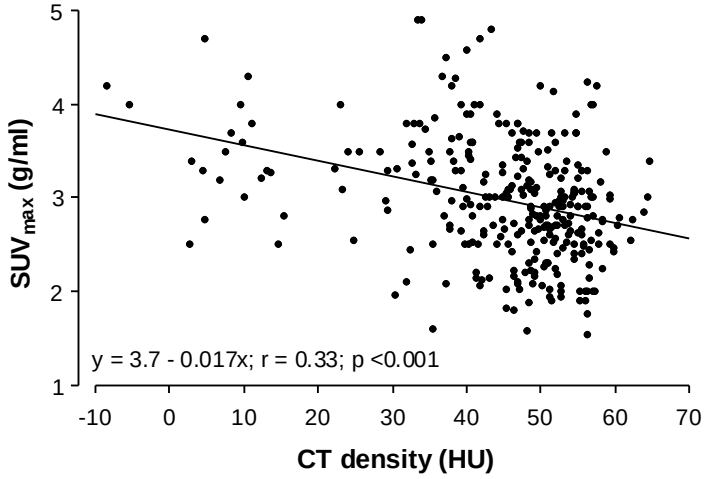

Fig 3.4. Relationship between CT density and SUV_{max}. Regression line and equation are shown. SUV_{max} tends to be increased in patients with fatty liver.

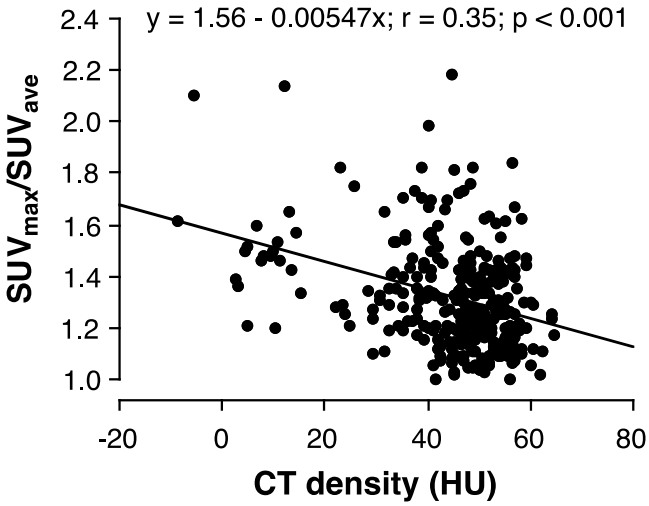

Figure 3.5. Correlation of SUV_{max}/SUV_{ave} with CT density. The line is the linear regression line (equation shown). The ratio correlates significantly with CT density.

Table 3.1.

Relationships between blood glucose (mmol/l), body weight (kg), CT density (HU) and liver SUV (based on body weight; g/ml).

y	x	regression equation	r	p <
glucose	weight	2.70 mmol/l + 0.0454x	0.34	0.001
CT density	glucose	57.5 HU – 2.00x	0.39	0.001
CT density	weight	70.1 HU – 0.316x	0.46	0.001
SUV_{max}	weight	1.78 g/ml + 0.015x	0.43	0.001
SUV_{max}	CT density	3.72 g/ml – 0.0166x	0.33	0.001
SUV_{ave}	weight	1.65 g/ml + 0.0078x	0.35	0.001
SUV_{ave}	CT density	2.42 g/ml + 0.0033x	0.10	0.1
SUV_{max}/SUV_{ave}	CT density	1.56 – 0.0055x	0.35	0.001

3.4. DISCUSSION

I found that SUV_{max} correlates inversely with CT density. However, CT density also correlates inversely with weight. This introduces bias in the correlation between

SUV_{max} and CT density because SUV is calculated using weight. The best whole body metric for calculating SUV was investigated by Sugawara et al (1999). They showed a strong correlation between SUV and weight in women with breast cancer. The subject of optimal whole body metric for calculating SUV is described in chapter 4. CT density also correlates inversely with blood glucose, indicating that glucose tends to be raised in hepatic steatosis.

In contrast to SUV_{max}, SUV_{ave} showed no correlation with CT density. I speculated that this is because the count rate from the liver is reduced by the fat in the liver because negligible FDG enters the fat of the hepatocytes, so in fatty areas of the liver the FDG signal is 'diluted'. Fat is heterogeneously distributed throughout the liver (Decarie et al 2011). In any region of interest, SUV_{max} will tend to avoid fatty areas (as it is recorded from the voxel with the highest count rate) and be relatively independent of this fat dilution effect, unlike SUV_{ave} which is taken as the average of all the voxels. In fatty liver with low CT density, therefore, SUV_{ave} will tend to be reduced, resulting in loss of correlation with CT density. Accordingly, SUV_{max}/SUV_{ave} correlated inversely with CT density. Indeed, this ratio may represent a new marker of hepatic fat. It should be noted that the effects of blood glucose and the whole body metric used to calculate SUV cancel out in this ratio. However, it still possible that in large persons, SUV values are more subject to low signal-to-noise ratio than in small persons and, as CT density correlates with weight, there may be a spurious bias in the correlation of SUV_{max}/SUV_{ave} with CT density. This is discussed later in chapter 12.

In chapter 6, I describe a procedure for correcting SUV_{ave} for the fat contained within the region from which it is recorded (fat-adjusted SUV_{ave}).

The relationship between SUV and blood glucose is discussed in chapter 5 in which it can be appreciated that the relationship between SUV and CT density is complex and depends on several factors. It easy to understand why the studies of previous of workers gave such conflicting findings.

Chapter 4: Influence of whole body metric on SUV

4.1. INTRODUCTION

FDG concentration in any tissue will be lower in a large patient compared with a small one if the two are given the same administered activity. So, in order to account for this, as mentioned in chapter 1, SUV has to be 'scaled' to a metric of whole body size.

It has been suggested that SUV should not be calculated using body weight because when it is based on body weight (SUV_W), it correlates positively with body weight (Sugawara et al 1999).[7] The appropriate metric of body size needs to be consistent with the distribution volume of the FDG, which is the administered activity divided by average tissue concentration of FDG throughout the whole body. The problem with weight for calculating SUV is that FDG uptake in adipose tissue (but not brown fat) is negligible so that SUV is overestimated in obese patients. It is not surprising, therefore, that SUV_W correlates strongly with weight. So it has been suggested that lean body mass (LBM) is more appropriate for calculating SUV, especially as SUV_{LBM} showed no correlation with body weight (Sugawara et al 1999, Tahari et al 2015). Body surface area (BSA) has also been suggested (Sugawara et al 1999).

However, correlating SUV_{LBM}, SUV_{BSA} and SUV_W with body weight is not valid because all these SUVs contain weight in their calculation. When the two co-ordinates of a relationship contain the same variable, the correlation coefficient will be

spuriously increased, unless that variable is measured with complete accuracy. If these rules were to be ignored, Sugawara et al (1999) should have been correlated SUV_{LBM} with LBM, not weight, and SUV_{BSA} should have been correlated with BSA.

Several different equations have been developed for estimating LBM but in general, they show rather poor agreement (Kim et al 2013, Erselcan et al 2002). Equations for estimating BSA are few and are not gender-specific. So the best whole body metric with which to calculate SUV remains uncertain.

The aim of the study in this chapter is to compare weight, LBM and BSA as metrics for calculating SUV, using an approach that avoids spurious correlations.

4.2. METHODS

4.2.1. Theory

The definition of SUV is as follows.

$$SUV = \frac{\text{tissue activity/ml}}{\text{administered activity}} \times \text{whole body metric} \qquad (4.1)$$

Tissue activity/administered activity is the fraction (F) of administered activity in the tissue. F/ml is then the fraction of administered activity per ml of tissue.

Re-arranging equation 4.1 gives

$$F/ml = SUV \times 1/\text{whole body metric} \qquad (4.2)$$

For an ideal whole body metric, plotting F/ml against 1/whole body metric in a population of patients would give a straight-line graph passing through the origin (i.e. no intercept) with a gradient equal to the mean population SUV of the tissue from which F/ml was derived. The aim of the study was to see which body metric best meets this requirement.

4.2.2. Patients

This was a retrospective study. Data are from 49 male patients and 51 female patients attending CISC for routine FDG PET/CT, mainly for management of cancer. As in all my studies, the patients gave informed consent for publication of any data arising from their PET/CT studies.

4.2.3. Imaging

PET/CT acquisition was as described in chapter 2.

4.2.4. Image analysis

A circular region of interest (ROI) of 3 cm diameter was drawn over the centre of the right lobe of the liver in a mid-section slice and maximum and average SUV values (SUV_{max} and SUV_{ave}) were recorded. Patients with visible suspicious focal hepatic pathology were not included.

4.2.5. Data analysis and statistics

The PET CT computer is programmed to calculate SUV using the patient's weight (i.e. SUV_W). SUV_W was therefore divided by the patient's weight to give F/ml (see equation 4.2). F/ml was then plotted against 100/weight, 100/LBM and 1/BSA. (I

multiplied the reciprocals of weight and LBM by 100 to reduce the number of zeros in their values.)

LBM was estimated from height and weight using the gender-specific formulae of Boer (1984). BSA was estimated from height and weight using the gender-nonspecific formula of Haycock et al (1978).

Relations between F/ml and the reciprocals of the 3 whole body metrics were quantified using Pearson's linear regression analysis. The standard errors (SE) of the intercepts of the regression equations were calculated (Altman 1991). The significance of the difference between any pair of intercepts was calculated using Student unpaired *t*-testing, where

$$t = \frac{\text{intercept}_1 - \text{intercept}_2}{(SE_1^2 + SE_2^2)^{0.5}} \quad (4.3)$$

Similarly, the significance of the difference between an intercept and zero was calculated from

$$t = \frac{\text{intercept}}{SE} \quad (4.4)$$

Significance was rejected if $p > 0.05$.

4.3. RESULTS

For all 3 body size metrics, correlation coefficients were higher with respect to SUV_{ave} than SUV_{max} for men, women and both genders combined. Results are therefore given only for SUV_{ave}.

The regression equations of F/ml against the reciprocals of the 3 body size metrics are shown in Table 4.1 and Figure 4.1.

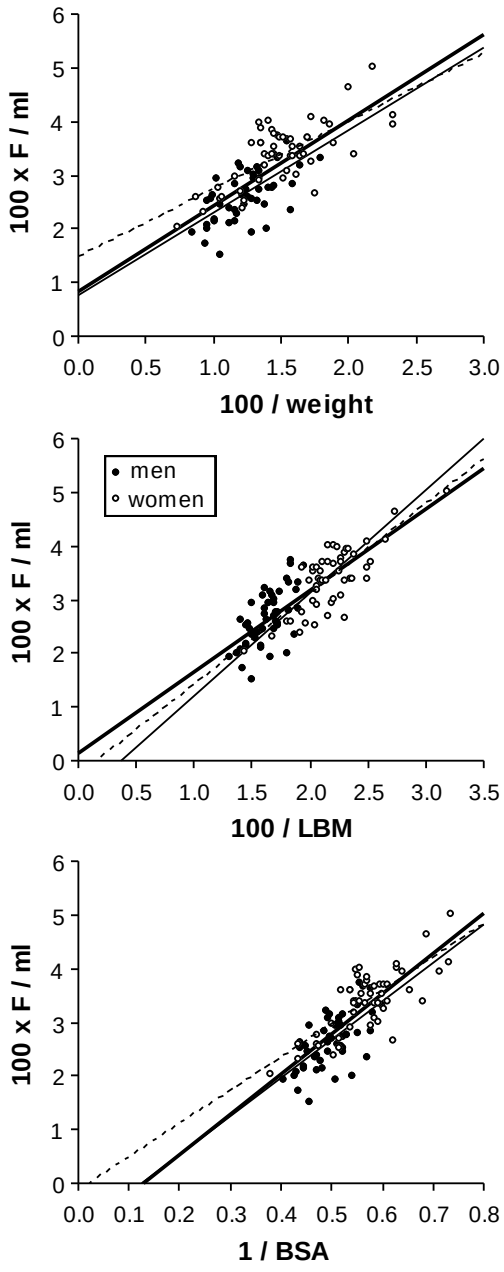

Fig 4.1. Linear correlation between 100 x F/ml and 100/W (upper panel), 100/LBM (middle panel) and 1/BSA (lower panel); dark circles: men (faint continuous regression line; n = 49); open circles: women (dashed regression line; n = 51). The regression line for all patients combined is bold. Regression equations and correlation coefficients are shown in Table 4.1.

When genders were combined, 100/weight gave an intercept that was significantly greater than zero ($p < 0.001$), while 1/BSA gave an intercept that was significantly less than zero ($p < 0.001$). 100/LBM, in contrast, gave an intercept not significantly different from zero.

When the genders were separated, the intercepts given by 100/weight and 1/BSA were significantly greater for women compared with men ($p < 0.01$) but there was no significant difference with respect to 100/LBM (Table 4.1).

Correlation coefficients were marginally higher for 100/LBM than for 100/weight and 1/BSA for women, men and both genders combined (Table 4.1).

Table 4.1: Regression equations for 100 * F/ml (y-axes) against reciprocals of body size indices (x-axes). Correlation coefficients are shown in brackets.

	All (n = 100)	**men (n = 49)**	**women (n = 51)**
100/W	^0.84 + 1.60x (0.75)	0.75 + 1.54x (0.64)	$^{\$}$1.51 + 1.26x (0.72)
100/LBM	0.14 + 1.52x (0.81)	-0.77 + 2.10x (0.65)	-0.27 + 1.68x (0.78)
1/BSA	*-0.96 + 7.48x (0.79)	-0.91 + 7.16x (0.65)	$^{\$}$-0.15 + 6.22x (0.76)

^Significantly greater than corresponding intercept for 100/LBM ($p < 0.001$);
*significantly less than corresponding intercept for 100/LBM ($p < 0.001$);
$^{\$}$significantly higher than corresponding intercept for men ($p < 0.001$ for 100/W; $p < 0.01$ for 1/BSA).

4.4. DISCUSSION

The whole body distribution volume of FDG is complex and influenced by many factors, including time before imaging, the presence or absence of tumour, the amount of body fat and the extent to which fat accumulates FDG, the FDG blood clearance rate (which is influenced by blood glucose) and renal function. So no whole body metric would be able to accurately define the volume of distribution in a heterogeneous population of patients.

Adipose tissue accumulates FDG but less than lean tissue, so SUV_W will be overestimated to an extent that depends on percentage body fat. In obese people, the FDG concentration of lean tissue will be relatively high compared to their weight. F/ml will therefore also be high relative to weight and so the reciprocal of weight should give a positive intercept when correlated with F/ml, as I found.

BSA in relation to body size is high in small individuals and low in large individuals. Thus, the surface area-to-volume ratio of a golf ball is higher than that of a soccer ball. This explains the negative intercept seen when F/ml is regressed on 1/BSA.

Because LBM excludes adipose tissue, SUV_{LBM} will be underestimated to an extent that depends on how much FDG accumulates in adipose tissue. However, the insignificant positive intercept observed with 100/LBM for genders combined suggests that adipose tissue in general accumulates minimal FDG.

The differences in the intercepts observed between men and women are consistent with the above conclusions. Thus women have approximately 10% more fat than men

(Deurenberg et al 1991) and accordingly the intercepts with respect to 100/W and 1/BSA were significantly higher in women. In contrast, because of the exclusion of body fat, there was no significant gender difference with respect to 100/LBM.

These 3 whole body indices have advantages and disadvantages. The advantage of weight is that it is easily and accurately measured. Its disadvantage is that adipose tissue in general accumulates less FDG than lean tissue. LBM has the disadvantage of uncertainty in its estimation. Thus, there are many equations described in the literature and they have been found to have poor agreement in their estimation of LBM (Kim et al 2013, Erselcan et al 2002). Inaccurate estimation of LBM would reduce the correlation between SUV_{LBM} and weight (Wahl et al 2009, Sugawara et al 1999, Tahari et al 2015), thereby weakening the claim, based on the observed low correlation between SUV_{LBM} and weight, that SUV_{LBM} is more reliable than SUV_{W}.

Estimation of LBM may also be more difficult in a cancer population because of the relatively high prevalence of cachectic patients. Nevertheless, despite these apparent disadvantages, 100/LBM correlated slightly better with F/ml than 100/W and 1/BSA (Table 1). BSA has no apparent advantages but several disadvantages, including its 2-dimensional nature and that the equations for its estimation are not gender-specific. BSA is lower, relative to body mass, in large individuals compared with small ones, accounting for its negative intercepts in the current study and for the finding of Sugawara et al that SUV_{bsa} correlates negatively with body weight (Sugawara et al 1999).

In conclusion, this study has confirmed that LBM is the preferred whole body metric to calculate SUV and should be taken up in routine clinical practice. LBM however is not perfect because of the uncertainty of equations for estimating LBM and the potential uptake of FDG in fatty tissues.

Chapter 5: Influence of blood glucose on SUV

5.1. INTRODUCTION

As described in chapter 1, the majority of the FDG signal from the liver arises from activity that is in rapid exchange between hepatocytes and hepatic blood via K_1 (hepatic blood flow) and k_2 (Fig 1.5). Hepatic FDG concentration therefore closely follows blood concentration, as shown by Choi et al (1994) (Fig 1.6). Indeed, it has been suggested that the liver is a good region for the blood pool signal in small animal PET because of the size limitations imposed by placing an ROI over the heart or a major blood vessel (Green et al 1998, Torizuka et al 1995). However, blood and liver FDG concentrations are not identical because of phosphorylation of FDG via k_3, mainly in hepatocytes but also other hepatic cells, including possibly inflammatory cells. As shown by Choi et al (1994), hepatic FDG concentration therefore slightly exceeds blood concentration; in other words, there is an excess signal from the liver relative to the blood pool signal that is the result of FDG phosphorylation. Choi et al (1994) showed that this excess signal was higher following a glucose load, presumably as a result stimulation of hexokinase (k_3) by insulin.

FDG and glucose compete with each other for uptake into the organs, so when blood glucose increases, tissue FDG clearance in general decreases (except in muscle in which FDG uptake increases in hyperglycaemia (Lindholm et al 1993, Namba et al 1994). Blood FDG concentration therefore also increases in hyperglycaemia, as shown by Choi et al (1994). Liver FDG activity should therefore vary with the blood glucose level, so it follows that to study the relation between hepatic steatosis and liver FDG accumulation, the blood glucose level should be taken into account.

However, none of the previous studies examining the relation between hepatic SUV and hepatic steatosis considered the influence of blood glucose.

In order to control for blood glucose and to detect the excess hepatic FDG signal, I divided the liver SUV by the blood pool SUV. Doing this has the advantage that the whole body metric for calculating SUV cancels out. Surprisingly none of the previous studies on liver SUV in hepatic steatosis expressed liver SUV in relation to blood pool SUV.

The aim of this chapter was to examine the relationship between liver SUV and blood glucose in the context of intrahepatic FDG kinetics.

5.2. METHODS

5.2.1. Patients

This was a retrospective study of 304 patients undergoing routine FDG PET/CT as described in chapter 2. I initially included a random consecutive group of 156 patients irrespective of blood glucose over a two-year period (2011-2012). To increase the numbers of patients with low or high blood glucose levels, I included 148 further patients imaged over a period from 2007-2012 who had blood glucose levels > 6 mmol/l (n =113) or < 4 mmol/l (n = 35). Fifteen and 101 patients had known diagnoses of types 1 and 2 diabetes mellitus, respectively.

5.2.2. Image analysis

For each patient, a single circular region of interest (ROI) of 3 cm diameter was drawn over the right lobe of the liver for measurement of liver SUV, using body

weight. Height was not recorded in this series of patients so I was unable to use lean body mass to calculate SUV. Identical ROIs were drawn on the PET and CT scans, avoiding any visible focal lesions present in either scan. ROIs were also drawn over the ascending aorta (AA), left ventricular cavity (LV) and descending aorta (DA) to record blood pool activity.

In this chapter, I used the maximum SUV for the 3 blood pool regions in order to minimize partial volume effects in the relatively small ROI over the AA and DA. Because the LV cavity is not so size-limited, I also measured SUV_{ave} for the LV cavity. I then divided liver SUV by LV SUV.

CT density of the liver was measured and used as an index of hepatic fat content, as described in chapter 2.

5.2.3. Statistical analysis

Relations between variables were quantified using Pearson's linear regression analysis or by least squares fitting to second order polynomials. Patients were also subdivided into 6 sub-groups based on blood glucose levels within the following ranges (patient numbers in brackets): <4 (59), 4-4.9 (76), 5-5.9 (38), 6-7.9 (38), 8-9.9 (58) and 10+ (35) mmol/l.

5.3. RESULTS

5.3.1. Relationships between blood glucose and liver SUV

Liver SUV_{ave} and SUV_{max} both increased with similar time courses as blood glucose increased up to levels of 8-10 mmol/l (Fig 5.1). Above these levels, liver SUV_{max} showed no further increase, while SUV_{ave} showed a slight decrease.

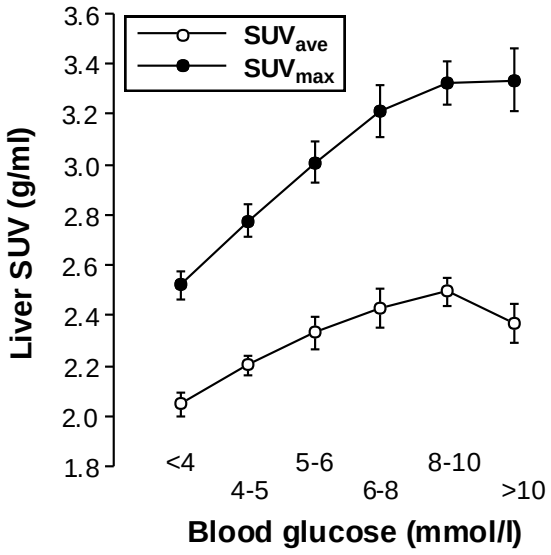

Fig 5.1. Relationships of liver SUV_{ave} and SUV_{max} with blood glucose shown as categorized data. Error bars = SEM.

The continuous datasets were better fitted by second order polynomials than by linear functions (Fig 5.2) and showed strong correlations between blood glucose and SUV.

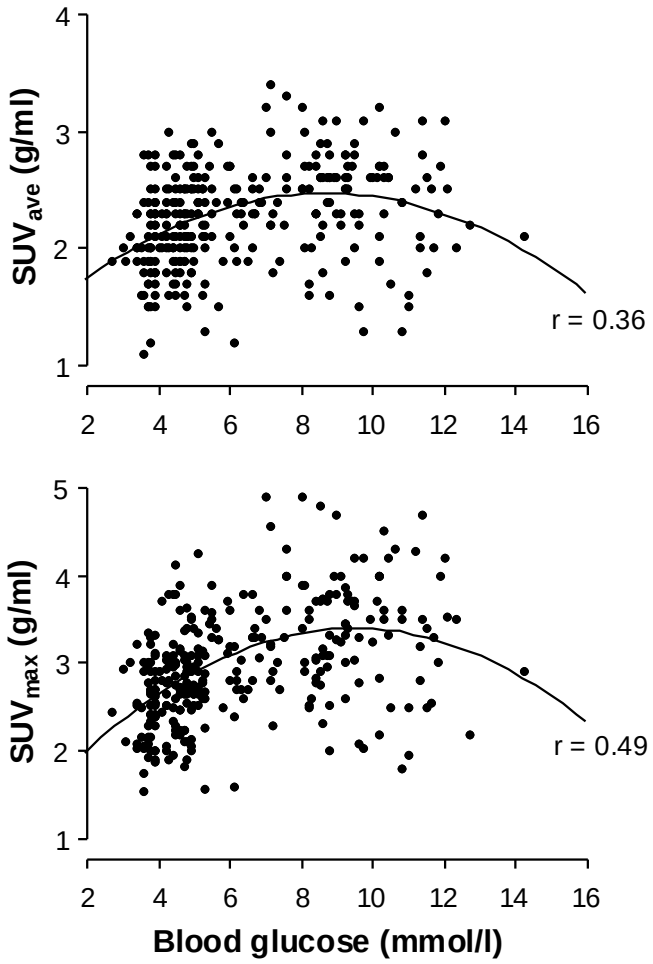

Fig 5.2. Relations of liver SUV_{ave} (upper panel) and SUV_{max} (lower panel) with blood glucose shown for continuous data. The curved lines are second order polynomial fits, as follows (x = blood glucose); upper panel: $SUV_{ave} = 1.24 + 0.28x - 0.016x^2$ ($r = 0.36$; $p < 0.001$); lower panel: $SUV_{max} = 1.13 + 0.48x - 0.025x^2$ ($r = 0.49$; $p < 0.001$).

The relationships of the 3 blood pool region SUV values with blood glucose were almost superimposed on each other and very similar to the relationship observed between blood glucose and liver SUV (Fig 5.3). Thus, for all 3 blood pool regions, SUV increased up to glucose levels of 8-10 mmol/l then showed a slight decrease up to glucose levels of 10+ mmol/l, similar to liver SUV_{ave}.

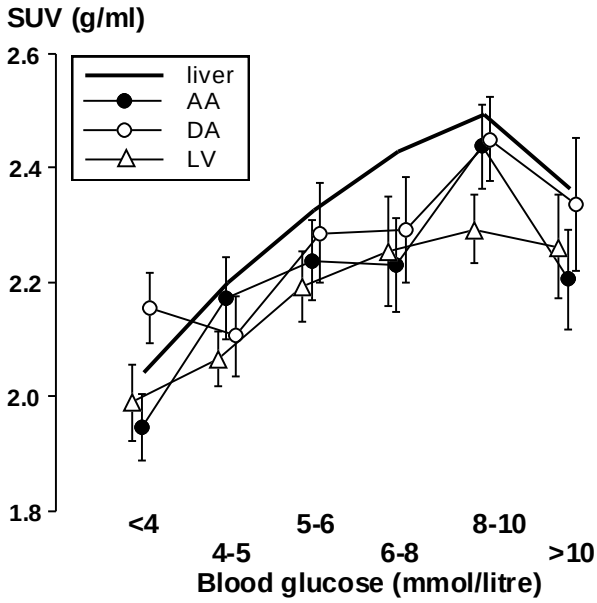

Fig 5.3. Relationships of maximum SUV of 3 blood pool regions with blood glucose shown as categorized data. Error bars = SEM. The continuous bold line is the relation of liver SUV_{ave} with glucose from Figure 1. AA – ascending abdominal aorta, DA – descending abdominal aorta, LV – left ventricular cavity (all SUV_{max}).

5.3.2. Relationships between liver SUV expressed in relation to LV SUV and CT density

Liver SUV_{max} divided by LV SUV_{ave} correlated significantly and inversely with CT density (Fig 5.4). The correlation was stronger when liver SUV_{max} was divided by LV SUV_{ave} rather than LV SUV_{max} probably because LV SUV_{max} is based on a single voxel and therefore more susceptible to 'noise' than LV SUV_{ave}.

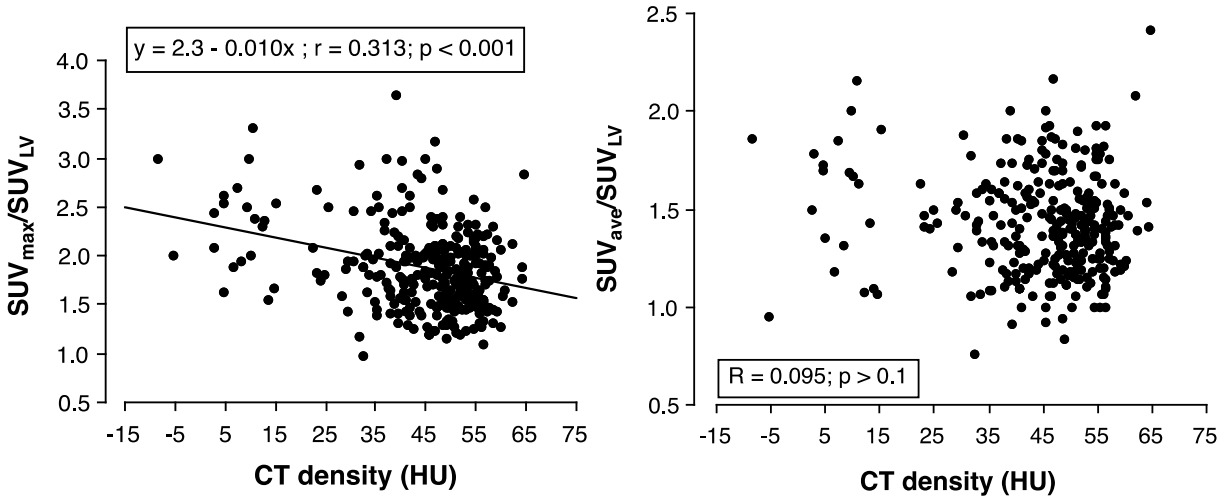

Fig 5.4. Relationships between liver SUV/LV SUV_{ave} and CT density; left panel: liver SUV_{max}/LV SUV_{ave}; right panel: liver SUV_{ave}/LV SUV_{ave}. No correlation is seen with liver SUV_{ave}/LV SUV_{ave}. Note that by dividing liver SUV by LV SUV, the effects of blood glucose and the whole body metric for calculating SUV cancel out.

In contrast to liver SUV_{max}, when liver SUV_{ave} was divided by LV SUV_{ave}, it showed no correlation with CT density, probably because at low values of CT density, liver SUV_{ave} is diluted by fat (see Figure 3.3).

5.4. DISCUSSION

As mentioned in chapter 1, previous publications that examined the relationship between liver SUV and hepatic steatosis (Bural et al 2010, Abikzer et al 2011, Lin et al 2011, Abele et al 2010, Kamikura et al 2010) have given contradictory results, some showing a positive relation between liver FDG uptake and fat content (Bural et al 2010), others a negative relation (Abikzer et al 2011, Lin et al 2011) and, some, no relation (Abele et al 2010). A further study found higher hepatic FDG uptake in patients with metabolic syndrome compared with those without (Kamimura et al

2010). One possible reason for this disagreement is that blood glucose was not considered.

Using dynamic PET with measurement of hepatic and blood FDG concentrations in healthy volunteers either fasted or after a glucose load, Choi et al (1994) showed that glucose administration resulted in a parallel increase in liver and blood FDG concentrations measured in absolute units (MBq/ml). There was also a small increase in the liver-to-blood concentration ratio, as a result of insulin-induced up-regulation of k_3 (Fig 1.6). Kubota et al (2011) showed a positive correlation between blood glucose and SUV_{ave} up to a glucose level of 7 mmol/l but curiously the relation was much stronger at 90 min post-injection compared with 60 min. Groheux et al (2013) demonstrated a positive correlation between blood glucose and liver SUV_{ave} that was not affected by time post-injection.

de Geus-Oei et al (2006) previously showed that all 3 blood pool regions used in the current study reflected arterial FDG concentration with reasonable accuracy, although Lammertsma's group favored the ascending aorta (van der Weerdt et al 2001, Lubberink et al 2004). The three separate blood pool regions gave correlations between their SUV values and blood glucose that were almost superimposed on each other and also on the liver SUV. An increase in blood pool SUV as blood glucose increased was expected but the decrease, although small, in values above 8-10 mmol/l, seen in all 3 regions, was not expected and is unexplained. It might be due to increased uptake in skeletal muscle in hyperglycaemia (Lindholm et al 1993, Namba et al 1994).

A confounding factor that should be considered is the effect of the signal-to noise ratio. This may be lower in larger, overweight people, and have the effect of increasing variability of SUV_{max} more than SUV_{ave}. Blood glucose tends to be higher in overweight people (see Table 3.1) and so this may contribute a spurious positive element to the relation between blood glucose and SUV_{max}. The signal-to-noise ratio issue is studied in this context in chapter 12.

In conclusion, the inverse relationship between CT density and liver SUV_{max}/LV SUV_{ave} suggests that hepatic FDG accumulation is increased in hepatic steatosis. This is probably the result of insulin resistance, with resulting hyperinsulinaemia and upregulation of k_3 (see chapter 8). Further implications of this study are firstly that it may explain why previous studies on the relation between hepatic steatosis and liver FDG uptake have been conflicting, and secondly, suggests that liver SUV is not valid as a reference region (comparator) for tumour uptake.

Chapter 6: Influence of hepatic fat on the SUV signal

6.1. INTRODUCTION

As described in chapter 3, I found that liver SUV_{max} correlated with hepatic fat (measured from CT density) but liver SUV_{ave} showed no correlation with hepatic fat. The ratio of liver SUV_{max}/SUV_{ave} also correlates with hepatic fat. In chapter 5, I went on to show that liver SUV_{max}/LV SUV_{ave} correlated with hepatic fat but liver SUV_{ave}/LV SUV_{ave} did not correlate with hepatic fat. I postulated that these findings were the result of dilution of the FDG signal by heterogeneously distributed fat, tending to reduce liver SUV_{ave} in a region of interest but not SUV_{max}. I therefore proposed the ratio of liver SUV_{max}/SUV_{ave} as a new marker of hepatic fat.

No previous studies examining the uptake of FDG by the liver have considered a possible signal dilution effect of fat. In this chapter, I describe the use of a procedure to adjust (or correct) the liver SUV for the dilution effect of fat. I then compared liver SUV indices, including 'fat-adjusted' SUV_{ave}, between patients with and without steatosis. I also minimised the effects of blood glucose by making this comparison in 6 separate blood glucose groups, as described in chapter 2.

6.2. METHODS.

6.2.1. Patients

This was a retrospective cohort study of 304 patients undergoing routine FDG-PET/CT at CISC, as described in the previous chapter and in chapter 1.

Image acquisition is as described in chapter 2.

6.2.2. Image analysis

For each patient, an ROI of 3 cm diameter was drawn over the right lobe of the liver, as described in the previous chapter. An ROI was also drawn over the left ventricular cavity (LV), carefully avoiding the myocardial walls, to record blood pool activity. SUV_{max} and SUV_{ave} were recorded for the liver using body weight. Average SUV (SUV_{LV}) was recorded for the left ventricular cavity. CT density of the liver was measured in Hounsfield units (HU) in the same ROI as for liver SUV.

6.2.3. Data Analysis

All 304 patients were subdivided into 6 sub-groups based on blood glucose level, as described in chapter 2.

SUV_{ave} was adjusted for hepatic fat content using an equation relating CT density to the percentage of liver that is fat that was described by Ricci et al (1997). They measured CT density in samples containing known amounts of %fat, and obtained the following equation.

$$\text{CT density (HU)} = 55.8 - (1.7 \times \%\text{fat}) \qquad (6.1)$$

It can be seen from this equation that 10% fat corresponds to a CT density of 39 HU.

In order to do the inverse; i.e. calculate the %fat from CT density in my patients, I re-arranged equation 6.1 to give

$$\%\text{fat} = (55.8 - \text{CT density})/1.7 \qquad (6.2)$$

Expressed as a proportion of instead of percentage, equation 6.2 is simply divided by 100. So

Proportion of the liver that is fat = (55.8 – CT density)/170 (6.3)

This proportion was subtracted from 1 to give the proportion of the liver that is lean (i.e. fat-free). Liver SUV_{ave} was then divided by the fat-free proportion to give fat-adjusted liver SUV_{ave}. SUV_{max} was not adjusted for hepatic fat.

6.2.4. Statistics

Liver SUV_{ave}, liver SUV_{max}, and fat-adjusted liver SUV_{ave} were compared between patients with and without hepatic steatosis using ANCOVA. I also compared liver SUV/SUV_{LV}. Numbers of patients with (≤40 HU) and without hepatic steatosis were 71 and 233, respectively.

6.3. RESULTS

6.3.1. Adjustment for liver fat

The theoretical relation between the percentage of fat in the liver and CT density, based on equation 6.2, is shown in Fig 6.1. It can be seen that in some patients with high CT density, the percentage became negative, probably reflecting experimental error.

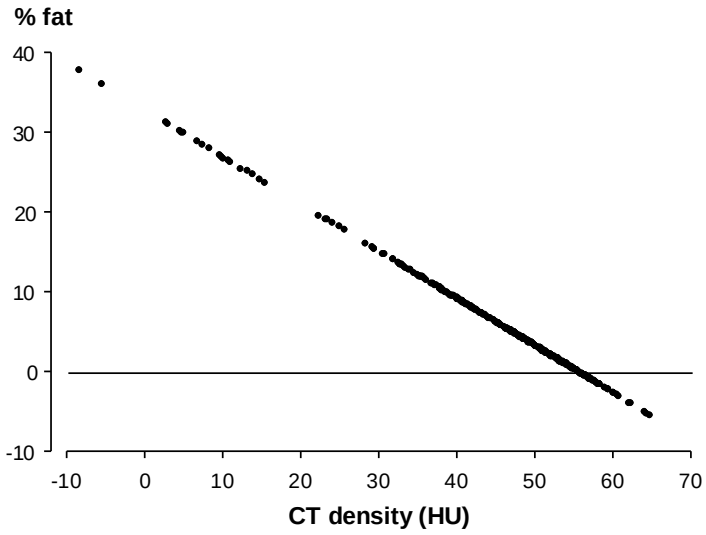

Figure 6.1. Theoretical relation between percent fat in the liver, determined from CT density using equation 6.2, and CT density. Note the presence of negative values in patients with high CT density.

6.3.2. Relationship between blood glucose and hepatic fat

Percentage hepatic fat increased exponentially with increasing blood glucose ($p < 0.001$) (Fig 6.2).

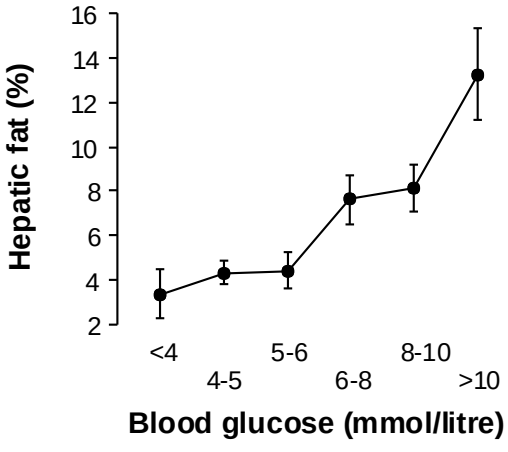

Figure 6.2. Relationship between blood glucose and % hepatic fat calculated using equation 6.2. Note that % fat increases exponentially as blood glucose increases.

6.3.3. Relationships between blood glucose and liver and left ventricular SUV

As shown in chapter 5, SUV_{LV} increased with blood glucose up to glucose levels of 8-10 mmol/l but tended to decrease between blood glucose groups of 8-10 and 10+ mmol/l. Liver SUV_{ave} showed a similar relation with blood glucose (Fig 6.3A). Liver SUV_{max} however showed not so much tendency to fall at high glucose levels. Fat-adjusted liver SUV_{ave} also correlated with blood glucose but continued to increase between blood glucose groups of 8-10 and 10+ mmol/l (Fig 6.3A).

The ratio of liver SUV_{ave}/SUV_{LV} did not correlate with blood glucose (Fig 6.3A, lower panel). In contrast, liver SUV_{max}/SUV_{LV} ($p < 0.001$) and fat-adjusted SUV_{ave}/SUV_{LV} both correlated positively ($p < 0.001$) and showed similar relations with blood glucose (Fig 6.3A).

6.3.4. Relationships between blood glucose and liver SUV; fatty liver versus non-fatty liver

The relationships between liver SUV_{ave} and blood glucose were similar between patients with and without hepatic steatosis (Fig 6.3B). In contrast, fat-adjusted liver SUV_{ave} in patients with steatosis was higher than those without steatosis ($p < 0.01$) (Fig 6.3B). The difference was ~0.4 g/ml across all blood glucose subgroups. Liver SUV_{max} was also different between patients with and without steatosis ($p < 0.005$) but it was slightly smaller (~0.3 g/ml) (Fig 6.3B).

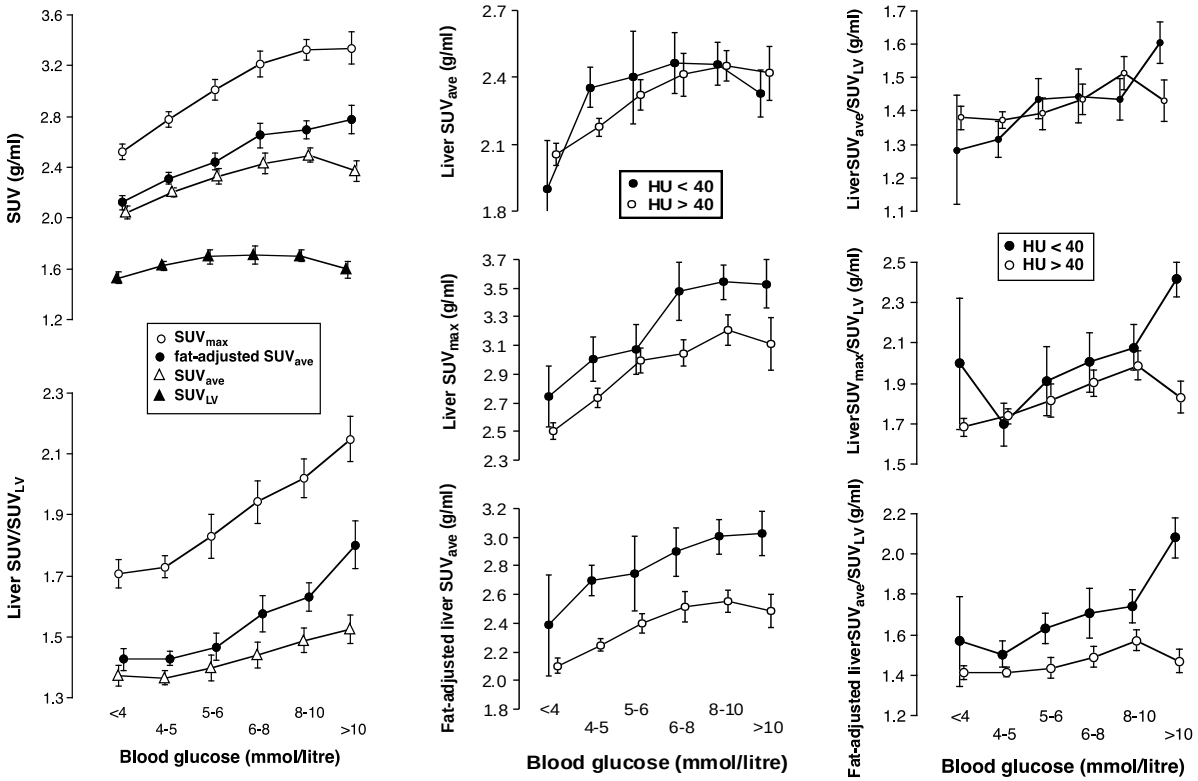

A **B** **C**

Fig 6.3.
A: Upper panel: relationships of liver SUV_{max} (open circles), SUV_{ave} (open triangles), fat-adjusted SUV_{ave} (closed circles) and SUV_{LV} (closed triangles) with blood glucose. Lower panel: relationships between liver SUV_{ave}/SUV_{LV}, SUV_{max}/SUV_{LV} and fat-adjusted SUV_{ave}/SUV_{LV} with blood glucose; all 3 relationships are significant ($p < 0.001$).

B: Relationships of liver SUV_{ave} (upper panel), SUV_{max} (middle panel) and fat-adjusted SUV_{ave} (lower panel) with blood glucose in patients with (closed circles) and without steatosis (open circles). SUV_{ave} does not correlate significantly with blood glucose in either group. SUV_{max} and fat-adjusted SUV_{ave} both correlate significantly with glucose in both groups ($p < 0.01$). The difference in liver SUV_{max} between the two groups is ~0.3 g/ml and in fat adjusted SUV_{ave} is ~0.4 g/ml ($p < 0.005$).

C: Relationships of SUV_{ave} /SUV_{LV} (upper panel), SUV_{max} /SUV_{LV} (middle panel) and fat-adjusted SUV_{ave} /SUV_{LV} (lower panel) with blood glucose in patients with (closed circles) and without steatosis (open circles). There was no significant relationship between SUV_{ave} /SUV_{LV} and blood glucose either in patients with or without steatosis. Fat-adjusted SUV_{ave} /SUV_{LV} correlated significantly with blood glucose in patients with hepatic steatosis ($p < 0.01$) but not in those without. SUV_{max} /SUV_{LV} correlated significantly with blood glucose in patients with ($p < 0.01$) or without steatosis ($p < 0.02$), though more strongly with those with steatosis. Moreover, in the group with blood glucose levels of 10+ mmol/l, SUV_{max} /SUV_{LV} was significantly higher in patients with steatosis ($p < 0.01$).

Error bars = SEM.

Liver SUV_{ave}/SUV_{LV} was similar between patients with and without steatosis ($p > 0.05$) but liver SUV_{max}/SUV_{LV} and fat-adjusted liver SUV_{ave}/SUV_{LV} were higher in patients with steatosis ($p < 0.01$; Fig 6.3C). None of these 3 expressions of liver SUV as ratios with SUV_{LV} showed any significant correlation with blood glucose in patients without steatosis but in contrast they all increased with increasing glucose in patients with steatosis ($p < 0.01$). The difference in liver SUV/SUV_{LV} between the two patient groups was most obvious in patients with blood glucose of 10+ mmol/l (Fig 6.3C).

6.4. DISCUSSION

Hepatic FDG kinetics is the key to understanding and evaluating the effects of blood glucose on hepatic FDG accumulation (Choi et al 1994). Blood FDG concentration would be expected to vary with blood glucose because FDG competes with glucose for tissue clearance. Hepatic SUV is largely, but not entirely, a blood pool SUV (Green et al 1998, Torizuka et al 1995) and is therefore affected by blood glucose similarly to left ventricular cavity SUV. In this chapter, I therefore divided the patients into blood glucose groups in order to examine the liver SUV differences between patients with and without steatosis without influence of blood glucose.

As expected, liver SUV correlated with blood glucose whether expressed as SUV_{ave}, SUV_{max} or fat-adjusted SUV_{ave}. However at high blood glucose levels, differences were seen. Thus SUV_{ave} tended to fall, SUV_{max} remained unaltered while fat-adjusted SUV_{ave} continued to increase. As can be seen from Fig 6.2, hepatic fat increases exponentially with increasing blood glucose, which may explain these differences.

Thus SUV_{ave}, but not fat-adjusted SUV_{ave}, is diluted by the fat at high blood glucose, while SUV_{max} may be slightly diluted by hepatic fat. It remains unclear however, why SUV_{LV} fell at high blood glucose.

It was pointed out in the previous chapter that in order to measure the excess hepatic FDG activity (from FDG phosphorylation) over and above that expected from blood pool SUV, it is helpful to express hepatic SUV values as ratios with left ventricular cavity SUV. It can then be seen from the lower panel of Fig 6.3A that liver SUV/SUV_{LV} increased with increasing blood glucose, especially SUV_{max}/SUV_{LV} and fat-adjusted SUV_{ave}/SUV_{LV}.

Figs 6.3B and 6.3C are the upper and lower panels of Fig 6.3A have been split into steatosis and non-steatosis groups. In Fig 6.3B, differences between the 2 groups are evident in liver SUV_{max} and fat-adjusted SUV_{ave}, but not in SUV_{ave}. Similar findings are seen between the 2 groups when the liver SUV values are divided by SUV_{LV} (Fig 6.3C). Interestingly, in Fig 6.3C, it can be seen that patients with steatosis show a stronger relationship with blood glucose than in those without.

In chapter 5, I showed that regions over the ascending aorta, descending aorta and left ventricular cavity gave very similar values of maximum SUV and showed similar relations with blood glucose. However, I used the left ventricular cavity for monitoring blood pool activity in the current study because its SUV_{ave} correlated more closely with glucose than the SUV values obtained from the regions over the aorta. The use of the left ventricular cavity as a surrogate for arterial FDG concentration has previously been validated (de Geus-Oei et al 2006).

I conclude that after correcting for both the effects blood glucose and of dilution of the hepatic FDG signal by heterogeneously distributed hepatic fat, FDG accumulation is increased, and shows a stronger relationship with blood glucose, in hepatic steatosis. The reasons for this are discussed in chapter 8.

Chapter 7: Correcting tumour SUV for blood glucose in FDG PET

7.1. INTRODUCTION

In FDG PET/CT for cancer management, quantification of tumour uptake is essential for monitoring treatment. This is most often by measurement of SUV. FDG competes with glucose for uptake into tumour, so tumour SUV is inversely related to blood glucose (Lindholm et al 1993). European Association of Nuclear Medicine (EANM) guidelines therefore recommend normalisation of tumour SUV to a blood glucose level of 5 mmol/l (Boellaard et al 2010). This recommendation assumes that tumour glucose utilisation rate (MRglu) is not affected by blood glucose, in which case MRglu would be equal to tumour glucose clearance multiplied by blood glucose.

i.e. MRglu = tumour glucose clearance x blood glucose (7.1)

(mmol/min = ml/min x mmol/ml)

FDG is a tracer for glucose; in other words, tumours trap FDG as though it was glucose, so assuming a lumped constant of one (i.e. that FDG and glucose are 'handled' by the tumour tissue identically)

MRglu = tumour FDG clearance x blood glucose (7.2)

Re-arranging

FDG clearance = MRglu/blood glucose (7.3)

In the brain, MRglu is constant (Namba et al 1994); in other words, the brain takes a constant supply of glucose irrespective of the blood glucose level. If tumours also

have a constant glucose utilisation rate, it can be seen from equation 2 that the relationship between tumour FDG clearance and blood glucose would be hyperbolic, i.e. have the form y = k/x, where k, the constant, is MRglu. So when blood glucose changes, FDG clearance changes in the opposite direction, as illustrated in Fig 7.1.

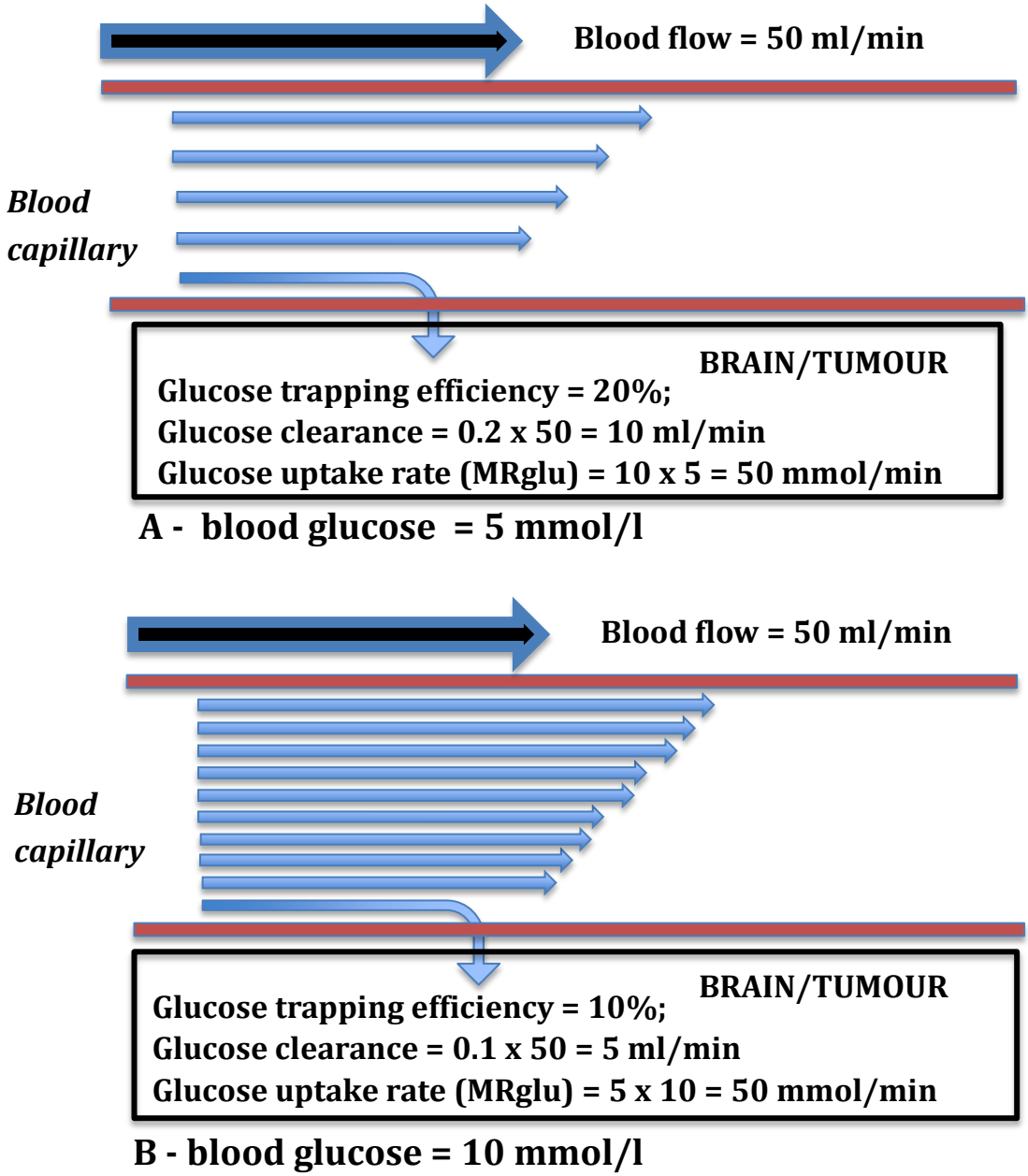

Fig 7.1. For a blood flow of 50 ml/min and trapping efficiency of 20%, glucose clearance would be 10 ml/min. If blood glucose concentration doubled from 5 mmol/l (panel A) to 10 mmol/l (panel B), then in order to maintain its MRglu of 50 mmol/min, brain or tumour would only need a trapping efficiency of 10%, which would give a glucose clearance of 5 ml/min.

By recommending normalisation to blood glucose, EANM guidelines therefore assume that tumour SUV is the same as tumour FDG clearance.

EANM guidelines also recommend that when blood glucose is >7 mmol/l, the study should be re-scheduled, although most departments would tolerate levels up to 10 mmol/l.

Liver SUV is thought to be relatively constant from patient to patient (Paquet et al 2004, Ramos et al (2001) so another method for quantifying tumour FDG uptake is to express tumour count rate as a ratio with liver count rate (Barrington et al 2104, Khandani et al 2005, Kumar et al 2004, van Kouwen et al 2005, Diederichs et al 1998). This method for example is used in the Deauville criteria for staging lymphoma (Barrington et al 2014).

As mentioned in earlier chapters, FDG exchanges rapidly between hepatocytes and blood before it gets phosphorylated to FDG-6-phosphate. The hepatic FDG concentration therefore closely follows the blood concentration. Because blood FDG concentration depends on blood glucose (Choi et al 1994), hepatic FDG activity will also depend on blood glucose (Kubota et al 2011, Groheux 2013), so the tumour-to-liver ratio will also depend on blood glucose.

The aim of the study in this chapter was to compare normalisation to blood glucose and scaling to liver as correction procedures for quantifying tumour FDG uptake. Tumour SUV is highly variable in patients with cancer, and depends on the type and

stage of tumour, and the effects of chemotherapy, so I used the brain as a substitute for tumours to examine the effects of blood glucose because, like tumours, the brain metabolically traps FDG.

7.2. METHODS

7.2.1. Patients

This was a retrospective study based on 304 patients undergoing routine FDG PET/CT, as described in earlier chapters. All patients attending our PET CT Unit are asked to give informed consent for use of any of their clinical data for publication. All patients in this study did so.

PET/CT acquisition and measurement of blood glucose was as described in earlier chapters.

7.2.2. Image analysis

Regions of interest (ROI) were drawn over the right lobe of the liver (avoiding any focal lesions and major blood vessels), frontal cortex, basal ganglia and cerebellum. The whole body sweep did not include frontal cortex and basal ganglia in 107 patients. SUV was recorded for all 4 regions. An ROI identical to the liver ROI drawn on the PET image was drawn on the CT scan for measurement of CT density. SUV in brain regions was multiplied by blood glucose and divided by 5 to give normalised SUV (nSUV).

7.2.3. Statistical analysis

Relations between variables were quantified using Pearson's linear regression analysis of continuous data. In addition, patients were categorised into 6 sub-groups based on blood glucose, as described in chapter 2. The patients were also subdivided into those with hepatic steatosis (CT density ≤ 40 HU; n = 71) and those without (> 40 HU; n = 233) (Boyce et al 2010, Zeb et al 2012).

7.3. RESULTS

7.3.1. Relationships of brain and hepatic SUV values with blood glucose

SUV of brain regions decreased as blood glucose increased. The opposite was seen with hepatic SUV, which increased with increasing blood glucose (Fig 7.1).

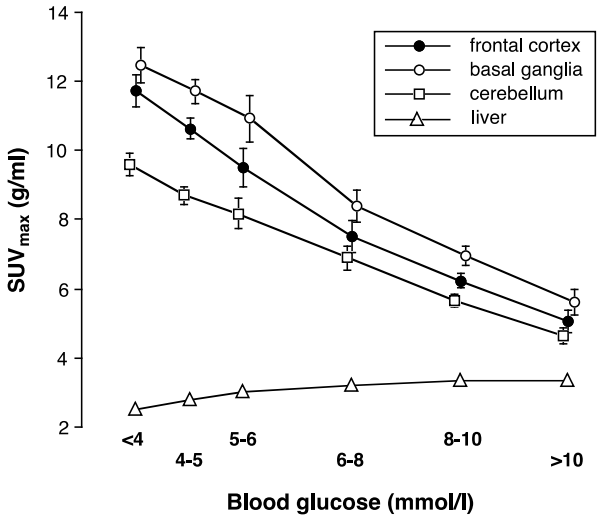

Figure 7.1. Relationships of brain SUV_{max} and liver SUV_{max} with blood glucose. Vertical bars = SEM. Note that SEM values for the liver are too small to be visible.

The relationship between cerebellar SUV_{max}, as a representative brain region, and blood glucose was better fitted with an exponential function (r = 0.75) than a

hyperbolic function (r = 0.60) (Fig 7.2). The exponential constant was -0.0993 mmol/l^{-1}, which means the SUV decreased by about 10% for every mmol/l increase in blood glucose. Corresponding exponential constants for frontal cortex and basal ganglia SUV_{max} were similar: -0.119 mmol/l^{-1} (r = 0.76) and -0.114 mmol/l^{-1} (r = 0.75). Exponential constants for brain SUV_{ave} were also similar: -0.113 (r = 0.77), -0.110 (r = 0.76) and -0.097 (r = 0.74) mmol/l^{-1} for frontal cortex, basal ganglia and cerebellum, respectively.

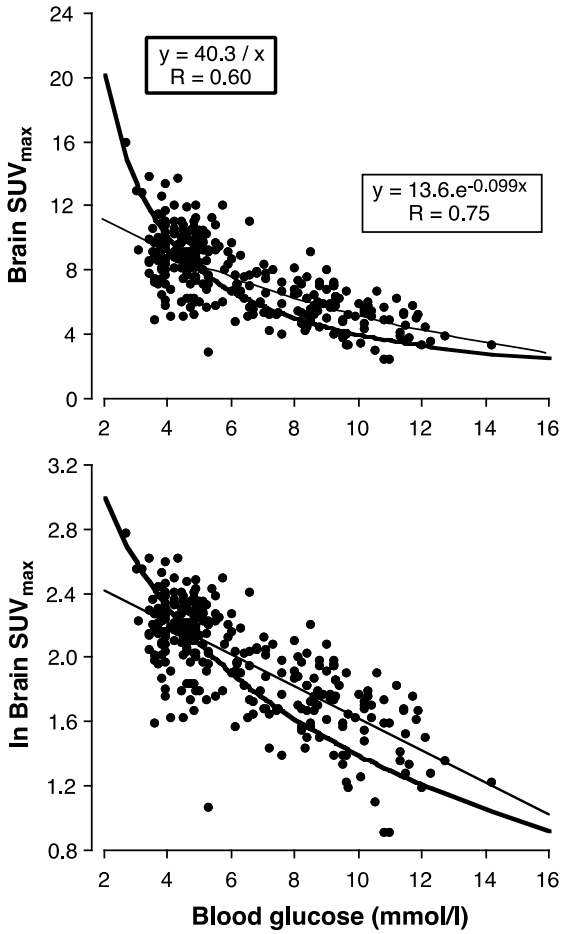

Figure 7.2. Relationship between cerebellar SUV_{max} and blood glucose. Equations are shown for least squares fits to hyperbolic (y = k/x; bold line) and exponential (fine line) functions. Upper panel: linear y-axis; lower panel: logarithmic y-axis.

7.3.2. Relation between cerebellum-to-liver SUV ratio and blood glucose

The cerebellum-to-liver SUV_{max} ratio declined as blood glucose increased (Fig 7.3). The relationship appeared hyperbolic (r = 0.83).

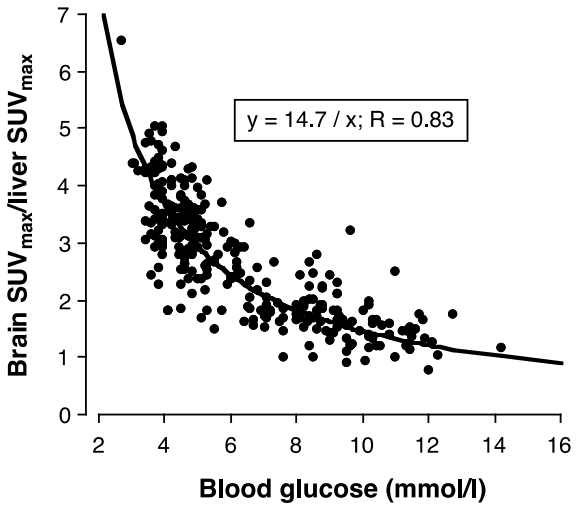

Figure 7.3. Relationship between cerebellum-to-liver SUV_{max} ratio (y) and blood glucose (x): y = 14.7/x.

7.3.3. Correction of brain SUV for blood glucose

Correction of tumour SUV for blood glucose by normalisation to 5 mmol/l (nSUV) aims to abolish the dependence of tumour SUV on blood glucose, and the same should apply to the brain. However, normalisation gave $nSUV_{max}$ values for the cerebellum that still correlated with blood glucose (Fig 7.4). There was a positive linear correlation up to blood glucose of 7 mmol/l ($r = 0.44$; $p < 0.0001$), but no further increase above 7 mmol/l. The overall relation was therefore better fitted with a second order polynomial ($r = 0.55$; $p < 0.0001$).

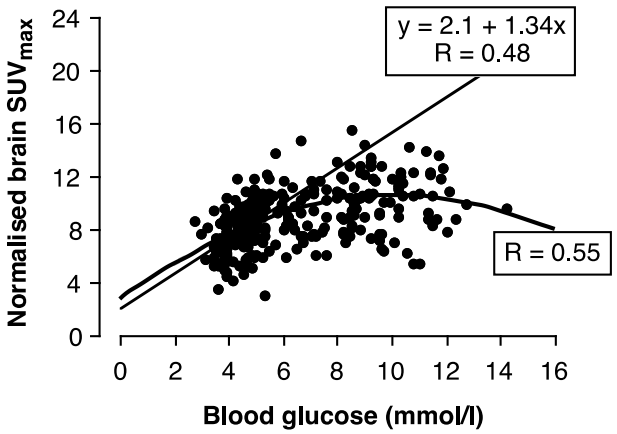

Figure 7.4. Relationships with blood glucose of cerebellar SUV_{max} normalised to blood glucose of 5 mmol/l. Straight line is linear fit to points up to blood glucose of 7 mmol/l. Bold curved line is second order polynomial fit to all data.

Division of cerebellar $nSUV_{max}$ by liver SUV_{max} almost abolished the relation of brain SUV with blood glucose ($r = 0.17$; $p < 0.01$; Fig 7.5).

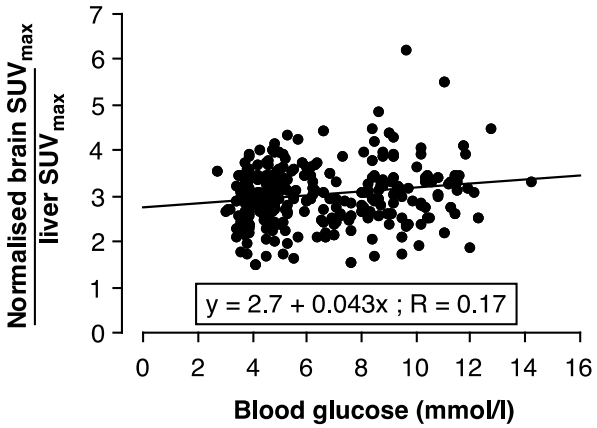

Figure 7.5. Relationship between blood glucose and cerebellar SUV normalised to blood glucose (nSUV) and then divided by liver SUV. Straight line is the linear fit to data points.

7.4. DISCUSSION

7.4.1. Brain SUV as a function of blood glucose

Hasselbalch et al (2001) and Namba et al (1994) found no change in cerebral MRglu in response to acute hyperglycaemia, so elevated blood glucose results in decreased FDG clearance into the brain (see equation 7.2). I found an inverse, non-linear relationship between brain SUV and blood glucose that was better fitted by an exponential function than a hyperbolic function. The fact that this relationship is more exponential than hyperbolic suggests that SUV is not a suitable surrogate for brain FDG clearance. The exponential constants were similar between the cerebellum, basal ganglia and frontal cortex. An inverse relationship between brain SUV and blood glucose has been shown previously by others (Claeys et al 2010, Ishizu et al 1994). Buchert et al (2009) for example showed that acute reversal of hyperglycaemia increased FDG uptake in the brain by up to 80%.

7.4.2. Validity of liver SUV for scaling tumour SUV

Liver SUV, in contrast to brain SUV, showed a positive relationship with blood glucose (Fig 7.1). The brain/liver SUV ratio therefore showed a strong inverse relationship with blood glucose (Fig 7.3). Assuming the brain can be regarded as a surrogate for tumours, this relationship shows that the liver cannot be used as a reference tissue for tumour FDG uptake. The relationship between brain/liver SUV ratio was close to hyperbolic, suggesting that this ratio is a better surrogate for FDG clearance than SUV.

7.4.3. Use of brain SUV as a surrogate for tumour FDG uptake

An important assumption underlying the use of brain as a surrogate for tumour FDG uptake is that MRglu in brain and tumours is independent of blood glucose. Hasselbach et al (2001) measured MRglu in the brain of normal subjects. They showed that during acute hyperglycaemia, when compared with normoglycaemia, global and regional MRglu in cortical and subcortical gray matter did not change. Namba et al (1994) directly measured tissue de-oxyglucose concentration in the rat brain at several different blood glucose concentrations and came to a similar conclusion. Most studies (Ishizu et al 1994, Lidholm et al 1993, Crippa et al 1997, Zhuang et al 2001) though not all (Hallett et al 2001, Busing et al 2013), have shown that tumour SUV also decreases at high blood glucose levels, as recognised by both the EANM and Society of Nuclear Medicine (SNM) guidelines (Boellaard et al 2010, Delbeke et al 2006). Thus Lindholm et al (1993) showed no change in tumour MRglu in response to oral glucose loading in 5 patients with head and neck cancer. Moreover, Crippa et al (1997) recorded a decrease in mean SUV of 20 hepatic colorectal metastatic deposits from 9.4 to 4.3 in a study in which patients were imaged on two separate occasions, fasting and following a glucose load that increased blood glucose from 5 to 9 mmol/l. Ishizu et al (1994) recorded a decrease in brain glioma SUV from 4.41 to 1.54 following an increase in blood glucose from 5.9 to 13.5 mmol/l.

7.4.4. Similarity of exponential relationships of brain and tumour SUV with blood glucose

Assuming an inverse exponential relation between tumour SUV and blood glucose, as for the brain, it can be calculated from the data of Lindholm et al (1993) that the

exponential constant for tumours is -0.1 to -0.15 mmol/l^{-1}. Based on the data of Crippa et al (1997), the constant would be about -0.2 mmol/l^{-1}, although their SUV values had very high standard deviations. Based on data of Ishizu et al (1994), the constant would be -0.093 mmol/l. These estimated exponential constants are broadly similar to those recorded in this study for the brain (-0.099 to -0.119 mmol/l^{-1}). Further work is needed to confirm that there is a universal exponential constant for tumours and whether its value is similar to that of the brain, i.e. ~0.1 mmol/l^{-1}.

7.4.5. Correction of tumour SUV for blood glucose

EANM guidelines recommend normalising tumour SUV to 5 mmol/l (Boellaard et al 2010). To be successful, this procedure is required to abolish the relationship between tumour SUV and blood glucose. Its validity in this respect is supported by some studies (Lee et al 2011, Nozawa et al 2013) but not by others (Hallett et al 2001).

Because of wide variations in tumour SUV, it is difficult to determine the relation of blood glucose with tumour SUV in large heterogeneous patient populations with different kinds of tumours at different stages of treatment. Nevertheless, Zhuang et al (2001) attempted to do this and recorded a weak inverse correlation between tumour SUV and blood glucose, but did not describe the nature of the relationship. Hallet et al (2001) found no significant correlation in 248 patients with lung cancer between tumour SUV and blood glucose. Differing levels of metabolic activity across tumours would not rule out a single exponential constant that could be universally applied to tumours, provided that tumour MRglu, like brain MRglu, is independent of blood glucose.

In the current study, normalisation of SUV (i.e. multiplying it by blood glucose) failed to abolish its dependence on blood glucose but instead generated a significant non-linear correlation (Fig 7.4). However, when brain $nSUV_{max}$ was divided by liver SUV_{max}, it showed almost no relationship with blood glucose (Fig 7.5). The success of this can be understood by replacing glucose clearance in equation 1 with brain-to-liver SUV ratio, as follows

$$MRglu = \frac{\text{brain SUV}}{\text{liver SUV}} \times \text{blood glucose} \qquad (7.4)$$

which indicates that when brain SUV is divided by liver SUV it becomes a better surrogate of FDG clearance.

Another attraction of dividing nSUV by liver SUV is that it avoids the issue of the best whole body metric for calculating SUV (Sugawara et al 1999), which cancels out.

7.4.6. Study limitations

Limitations of the study include its retrospective design and heterogeneous patient population. Whilst focal liver pathology was avoided when drawing the liver ROI, it is possible that covert pathology, such as diffuse colorectal micro-metastases, may have increased liver SUV. Moreover, the frontal cortex and basal ganglia were included in the whole body sweep in only two-thirds of the patients, although patient numbers were still high.

7.4.7. Conclusion

In conclusion, expressing tumour FDG uptake in relation to liver SUV is not valid. Indeed, the ratio of tumour-to-liver SUV is even more dependent on blood glucose than SUV. Normalisation of brain SUV to blood glucose fails to abolish its relation with blood glucose and is therefore also invalid. Combining the two correction procedures, however, gives corrected values that show almost no relation with blood glucose.

Chapter 8: Measurement of hepatic FDG clearance and glucose utilisation rate by dynamic imaging

8.1. INTRODUCTION

Previous chapters have described the problems of SUV for the quantification of liver FDG accumulation. A better approach to the question of whether or not hepatic steatosis is associated with increased FDG uptake is to measure hepatic FDG clearance. As mentioned in the previous chapter, multiplication of FDG clearance with blood glucose gives the glucose utilisation rate (MRglu). In this chapter, I therefore aimed to measure hepatic FDG clearance and hepatic MRglu using dynamic PET and Patlak-Rutland graphical analysis in a series of patients randomly and prospectively selected from routine clinical referrals to CISC for FDG PET/CT. Hepatic steatosis and obesity are strongly associated (Farrell & Larter 2006), so in addition to studying the relations of FDG clearance and MRglu with hepatic steatosis, I also studied the relations of FDG clearance and MRglu with body mass BMI.

8.2. METHODS

8.2.1. Patients

Sixty patients (47 men, age range 28-84, and 13 women, age range 40-67) having routine, clinically indicated PET/CT for the management of cancer were prospectively recruited for this study and gave informed consent for the additional dynamic imaging required. There were 20 patients with known lymphoma, of whom 12 had metabolically active lymphoma and 8 had inactive lymphoma. Twenty-six patients had metabolically active non-haematological malignancy and 14 had normal PET/CT. Twelve patients had received chemotherapy within 6 months of their scan, 19 had

received chemotherapy more than 6 months previously (range 8 months – 10 y) and 29 patients had received no previous chemotherapy (chemotherapy-naïve). Five patients were known to have type-2 diabetes mellitus. There were none with type-1 diabetes mellitus.

The pathologies of alcoholic and non-alcoholic liver disease are different (Ma et al 2009). Steatohepatitis resulting from toxins, including alcohol, is associated with a predominantly neutrophilic infiltrate whereas non-alcoholic steatohepatitis is associated with a predominantly lymphocytic infiltrate (Ma et al 2009) so I did not recruit patients reporting or suspected of high alcohol intake.

8.2.2. Imaging

All patients had routine whole-body PET/CT as described in chapter 2. In addition to their routine imaging, they consented to additional dynamic imaging over the liver at one frame per min for 30 min starting after FDG injection in a single bed position with detectors over the torso (Fig 8.1).

Fig 8.1. Dynamic series of images of one minute each following intravenous injection of FDG. CT was switched off so the images are not corrected for attenuation. Regions of interest over liver and abdominal aorta used for Patlak-Rutland analysis are shown in one of the slices.

CT was switched off so there was no additional radiation dose over and above that from the routine clinical study. Each patient gave informed consent to undergo the additional dynamic study, as this is not part of our routine scanning protocol. Ethical approval for the additional procedure was given by a National Research Ethics Committee.

8.2.3. Image analysis

Images were analysed using *HERMES* software. An ROI of 3 cm was placed over the right lobe of the liver in about 30 axial slices. The counts in each slice were summed. The same was done for the abdominal aorta with an ROI of 1.6 cm diameter.

Hepatic FDG clearance was measured using Patlak-Rutland analysis which is a graphical technique for calculating tissue tracer clearance from dynamic data. Rutland originally described it for single photon imaging (I-131 hippuran renography; Rutland 1979) and then Patlak et al described it in more detail for PET (Patlak et al 1983).

Patlak-Rutland analysis is only valid for kinetic models where transport of tracer is unidirectional along a single transport pathway from one compartment to another.

Although the model shown in Chapter 1 (Fig 1.6) has 3 compartments, mixing of FDG between blood and hepatocytes is rapid because K_1 (hepatic blood flow) and k_2 are high, so the first compartment is 'free' un-phosphorylated FDG in the liver (Choi et al 1994, Iozzo et al 2007, Munk et al 2001) (Fig 8.2).

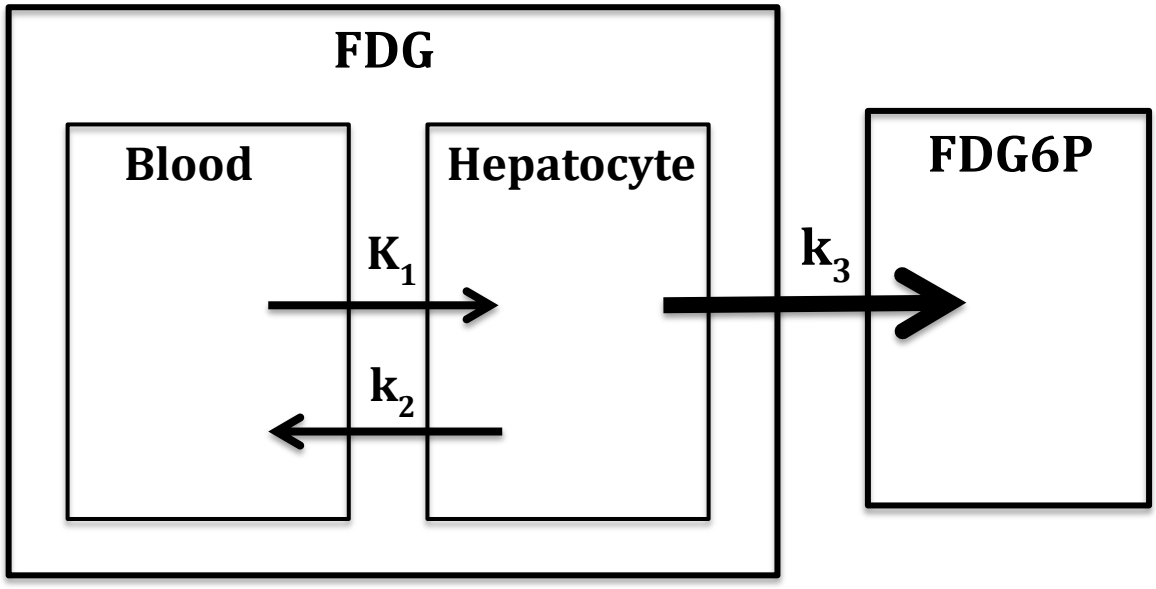

Fig 8.2. Model of intrahepatic FDG kinetics in which the 'free' FDG is shown as one compartment and phosphorylated FDG (FDG6P) as another. Once mixing of FDG is completed in first compartment, the clearance measured by Patlak-Rutland analysis is the result of transport along k_3. De-phosphorylation (k_4) is considered to be negligible and can be ignored (see Table 1 and Results).

Although k_3 is much lower than K_1 and k_2, it is still much higher than k_4 (glucose-6-phosphatase), which can be ignored so clearance of FDG is by phosphorylation to FDG-6-phosphate (FDG6P) along k_3 (hexokinase).

Between the time of injection and any time, t, after injection, the amount of FDG trapped by phosphorylation in hepatocytes and converted to FDG6P is equal to hepatic FDG clearance multiplied by the area under the blood FDG concentration-time graph up to time t.

hepatic FDG6P = FDG clearance x area under blood FDG concentration curve (8.1)

In PET, however, tissue tracer uptake is measured as the tissue concentration (MBq/ml) so clearance is expressed as clearance per unit tissue volume (ml/min/ml) and is called Ki (input constant).

So

hepatic FDG6P concentration = Ki x area under blood FDG concentration curve (8.2)

The hepatic FDG6P concentration is the concentration of FDG6P throughout the whole liver.

A ROI over the liver records hepatic FDG6P concentration *plus* the concentration of FDG in the liver that has not been phosphorylated. As mentioned above, this 'free' FDG distributes rapidly in a space that includes the hepatic capillary blood, hepatic interstitial space and hepatocytes (Fig 8.2).

So, adding free FDG concentration throughout the whole liver to both sides of equation 8.2,

Hepatic (FDG6P + free FDG) concentration = (Ki x area) + hepatic free FDG concentration (8.3)

In Patlak-Rutland theory, both sides of equation 8.3 are then divided by the blood FDG concentration to give

$$\frac{\text{hepatic (FDG6P + free FDG) conc.}}{\text{blood FDG conc.}} = \frac{\text{Ki x area}}{\text{blood FDG conc.}} + \frac{\text{hepatic free FDG conc.}}{\text{blood FDG conc.}} \quad (8.4)$$

Because FDG mixes rapidly between liver and blood, the concentration of free FDG in the liver is proportional to the blood FDG concentration, so hepatic FDG concentration/blood FDG concentration is a constant called the volume of distribution (V(0)).

The area under the blood FDG concentration-time curve has units of (min x MBq/ml), so dividing it by the blood FDG concentration (MBq/ml) gives time that is called 'normalized' time. For a graph that is declining (as in any blood clearance curve), normalized time exceeds 'clock' time (see Fig 8.3 and example data below). So, re-writing equation 8.4,

$$\frac{\text{hepatic (FDG6P + FDG) concentration}}{\text{blood FDG concentration}} = (\text{Ki x normalized time}) + V(0) \quad (8.5)$$

Equation 8.5 is a linear equation in which Ki is the gradient and V(0) is the intercept (see Fig 8.3).

CT was switched off so I was unable to correct for photon attenuation. I was therefore unable to measure hepatic and blood FDG concentrations (MBq/ml) but instead only counts. Hepatic counts were recorded from a series of regions of interest (ROI) placed on multiple cranio-to-caudal liver 'slices'. Blood counts were recorded from 'blood pool' ROIs over the right and left ventricular cavities and multiple slices of abdominal aorta (see Fig 8.1). The area under the blood concentration-time curve is obtained as the running sum of blood pool counts from 0-30 min. For each 1 min frame, the running sum up to that frame was divided by blood pool counts in the frame to give normalized time. For each frame, hepatic counts were divided by blood pool counts and plotted against normalized time (Fig 8.3C).

Example data for an individual patient is given as follows.

Time (min)	Aorta (counts/frame)	Liver (counts/frame)	Liver counts/aorta counts	Running sum of aorta counts	Normalised time (min)
1	682,728.00	821,252.00	1.202897787	682,728.00	1
2	316,773.00	2,602,766.00	8.216502038	999,501.00	3.155259444
3	291,604.00	2,172,375.00	7.449743488	1,291,105.00	4.427597015
4	244,415.00	1,965,492.00	8.04161774	1,535,520.00	6.282429474
5	218,408.00	1,825,494.00	8.35818285	1,753,928.00	8.030511703
6	221,580.00	1,720,262.00	7.76361585	1,975,508.00	8.915551945
7	198,036.00	1,655,637.00	8.360282979	2,173,544.00	10.9754994
8	193,144.00	1,536,327.00	7.954308702	2,366,688.00	12.25348962
9	174,598.00	1,451,878.00	8.315547715	2,541,286.00	14.55506936
10	165,761.00	1,361,305.00	8.212456489	2,707,047.00	16.33102479
11	159,865.00	1,420,706.00	8.886910831	2,866,912.00	17.93333125
12	152,363.00	1,324,789.00	8.694952187	3,019,275.00	19.8163268
13	154,141.00	1,347,395.00	8.74131477	3,173,416.00	20.58774758
14	141,848.00	1,182,603.00	8.337114376	3,315,264.00	23.37194744
15	136,858.00	1,168,100.00	8.535123997	3,452,122.00	25.22411551
16	133,421.00	1,246,101.00	9.339616702	3,585,543.00	26.87390291
17	130,332.00	1,155,633.00	8.86684007	3,715,875.00	28.51084154

18	122,297.00	1,118,957.00	9.149504894	3,838,172.00	31.38402414
19	115,679.00	1,107,010.00	9.569671245	3,953,851.00	34.17950536
20	114,646.00	1,067,247.00	9.309064424	4,068,497.00	35.48747449
21	110,339.00	1,066,759.00	9.668014029	4,178,836.00	37.8727014
22	114,474.00	1,071,627.00	9.361313486	4,293,310.00	37.50467355
23	106,700.00	1,070,386.00	10.03173383	4,400,010.00	41.23720712
24	106,695.00	983,997.00	9.222522143	4,506,705.00	42.2391396
25	97,319.00	988,526.00	10.15758485	4,604,024.00	47.30858311
26	95,495.00	944,572.00	9.891324153	4,699,519.00	49.21219959
27	97,968.00	941,201.00	9.607228891	4,797,487.00	48.96993916
28	91,938.00	943,019.00	10.25711893	4,889,425.00	53.1817638
29	89,719.00	937,874.00	10.45346025	4,979,144.00	55.49709649
30	87,151.00	892,879.00	10.24519512	5,066,295.00	58.13237943

Inspection of the Patlak-Rutland plots revealed that they were essentially linear from 2-30 min (Fig 8.3C), consistent firstly with rapid mixing and secondly with a low value of k_4. The first 2 frame values, during which mixing of FDG between blood and the hepatic tissue distribution volume appears to be completed, were therefore not included in the Patlak-Rutland plot.

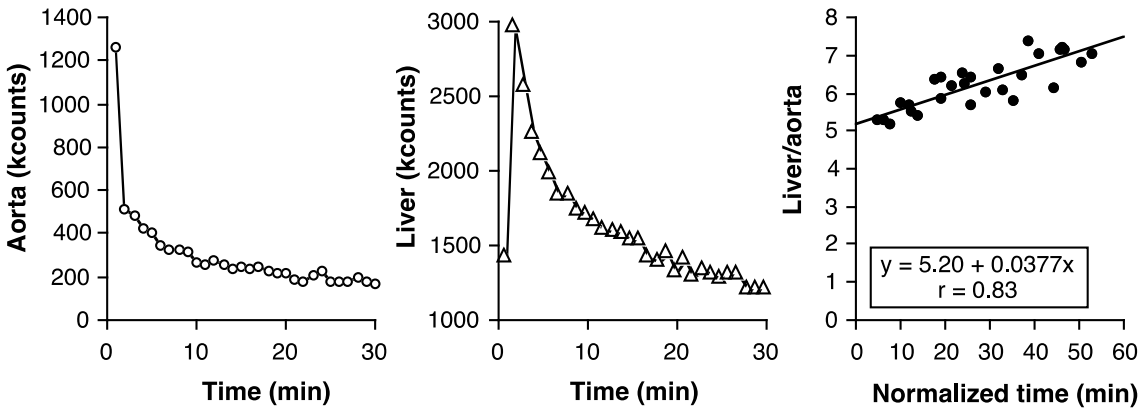

Fig 8.3. Time-count curves for the aortic blood pool (left panel), liver (middle panel) and Patlak-Rutland plot (right panel) based on these curves.

As already mentioned, I could measure counts only and not tracer concentrations. I could not therefore measure Ki and V(0) in absolute units so I divided the gradient of the Patlak-Rutland plot by the intercept to give Ki/V(0). All the factors that relate gradient to Ki are the same as those that relate intercept to V(0), so when the gradient divided by the intercept, they cancel out. Expressing hepatic FDG clearance as Ki/V(0) allows the use of ROI dimensions of any size and images un-corrected for photon attenuation (as is the case when CT is switched off). It also corrects for the diluting effect of hepatic fat.

Ki/V(0) was multiplied by 100 to give hepatic FDG clearance in units of ml/min/100 ml, and then multiplied by the blood glucose concentration (μmol/ml) to give hepatic MRglu in units of μmol/min/100 ml, assuming a lumped constant of unity (Iozzo et al 2003).

Body mass index (BMI) was measured as weight/height^2 (kg/m^2). Patients were classified as obese if BMI was ≥ 30 kg/m^2 and as having hepatic steatosis if CT density was ≤ 40 HU (Boyce et al 2010).

8.3. RESULTS

8.3.1. Effect of chemotherapy

Mean CT density in the 29 patients who had never received chemotherapy (chemotherapy-naïve patients) was 46 ± 9 HU compared with 43 ± 9 HU in the 12 patients with a history of recent chemotherapy ($p > 0.05$). Patients with long-since previous chemotherapy had a mean CT density of 47 ± 11 HU ($p > 0.05$). Corresponding mean values of BMI were 28 ± 5, 28 ± 8 and 26 ± 4 kg/m^2 ($p > 0.05$).

There was no significant difference in MRglu between patients with recent chemotherapy (2.57 ± 1.35 □mol/min/min) and chemotherapy-naïve patients (2.26 ± 1.41 □mol/min/min). So chemotherapy had no effect on my results.

8.3.2. Prevalence of hepatic steatosis in obese and non-obese patients

Of the 60 patients, 19 (32%) had hepatic steatosis and 18 (30%) were obese. Thirty-four had neither steatosis nor obesity, while 11 had both. Of the 19 with steatosis, 8 (42%) were not obese (and 5 [26%] were not even overweight [< 25 kg/m^2]), while of the 18 who were obese, 11 (61%) had hepatic steatosis and 7 did not.

8.3.3. Blood glucose levels

Blood glucose levels were slightly but significantly higher in patients with hepatic steatosis (6.4 ± 1.5 mmol/l) compared with those without (5.7 ± 0.6 mmol/l; $p < 0.02$) and in obese subjects (6.3 ± 1.5 mmol/l) compared with non-obese (5.7 ± 0.7 mmol/l; $p < 0.05$).

8.3.4. Hepatic FDG clearance and MRglu

The single bed position used for the dynamic data acquisition resulted in inadequate inclusion of the right and/or left ventricular blood pool regions in several patients. The aortic blood pool was therefore used exclusively for measuring blood pool counts for Patlak-Rutland analysis in all patients.

The liver and aortic blood pool time-activity curves followed similar time courses, reflecting the closeness with which the hepatic FDG concentration resembles blood concentration (Fig 8.3). Relative to the intercept, Patlak-Rutland analysis of dynamic

hepatic and aortic blood pool activity therefore generated a shallow positive gradient that appeared to be linear from 2-30 min (Fig 8.3).

There were strong negative correlations between CT density and hepatic FDG clearance ($r = -0.52$; $p < 0.0001$) and between CT density and MRglu ($r = -0.56$; $p < 0.0001$; Figs 8.4 and 8.5). In contrast, whilst BMI correlated significantly with MRglu ($r = 0.32$; $p = 0.013$), it showed an insignificant correlation with hepatic FDG clearance ($r = 0.21$; $p = 0.11$; Figs 8.4 and 8.5).

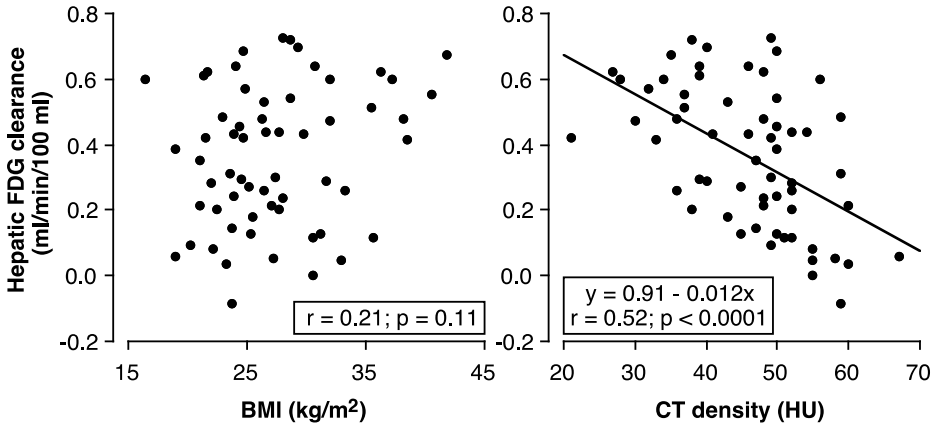

Fig 8.4. Relationships of hepatic FDG clearance with BMI (left panel) and CT density (right panel).

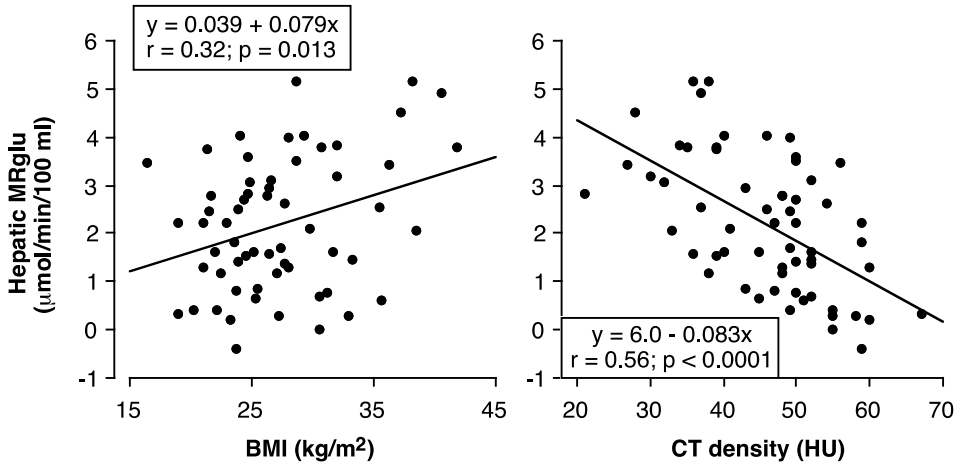

Fig 8.5. Relationships of MRglu with BMI (left panel) and CT density (right panel).

In line with the above correlations, MRglu was higher in patients with hepatic steatosis (3.26 ± SD 1.26; n = 19) than in those without (1.70 ± 1.18; n = 41; $p < 0.001$) but the difference between obese (2.48 ± 1.65; n = 18) and non-obese patients (2.07 ± 1.28; n = 42) was not significant (Fig 8.6). There was no significant difference in MRglu between 8 non-obese (2.89 ± 1.41) and 11 obese (3.52 ± 1.13) patients with hepatic steatosis (Fig 6). However, MRglu in these 11 obese patients with hepatic steatosis was higher than in 7 obese patients without hepatic steatosis (0.84 ± 0.71; $p < 0.001$) (Fig 8.7). A similar pattern of results was observed with respect to hepatic FDG clearance instead of MRglu (Figs 8.6 and 8.7). Thus, clearances were 0.51 ± 0.16 ml/min/100 ml in steatosis versus 0.30 ± 0.21 ml/min/100 ml in non-steatosis patients ($p < 0.001$) and 0.39 ± 0.23 ml/min/100 ml in obese patients versus 0.36 ± 0.21 ml/min/100 ml in non-obese patients ($p > 0.05$).

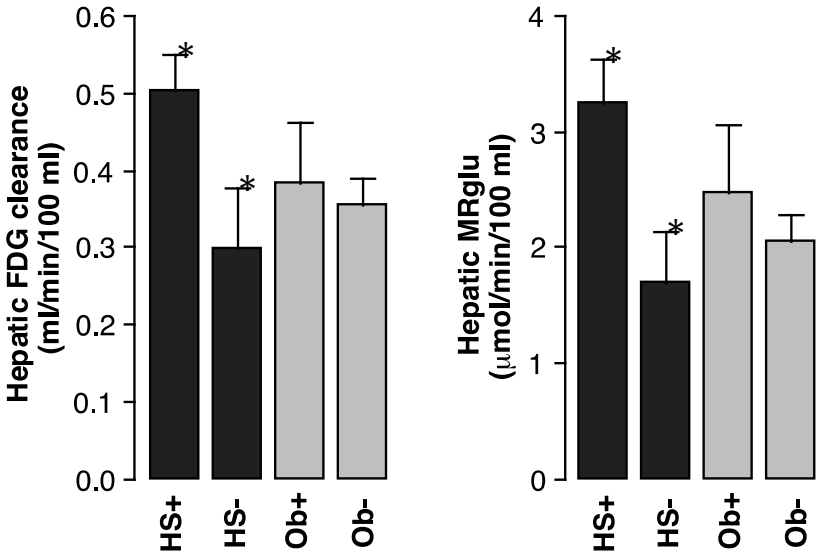

Fig 8.6. Hepatic FDG clearance and MRglu are increased in patients with hepatic steatosis (HS+) compared with those without (HS-). In contrast, there are no significant differences between obese (Ob+) and non-obese (Ob-) patients (*$p < 0.001$; bars = standard error of the mean).

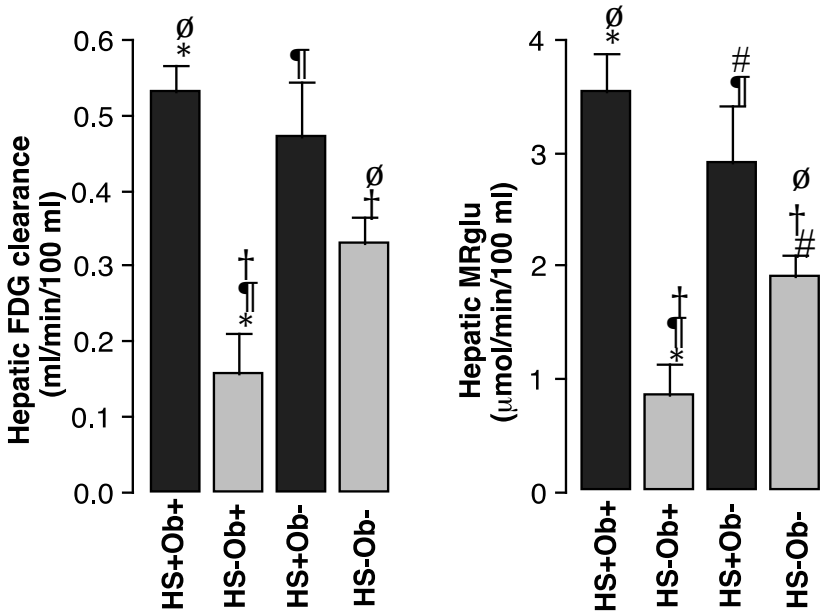

Fig 8.7. Hepatic FDG clearance and MRglu are increased in patients with hepatic steatosis (HS+), whether or not they are obese (Ob+). In contrast, obese patients only have increased FDG clearance and MRglu when they also have hepatic steatosis (*p <0.001; øp < 0.01; ¶p < 0.01; #p < 0.05; †p < 0.05; symbols identify paired columns for unpaired *t*-test; bars = standard error of mean).

Of the 5 patients with type-2 diabetes mellitus, 4, all with hepatic steatosis (CT density 36, 37, 37 and 38 HU), had high values of hepatic FDG clearance (mean 0.57 ± 0.11 ml/min/100 ml) and MRglu (4.45 ± 1.27 □mol/min/100 ml). In contrast, one patient without hepatic steatosis (CT density 50 HU) had low values (0.13 ml/min/100 ml and 0.78 □mol/min/100 ml, respectively).

8.4. DISCUSSION

Previous studies (Bural et al 2010, Abikzer et al 2011, Lin et al 2011, Abele et al 2010, Kamikura et al 2010) examining the relationship between hepatic steatosis and hepatic FDG uptake have been based on SUV as the measure of FDG uptake.

However, as I have already shown in previous chapters, the relationship between steatosis and hepatic SUV is complicated by several factors. These factors have been largely overlooked in these previous studies. The approach I used in the current study avoided all of these problems.

In this study I have clearly demonstrated increased hepatic glucose utilization rate in steatosis. Hepatocytes contain glucose-6-phosphatase, which dephosphorylates FDG-6-phosphate. This pathway, represented by k_4 in Fig 1.6, has been shown by several authors to have a very low rate constant based on modeling approaches to hepatic FDG kinetics (Iozzo et al 2003, Munk et al 2001). This means that, over the short term, FDG clearance and MRglu will be determined by k_3, which reflects the FDG phosphorylation rate by hexokinase. However, because of glucose-6-phosphatase, the hepatocyte will not metabolically trap FDG over the *long* term, especially if the subject is fasting. The Patlak-Rutland plot would therefore be expected to be convex upwards, ultimately becoming horizontal when FDG phosphorylation and de-phosphorylation rates become equal. However, two previous studies using Patlak-Rutland analysis to measure liver glucose utilization rate (Iozzo et al 2003, Munk et al 2001) also, like me, recorded linear plots with no hint of convexity, even up to 120 min (Munk et al 2001), implying a low value for k_4.

As given by Choi et al (1994), the equations relating Ki, V(0), K_1, k_2 and k_3 are as follows:

$$Ki = K_1.k_3 /(k_2 + k_3) \quad (8.6)$$

$$V(0) = K_1 /(k_2 + k_3) \quad (8.7)$$

Dividing equation 8.6 by equation 8.7 gives

$$Ki/V(0) = k_3. \qquad (8.8)$$

As can be seen from equation 8.8, Ki/V(0) is the same as k_3. It is re-assuring, therefore, that the values I obtained for Ki/V(0) are similar to values of k_3 reported in the literature (Table 1). Thus, my mean value of Ki/V(0) for all patients is about 0.4 ml/min/100 ml, which is similar to the values of k_3 of 0.5 and 0.43 ml/min/100 ml obtained respectively by Choi et al (1994) and Iozzo et al (2003). The two previous studies that used Patlak-Rutland analysis to study hepatic glucose utilisation (Iozzo et al 2003, Munk et al 2001) found it to be robust and obtained values for Ki/V(0) ranging between 0.21 and 0.45 ml/min/100 ml, similar to the values obtained in my study (Table 8.1).

Iozzo et al (2003) measured Ki/V(0) during hyperinsulinemic euglycemic clamp and during fasting (Table 1*)*. Physiological hyperinsulinemia, mediated through an acute glucose load, increases the liver-to-blood FDG concentration ratio in normal subjects by up-regulating k_3 (Keramida et al 2014). Hepatic steatosis is associated with insulin resistance (Farell et al 2006, Garg et al 2002) in which insulin levels are increased despite hyperglycaemia. According to the data of Iozzo et al (2003), k_3, but not k_4, appears to be unaffected by insulin resistance. Thus, Iozzo et al (2003) showed that compared with fasting values, k_3 increased more during euglycaemic hyperinsulin-aemic clamp in patients with insulin resistance than in normal subjects (Table 1).

Table 8.1.

Values of K_1, k_2, k_3, k_4, Ki/V(0) and MRglu in normal subjects and patients with altered insulin sensitivity (IS) (from Choi et al (*12*), Iozzo et al (*18*), Munk et al (*19*), Borra et al (*2*) and my study).

		K_1	k_2	k_3	k_4	Ki/$^{\Delta}$V	MRglu
Fasting	Choi	86	98	0.50	1.6	0.40	2.1
Iozzo	*normal IS*	62	76	0.43	0.0047	0.23	1.3
	low IS	64	79	0.29	~0	0.21	1.1
Munk (pigs)		80	98	1.2	1.7	0.37	
Hyperglycemia	Choi	106	118	º1.3	1.4	1.1	9.6
¶Hyperinsulinemia	Iozzo						
	normal IS	60	74	0.57	0.0002	0.39	2.0
	high IS	62	77	0.50	~0º	0.42	º2.1
	low IS	68	88	º0.59	0.0034	º0.45	º2.4
Type-2 diabetes	Borra						$^{\#}$2.5
Healthy subjects	Borra						3.6
Hepatic steatosis	(my study)					0.51	3.3
No hepatic steatosis	(my study)					*0.30	*1.7
Type-2 diabetics with steatosis	(my study)					0.57	4.5

Units: ml/min/100 ml, except MRglu (μmol/min/100 ml);
*$p < 0.001$ vs steatosis; º$p < 0.05$ vs fasting; $^{\#}p < 0.01$ vs healthy
¶Euglycemic hyperinsulinemic clamp
$^{\Delta}$V: total liver volume except in my studies where it is V(0)

So, in insulin resistance, k_3 is up-regulated as a result of hyperinsulinaemia and promotes increased hepatic glucose accumulation. Accordingly Iozzo et al (2003) found increased Ki/V(0) from Patlak-Rutland analysis in hyperinsulinaemia, including patients with insulin resistance. Conversely, glucose-6-phosphatase becomes insensitive to insulin in insulin resistance. Thus Iozzo et al (2003) found that during hyperinsulinaemia, k_4 was much higher in patients with insulin resistance compared to normal subjects.

In fasting subjects with insulin resistance, therefore, k_3 and k_4 are *both* up-regulated (Fig 8.8). Although we did not measure blood insulin levels in our patients, up-regulation of k_3 from hyperinsulinaemia is the likeliest explanation for the increased MRglu of hepatic steatosis.

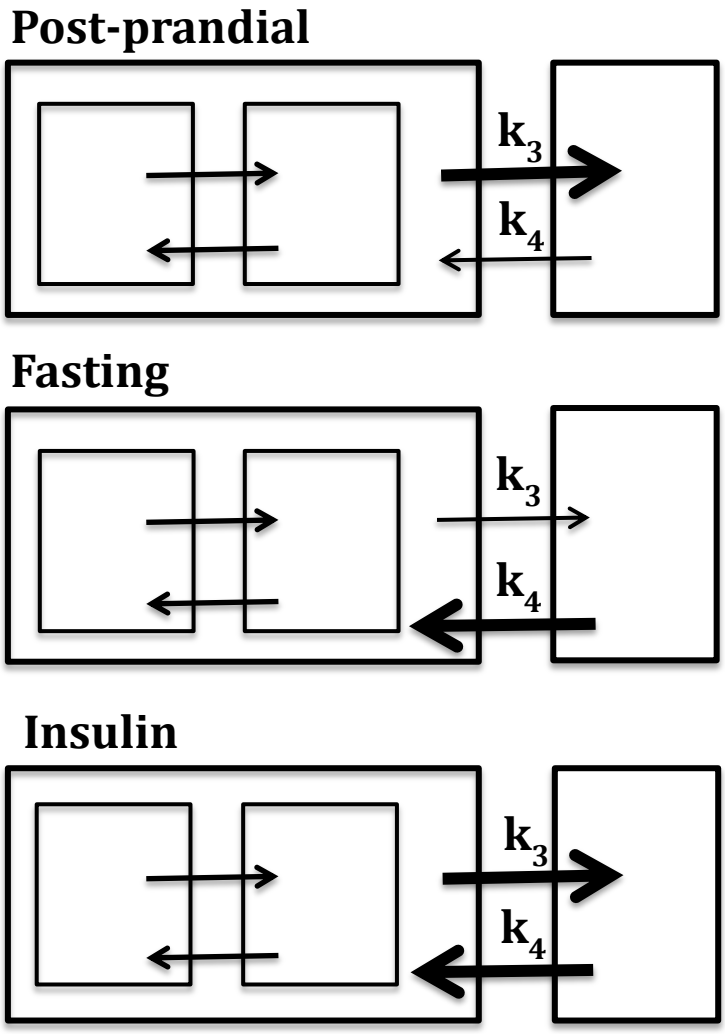

Fig 8.8. Models of intrahepatic FDG kinetics in the post-prandial state, fasting and insulin resistance. After a meal, insulin level is raised and by activating k_3 promotes glyconeogenesis. When fasting, insulin levels are low and the blood glucose level is maintained as a result of activation of k_4. In insulin resistance, insulin level is raised and activates k_3, which remains sensitive to insulin, but k_4 is insensitive to insulin in insulin resistance and remains inappropriately activated. (Based on Iozzo et al 2003.)

A possible alternative explanation is that hepatic steatosis is associated with increased MRglu as a result of FDG uptake in activated intrahepatic leukocytes; i.e. with steatohepatitis.

Whilst obesity is thought to be associated with insulin resistance, I found that hepatic FDG clearance and MRglu were not increased in obese individuals who did not also have hepatic steatosis. Conversely, non-obese patients with steatosis had increased FDG clearance and MRglu. These data clearly show that hepatic steatosis, and not obesity *per se,* is associated with increased glucose utilization and probably with insulin resistance. In other words, obesity appears to be linked to insulin resistance via hepatic steatosis.

Hepatic steatosis is very common and generally thought to be a complication of obesity. It is estimated that ~75% of obese Caucasians have steatosis (Farell et al 2006), and my study confirms this with a prevalence of 61%. However, although my patients are not healthy and their numbers are small, I also found that 42% of patients with hepatic steatosis were not obese. This is higher than previously reported, for example 16% (Bellentani et al 2000), and according to my data cannot be attributed to chemotherapy. This has implications for screening patients for hepatic steatosis because it is clear that screening cannot be limited to obese subjects. As the prevalence of obesity is expected to increase, screening for hepatic steatosis will soon become a major healthcare requirement.

Limitations of this study include the recruitment of patient volunteers with co-existing morbidity, the absence of control for alcohol intake and the absence of data on central

obesity as opposed to BMI. Moreover, although I suggest that insulin resistance is the explanation for the increased FDG clearance and MRglu in hepatic steatosis, I did not measure blood insulin levels, nor do I have any liver biopsy data. Fat distribution in the liver is known to be heterogeneous, so measurement of CT density in a single ROI may be misleading. Moreover, CT itself is not regarded as the gold standard imaging technique for quantifying hepatic steatosis and inferior to MRI and MR spectroscopy (Iozzo et al 2007, Bohte et al 2011).

In conclusion, hepatic FDG clearance and glucose utilisation rate are increased in hepatic steatosis. This is probably the result of insulin resistance, hyperinsulinemia and an increase in k_3, but possibly also superimposed increased glucose utilization rate in non-hepatocyte cells, especially inflammatory cells. This is of potential interest in relation to the use of FDG PET for imaging hepatic inflammation, which could open the way to imaging inflammatory liver disease at an early stage before the development of irreversible hepatic fibrosis.

Chapter 9: Limitations of standardised uptake value as a surrogate for splenic clearance of FDG

9.1. INTRODUCTION

There has been recent interest in the metabolic activity of the spleen, assessed using PET and FDG, especially in relation to raised inflammatory markers (Nam et al 2010, Nunez et al 2005), inflammatory disease (Wollenweber et al 2014, Kim E et al 2014, Kim K et al 2014, Emami et al 2015) and viral infections, including HIV (Valour et al 2012). Splenic metabolic activity is also increased in lymphoma even in the absence of focal splenic abnormalities on PET/CT (Salaun et al 2009, Rini et al 2003, Liu et al 2009).

In cardiology, the term 'cardiosplenic axis' has been used to describe increased splenic metabolic activity in patients with a recent acute cardiac event (Wollenweber et al 2014, Kim E et al 2014, Emami et al 2015). An important relationship between the spleen and atheroma was discovered by Dutta et al (2012) who showed in atheroma susceptible ApoE --/-- mice that the progression of atheroma was accelerated following myocardial infarction. This was related to the production of bone marrow progenitor cells that seeded the spleen to become monocytes. The acceleration of atheroma after infarction was prevented by sympathetic blockade or splenectomy. Further work in humans confirmed that inflammatory peri-infarction activity correlates with splenic metabolic activity (Wollenweber et al 2014) and appears to be a predictor of future cardiovascular events (Emami et al 2015). This has led to the slogan that "myocardial infarction begets myocardial infarction" (Joshi et al 2015).

Only one study measured splenic metabolic activity as splenic FDG clearance using dynamic PET imaging and Patlak-Rutland analysis (Wollenweber et al 2014), as described in the previous chapter, and all the others quantified splenic FDG accumulation from delayed whole body imaging using splenic SUV (Emami et al 2015) or the ratio of splenic-to-liver uptake (Salaun et 2009).

There are many ways of expressing SUV. It was shown in chapter 7 that brain SUV divided by liver SUV is a closer reflection of brain FDG clearance than SUV alone. Division of tissue SUV by liver SUV or a blood pool SUV therefore creates further variants of tissue SUV. As with other SUVs, blood pool SUV may be maximum or average, and, in the case of the liver, adjusted for hepatic fat, as described in chapter 6.

As shown below, splenic FDG clearance and MRglu measured from dynamic imaging and Patlak-Rutland graphical analysis are higher in patients with lymphoma compared with those without lymphoma. The purpose of the current study was to test which of these various forms of expressing SUV were also different between patients with lymphoma compared with those without lymphoma; in other words, which, if any could identify this difference.

9.2. METHODS

9.2.1. Patients

The patient population is the same as in chapter 8, namely 60 randomly selected patients (47 men, age range 28-84, and 13 women, age range 40-67) having routine, clinically indicated PET/CT for the management of cancer. Twenty patients had

lymphoma (Hodgkin's lymphoma [n = 2] and non-Hodgkins's lymphoma [n = 18], including 2 with follicular lymphoma and 6 with diffuse large B-cell lymphoma). Of the remaining 40 patients, 38 had a range of other malignancies or suspected malignancies. Two had suspected inflammatory disease but had normal PET/CT.

9.2.2. Imaging

All patients had routine whole-body PET/CT 60 min post-injection of ~400 MBq FDG, as described in chapter 2. Patients fasted for 6 h before FDG injection. Blood glucose was measured using a glucometer as described previously. In addition to routine imaging, patients consented to additional dynamic imaging at one frame per min for 30 min starting immediately following FDG injection in a single bed position with the detectors over the torso and CT switched off.

9.2.3. Image analysis

Images were analysed using *HERMES* software. Splenic FDG clearance was measured using Patlak-Rutland analysis. Splenic activity was measured from a series of regions of interest (ROI) placed on multiple cranio-to-caudal transaxial images. Blood pool activity was obtained by summation of counts in multiple transaxial 'slices' of abdominal aorta, as described in chapter 8.

The gradient of the Patlak-Rutland plot is proportional to hepatic FDG clearance and the intercept is proportional to the splenic distribution volume of FDG, analogous to Ki and V(0) described in studies of intrahepatic FDG kinetics and hepatic MRglu (Choi et al 1994, Iozzo et al 2003, Munk et al 2001, chapter 8). The first 2 frame

values, during which mixing of tracer between blood and splenic tissue distribution volume was assumed to take place, were not included in the Patlak-Rutland plot.

The gradient of the Patlak-Rutland plot was divided by the intercept to give Ki/V(0) and multiplied by 100 to give splenic FDG clearance in units of ml/min/100 ml. Splenic FDG clearance was then multiplied by the blood glucose concentration (μmol/ml) to give splenic MRglu in units of μmol/min/100 ml. As explained in the previous chapter, dividing the gradient by the intercept permits the use of ROI dimensions of any size and use of images un-corrected for photon attenuation because all the factors relating gradient to Ki are the same as those relating intercept to V(0).

SUVs were recorded from regions of interest over the liver (3 cm diameter), spleen (2.5 cm) and left ventricular (LV) cavity (1.5 cm) in the 60 min routine PET/CT scan. The computer calculates SUV using body weight. It was re-scaled for LBM estimated from height, weight and gender using the formulae of Boer (1984). SUV_{max} and SUV_{ave} were recorded for all 3 regions. For the liver, SUV_{ave} was adjusted for hepatic fat, as described in chapter 6. Note that the whole body metric for scaling SUV cancels out when splenic SUV is expressed as a ratio with LV SUV or liver SUV.

9.2.4. Statistical analysis

Correlations between variables were quantified using Pearson's correlation analysis. Significance of differences between the mean values (± standard deviation [SD]) of the two patient groups was tested using Student's unpaired *t*-test. A p value of < 0.05 was taken to indicate statistical significance.

9.3. RESULTS

Mean blood glucose levels were the same (5.9 mmol/l) in patients with and without lymphoma (Table 1). Examples of time-activity curves and corresponding Patlak-Rutland plots are shown for patients without (Fig 9.1A) and with (Fig 9.1B) lymphoma. The plots are clearly linear between 2 and 30 min, suggesting essentially complete mixing of FDG within its volume of distribution by 2 min.

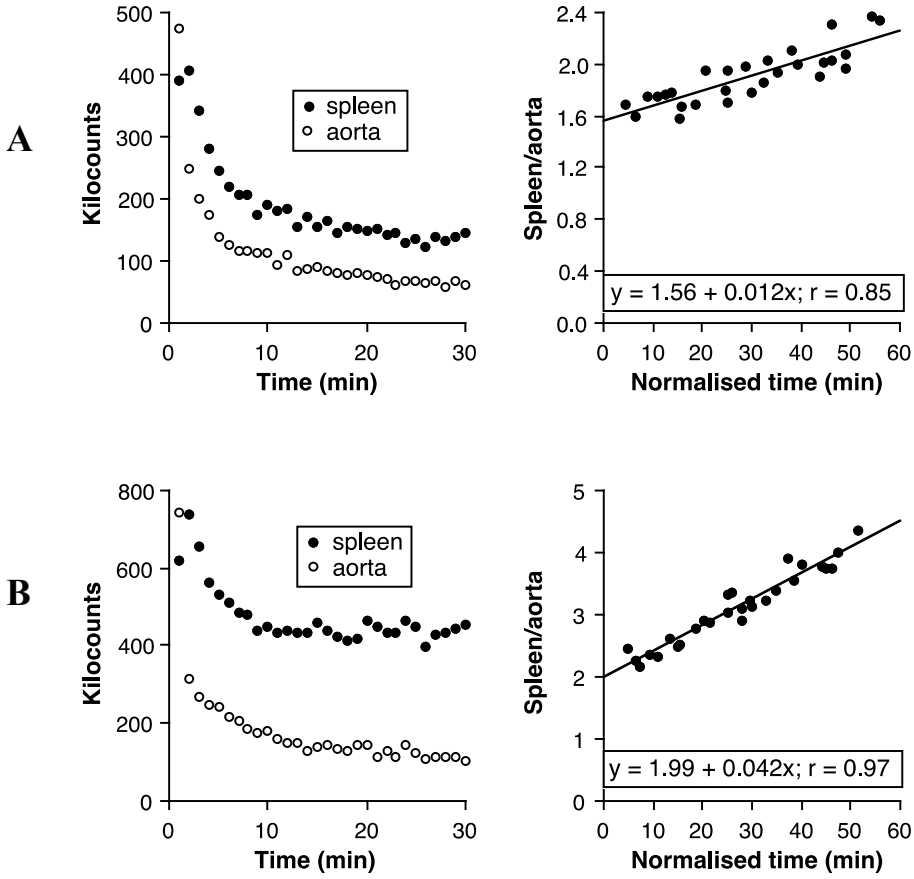

Fig 9.1. Examples of aortic (left panels) and splenic (right panels) time-activity curves and corresponding Patlak-Rutland plots. Note that the plots are linear between 2 and 30 min.
A. Patient without lymphoma with a splenic SUV_{ave} (weight) of 1.76. Splenic FDG clearance and MRglu were 0.74 ml/min/100 ml and 4.31 μmol/min/100 ml, respectively
B. Patient with lymphoma with a splenic SUV_{ave} of 2.65. Splenic FDG clearance and MRglu were 2.12 ml/min/100 ml and 12.29 μmol/min/100 ml, respectively.
Note that whilst there are approximate 3-fold differences in FDG clearance MRglu between these 2 patients, the difference in SUV_{ave} is only marginal.

Splenic FDG clearance and MRglu were both significantly higher in patients with lymphoma (0.75 ± 0.55 ml/min/100 ml and 4.60 ± 3.83 μmol/min/100 ml, respectively) than in those without (0.53 ± 0.29 ml/min/100 ml and 3.07 ± 2.01 μmol/min/100 ml, respectively). In contrast, splenic SUV was not significantly different between the two groups whether expressed as maximum or average, scaled using LBM or weight, or expressed as a ratio with left ventricular SUV or liver SUV, including liver SUV adjusted for fat (Table 9.1).

Relatively strong trends towards differences between patients with and without lymphoma were seen for SUV based on weight but not SUV based on LBM. However, this can be accounted for by the difference in body weight between the two groups, which also showed a strong trend for patients with lymphoma to be heavier (Table 9.1). No such trend was seen for LBM, underlining the tendency for SUV to be overestimated in heavy patients.

TABLE 9.1. Splenic FDG clearance, MRglu and SUV indices (SD) compared between patients with and without lymphoma. No SUV index was significantly different between patients with lymphoma and those without.

	no L (n = 40)	**L (n = 20)**	**%**	**p**
glucose (mmol/l)	5.9 (0.7)	5.9 (1.5)	0	1.000
body weight (kg)	80.6 (16.4)	88.2 (18.6)	9.4	0.111
lean body mass (kg)	58.7 (9.3)	61.9 (9.8)	5.1	0.220
FDG clearance (ml/min/100 ml)	0.52 (0.30)	0.75 (0.55)	43.3	0.039
MRglu (μmol/min/100 ml)	3.07 (2.01)	4.60 (3.83)	50.4	0.046
SUV_{ave} (weight)	1.92 (0.34)	2.10 (0.58)	10.4	0.102
SUV_{max} (weight)	2.33 (0.45)	2.59 (0.74)	11.4	0.091
SUV_{ave} (LBM)	1.39 (0.22)	1.47 (0.36)	6.3	0.251
SUV_{max} (LBM)	1.70 (0.29)	1.82 (0.46)	7.0	0.224
SUV_{ave}/LV SUV_{ave}	1.15 (0.25)	1.18 (0.32)	2.3	0.735
SUV_{ave}/LV SUV_{max}	1.00 (0.22)	0.98 (0.22)	-1.6	0.788
SUV_{max}/LV SUV_{ave}	1.41 (0.30)	1.46 (0.45)	3.8	0.584
SUV_{max}/LV SUV_{max}	1.22 (0.26)	1.22 (0.33)	-0.2	0.969
SUV_{ave}/liver SUV_{ave}	0.83 (0.12)	0.88 (0.21)	5.5	0.278
SUV_{ave}/liver SUV_{max}	0.62 (0.10)	0.64 (0.14)	3.1	0.551
SUV_{max}/liver SUV_{ave}	1.01 (0.15)	1.08 (0.28)	6.7	0.220
SUV_{max}/liver SUV_{max}	0.76 (0.12)	0.78 (0.25)	3.7	0.462
SUV_{ave}/^{f}liver SUV_{ave}	0.78 (0.11)	0.83 (0.18)	5.9	0.231
SUV_{max}/^{f}liver SUV_{ave}	0.95 (0.13)	1.02 (0.25)	7.1	0.170

no L = no lymphoma; L = lymphoma.
% = percent difference between lymphoma and no lymphoma.
p = significance of difference between lymphoma and no lymphoma.
^{f}liver SUV = liver SUV adjusted for hepatic fat (see chapter 6).

Splenic SUV_{max} and SUV_{ave} correlated weakly with splenic FDG clearance (Table 9.2). Correlations with splenic FDG clearance were slightly stronger and reached significance when SUV was based on LBM rather than weight. SUVs also correlated with FDG clearance when expressed as ratios with LV SUV, especially SUV_{ave} (Table 9.2). However, splenic SUV_{max} and SUV_{ave} correlated most strongly with FDG clearance when expressed as ratios with liver SUV, especially liver SUV_{ave}. Adjusting liver SUV_{ave} for hepatic fat, however, did not improve these correlations.

Table 9.2. Correlation coefficients (r) for relationships between SUV indices and splenic FDG clearance. The strongest correlations are seen when spleen SUV is divided by liver SUV.

	r	**p**
SUV_{ave} (weight)	0.24	0.065
SUV_{max} (weight)	0.24	0.065
SUV_{ave} (LBM)	0.25	0.054
SUV_{max} (LBM)	0.26	0.045
SUV_{ave}/LV SUV_{ave}	0.26	0.045
SUV_{ave}/LV SUV_{max}	0.17	0.194
SUV_{max}/LV SUV_{ave}	0.26	0.045
SUV_{max}/LV SUV_{max}	0.18	0.169
SUV_{ave}/liver SUV_{ave}	0.39	0.002
SUV_{ave}/liver SUV_{max}	0.29	0.025
SUV_{max}/liver SUV_{ave}	0.39	0.002
SUV_{max}/liver SUV_{max}	0.32	0.013
SUV_{ave}/^{f}liver SUV_{ave}	0.39	0.002
SUV_{max}/^{f}liver SUV_{ave}	0.39	0.002

In the 40 patients without lymphoma, splenic MRglu was 3.07 ± 2.01 μmol/min, significantly higher than hepatic MRglu, which was 2.01 ± 1.38 μmol/min ($p = 0.003$, paired *t*-test), indicating that in the apparent absence of hepatic or splenic disease, splenic metabolic activity is physiologically greater than hepatic metabolic activity.

9.4. DISCUSSION

My results show that SUV indices cannot reliably identify differences in splenic FDG clearance and glucose utilisation rate that exist between these two clinically heterogeneous populations, one with and one without lymphoma. Nor did I find strong correlations between SUV indices and splenic FDG clearance. Moreover, when SUV is scaled to body weight, there is a strong tendency for it to be overestimated in overweight persons (Sugawara et al 1999), potentially leading to misleading results when compared between two patient groups with different mean weights. Whenever SUV (weight) is used, body weight must be taken into account. SUV should preferably be based on LBM.

When splenic SUV was expressed as a ratio with blood pool SUV, which eliminates whole body metric scaling issues, correlations with FDG clearance were moderately strong, and stronger than those given by SUV indices alone, underlining my findings reported in chapter 7 that SUV is a closer reflection of FDG clearance when it is expressed as a ratio with blood pool SUV. The liver is essentially a blood pool SUV (Green et al 1998), so when it was used as the denominator in the splenic-to-blood pool SUV ratio it also gave a moderately strong correlation. In fact it gave the strongest correlation probably because it gives better count statistics than the LV cavity and is less susceptible to partial volume artefacts.

Patlak-Rutland analysis has previously been used by Wollenweber et al (2014) to measure splenic FDG clearance in patients with myocardial infarction. They expressed splenic clearance in the same units as mine, namely ml/min/100 ml tissue. However, they measured splenic and plasma FDG concentrations in absolute units so their 100 ml refers to total splenic tissue volume. This is likely to be higher than the distribution volume of FDG in the spleen that is obtained as the intercept of the Patlak-Rutland plot. Nevertheless, their range of MRglu values is very similar to that obtained in my study, implying that V(0) approaches total splenic volume.

Interestingly, MRglu is higher in the spleen than in the liver. The difference cannot be explained by differences in V(0) between the two organs as for both of them the evidence suggests that V(0) is close to total tissue volume.

Limitations of the study include the following.

1. The patient populations were unselected.
2. Both groups were heterogeneous in terms of pathology, and the group with lymphoma had various forms of the disease. However, it was not my aim to evaluate splenic MRglu in lymphoma in the context of clinical diagnosis and management but instead to evaluate the reliability of SUV indices that have been used previously as surrogates for splenic FDG clearance and MRglu.
3. Data from the dynamic studies were not corrected for attenuation and left as raw count rates rather than the absolute FDG concentrations that would be needed, either from blood sampling or measurement of tracer concentration in a blood pool region, to obtain clearance per unit of splenic volume. This required me to express the

Patlak-Rutland gradient as a quotient with the intercept in order to cancel out all the factors that respectively relate the gradient to clearance and the intercept to distribution volume. Although this approach is convenient and simplifies the dynamic study, uncertainty remains as to what anatomical volume V(0) represents. However, as mentioned above, our range of splenic FDG clearances is similar to the range obtained by Wollenweber et al (2014) who measured absolute concentrations, suggesting that V(0) is close to total volume, as is the case for the liver (Choi et al 1994. The linearity of the Patlak-Rutland plots from 2 min suggests that mixing of FDG in its splenic distribution volume is rapid.

In conclusion, in future studies on splenic metabolic activity in malignancies such as lymphoma and especially in the settings of atheroma and myocardial infarction, it is recommended that SUV is not used but instead replaced with more robust measures of clearance based on dynamic imaging. Using the technique described here, the data appear sufficiently robust and are relatively easily acquired, there is no need for attenuation correction or measurement of absolute FDG concentrations, and there is no additional radiation exposure. Surprisingly, I found the metabolic activity of the spleen to be greater than that of the liver, perhaps reflecting the high rate of blood cell destruction, especially neutrophils (Peters et al 2004), that takes place physiologically within the spleen.

Chapter 10: Regional variability of liver FDG accumulation as a marker of the heterogeneity of intrahepatic fat distribution

10.1. INTRODUCTION

Fat distribution within the liver, like the distribution of inflammation, is often heterogeneous (Decarie et al 2011). There are very few previous publications in the literature that have measured the heterogeneity of hepatic fat distribution. I postulated that such heterogeneity might be an independent marker of hepatic pathology. Using the SUV_{max}/SUV_{ave} ratio and CT density as markers of hepatic fat, the aim of the study in this chapter was to draw multiple regions of interest in single livers and quantify the regional variabilities of CT density and SUV indices as potential measures of hepatic fat distribution and possibly also of intrahepatic inflammation, which like fat is often heterogeneously distributed throughout the liver.

10.2. METHODS

10.2.1. Patients

This was a retrospective study of 24 patients (12 males, 12 females; age range 24-81) who were anonymously selected from the routine clinical database during a 3-month period of referrals for routine FDG PET/CT for the management of cancer. CT density was measured in a 3 cm ROI placed over the right lobe of the liver. I tried to ensure a population with a reasonably wide range of fatty livers (13 - 68 HU). Patients with diabetes, known liver disease, liver abnormalities on PET/CT, recent chemotherapy (within 6 months), excess alcohol intake or blood glucose outside the range of 4.5-7.5 mmol/l were not selected. Lean body mass (LBM), body mass index (BMI) and % whole body fat were measured using the equations described in chapter 2. PET/CT acquisition was as described in chapter 2.

10.2.2. Image analysis

For each patient, 12 small ROI (with circular diameter of 2 cm) were drawn in 3 tomographic axial slices of the liver (4 per slice) without overlap (Fig 10.1).

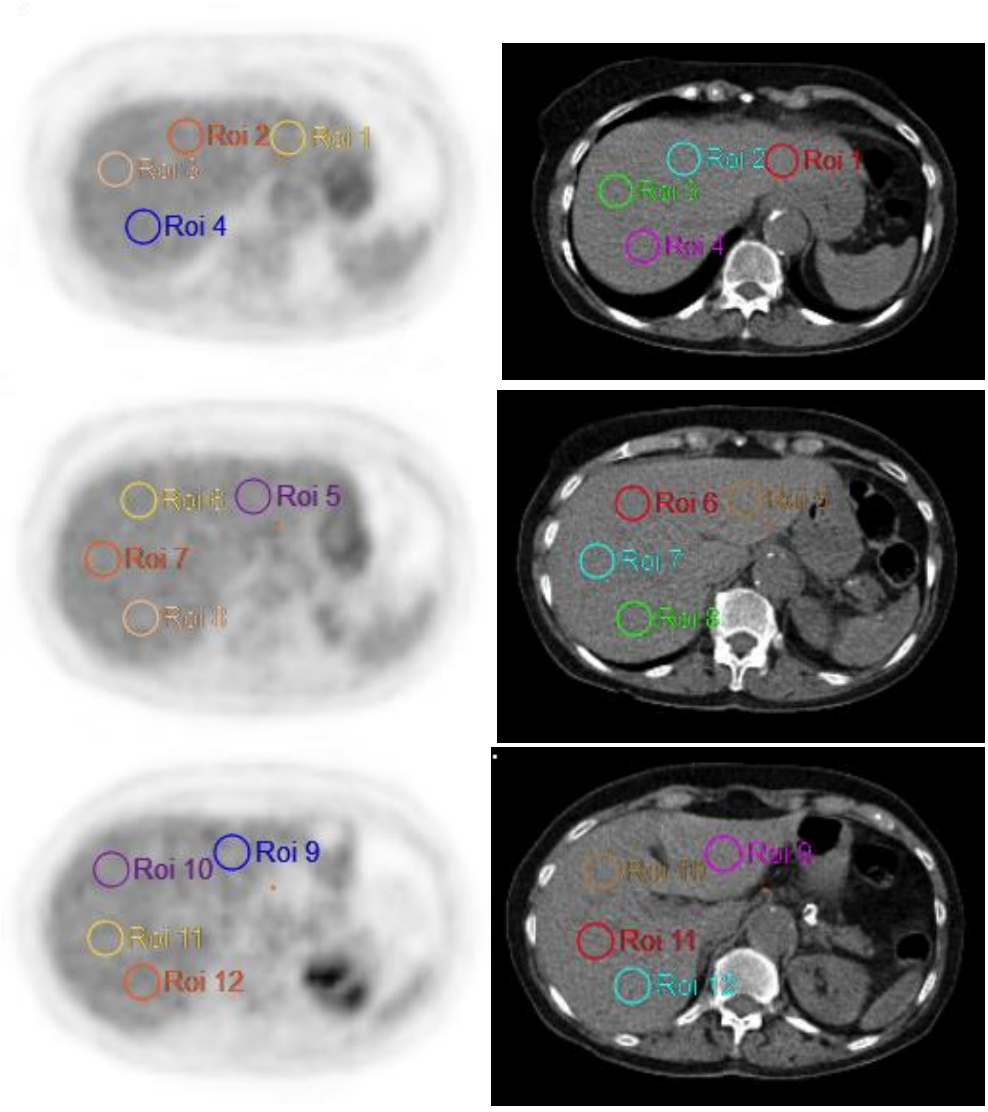

Fig 10.1. Placement of 4 ROI within each of 3 different transaxial sections of PET (left panels) and corresponding sections of CT (right panels); 'slicing' is from top to bottom.

SUV_{max} and SUV_{ave}, scaled to LBM and to body weight, were recorded in each small ROI as MBq/ml multiplied by LBM/administered activity or weight/ administered activity. SUV_{ave} was also recorded from an ROI over the left ventricular cavity (SUV_{LV}) using weight. Liver SUV values based on weight were then divided by SUV_{LV}, which meant that weight canceled out. CT density in Hounsfield Units (HU) was recorded in each small liver ROI. The mean values (± standard deviation [SD]) for CT density, SUV_{max}, SUV_{ave} and SUV_{max}/SUV_{ave}, based on these small ROI, were calculated for each patient. The mean values of SUV_{max}/SUV_{LV} and SUV_{ave}/SUV_{LV} were also calculated. There is only one value for SUV_{LV} in each patient so the SDs of the liver SUVs remain the same after they have been divided by SUV_{LV}.

Patients were divided into those with hepatic steatosis (CT density ≤40 HU; n = 12) and those without (n = 12) (Boyce et al 2010, Zeb et al 2012).

10.2.3. Statistics

Correlations were based on Pearson correlation analysis. The coefficients of variation (CV) of hepatic SUV indices were calculated for each individual liver from the 12 small ROIs as the ratio of SD to mean. Differences between steatosis and non-steatosis groups were tested using Student's unpaired *t*-test. Because CT density may be negative, it is not valid to use CV of CT density so I used SD instead. Note that the CVs of SUV indices are independent of the whole body metric used for calculating SUV. A p value of > 0.05 was taken to indicate no statistical significance.

10.3. RESULTS

CT density measured from the single 3 cm ROI ranged from 46 to 68 (mean 55 ± SD 6) HU in the 12 patients without steatosis and between 13 and 39 (mean 29 ± SD 8) HU in the 12 patients with steatosis. It correlated very closely with mean values of CT density based on the 12 small ROI (r = 0.97).

Body weight, BMI and %body fat were higher in the patients with steatosis, diagnosed from CT density in the single 3 cm ROI, but there was no significant difference in blood glucose and LBM (Table 10.1).

Table 10.1.
Mean values (SD) of blood glucose and body size metrics of patients with and without steatosis (diagnosed from a single 3 cm ROI over the right lobe of the liver).

	No steatosis (n = 12)	Steatosis (n = 12)	p
Body weight (kg)	69 (14)	92 (19)	0.003
Lean body mass (kg)	53 (9)	58 (11)	0.25
Body mass index (kg/m^2)	23.4 (3.7)	32.7 (6.8)	0.0005
Whole body fat (%)	22.6 (8.8)	36.5 (8.5)	0.001
Blood glucose (mmol/l)	5.8 (0.9)	6.2 (0.8)	0.28

Mean SUV_{max}/SUV_{ave} based on the small ROIs in the patients with steatosis was significantly higher compared with the non-steatosis group (p = 0.02; Table 10.2). Mean values of SUV_{max} and SUV_{ave} were significantly different between the two groups when calculated using body weight but not when calculated using LBM. SUV_{max}/SUV_{LV} but not SUV_{ave}/SUV_{LV} was significantly higher in steatosis (Table 10.2).

Table 10.2.
Mean values (SD) of mean SUV indices and CT density based on the 12 small ROI compared between patients with and without steatosis (diagnosed from a single separate 3 cm ROI). Note that there is a significant difference between patients with and without steatosis with respect to SUV calculated using body weight but not SUV calculated using LBM.

	No steatosis (n = 12)	Steatosis (n = 12)	p
CT density	55.2 (4.0)	32.6 (9.2)	-
SUV_{ave}(LBM)	1.57 (0.31)	1.56 (0.23)	0.99
SUV_{max} (LBM)	1.80 (0.36)	1.87 (0.26)	0.59
SUV_{ave}(weight)	2.02 (0.36)	2.47 (0.34)	0.006
SUV_{max} (weight)	2.32 (0.42)	2.96 (0.41)	0.001
SUV_{ave}/SUV_{LV}	1.24 (0.16)	1.42 (0.29)	0.09
SUV_{max}/SUV_{LV}	1.42 (0.19)	1.70 (0.33)	0.02
SUV_{max}/SUV_{ave}	1.15 (0.053)	1.20 (0.042)	0.02

Mean SUV_{max}/SUV_{ave} correlated with mean CT density (Fig 10.2) but none of the other SUV indices correlated with CT density (Table 10.3).

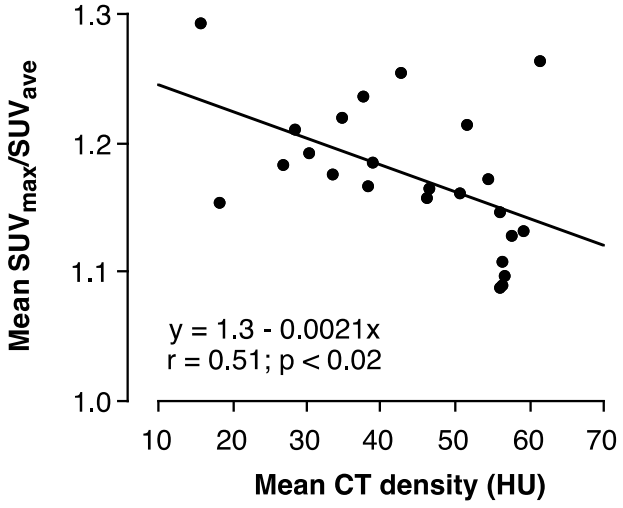

Fig 10.2. Relationship of mean SUV_{max}/SUV_{ave} with mean CT density based on the 12 small ROI. Least squares linear fit and regression equation are shown.

Table 10.3.
Correlation coefficients of relationships between mean SUV indices and mean CT density (CTD) in 12 hepatic ROI.

	r	p
SUV_{ave} (LBM)	0.00	1.00
SUV_{max} (LBM)	-0.13	0.54
SUV_{ave}/SUV_{LV}	-0.06	0.78
SUV_{max}/SUV_{LV}	-0.17	0.43
SUV_{max}/SUV_{ave}	-0.51	0.02

Mean CV of SUV_{max}/SUV_{ave} based on the small ROIs was significantly higher in patients with steatosis compared with those without (Table 10.4). The mean CV of SUV_{ave} was also higher in steatosis but, in contrast, the mean CV of SUV_{max} was not significantly different between the two groups. The mean SD of CT density was higher in patients with steatosis but not significantly higher. Note that the CVs of SUV_{max} and SUV_{ave} remain unchanged when they are divided by SUV_{LV} and so are not shown.

Table 10.4.
Variability of CT density (HU), expressed as mean SD, and of SUV indices, expressed as mean CV (%), in the 12 small ROI compared between patients with and without steatosis (diagnosed from a separate single 3 cm ROI). Standard deviation of mean variability is shown in brackets.

	No steatosis (n = 12)	Steatosis (n = 12)	p
SD of CT density	4.3 (1.8)	6.0 (3.3)	0.13
CV of SUV_{ave}	8.6 (3.0)	11.7 (3.8)	0.04
CV of SUV_{max}	10.2 (4.0)	12.9 (2.8)	0.08
CV of SUV_{max}/SUV_{ave}	5.0 (1.5)	7.1 (1.2)	0.001

The CV of SUV_{max}/SUV_{ave} correlated with mean CT density (r = -0.67; p = 0.003; Fig 10.3), but the CVs of SUV_{ave} and SUV_{max} did not correlate with mean CT density (r = -0.39; p = 0.06 and r = -0.33; p = 0.12, respectively). None of these CVs showed any significant correlation with the SD of CT density.

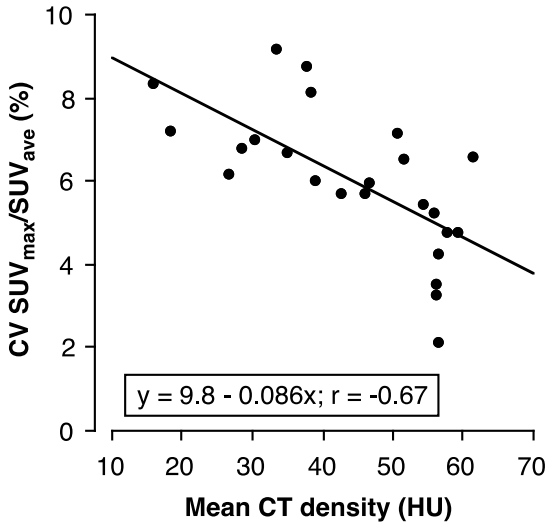

Fig 10.3. Relationship of the CV of SUV_{max}/SUV_{ave} with mean CT density based on the 12 small ROI. Least squares linear fit and regression equation are shown.

10.4. DISCUSSION

The main conclusions of this study are firstly that SUV_{max}/SUV_{ave} is a metric of hepatic fat, secondly that SUV_{max}/SUV_{ave} is more regionally variable in hepatic steatosis and thirdly that this regional variability may be a measure of the heterogeneity of hepatic fat distribution.

CT density is accepted as a measure of fat in the liver, with low density indicating steatosis (Boyce et al 2010, Zeb et al 2012). My results suggest that SUV_{max}/SUV_{ave} is

also a measure of hepatic fat. This is because hepatic fat, which is heterogeneously distributed throughout the liver (Decarie et al 2011), accumulates negligible FDG in comparison with lean liver parenchyma, so whilst SUV_{max} is selectively located in a relatively fat-free area of liver within the ROI, SUV_{ave} reflects the signals from all voxels, including those containing fat.

There was greater variation in SUV_{max}/SUV_{ave} in fatty as compared with non-fatty livers (Table 10.4). The CV of SUV_{ave} was also significantly greater in steatosis, probably reflecting the varying dilutional effect on the FDG signal of heterogeneously distributed hepatic fat. Although this supports the notion that SUV_{max} avoids fat, the CV of SUV_{max} was higher than that of SUV_{ave} in both patient groups (Table 10.4). This is probably because SUV_{max} is selected from a single voxel and so is more dependent on signal-to-noise ratio. In contrast, being an average based on many voxels, SUV_{ave} is less dependent on the signal-to-noise ratio. Patients with hepatic steatosis are generally obese. If as a result of obesity there was a low signal-to-noise ratio it could explain why SUV_{max}/SUV_{ave} is increased in hepatic steatosis. However, against this, the CV of SUV_{max} was not significantly different between steatosis and non-steatosis groups (Table 10.4). Moreover, there was less between-patient variation (as opposed to within-patient variation) in SUV_{max}/SUV_{ave} in the steatosis group (Table 10.2). The problems of inter-dependent correlations in this field of work have been emphasized in earlier chapters and discussed further in chapter 12.

I conclude that SUV_{max}/SUV_{ave} is a marker of hepatic fat and that its regional CV throughout the liver may be a quantitative marker of the heterogeneity of intrahepatic fat distribution, which itself may be an independent marker of liver disease. Further

work using texture analysis of diagnostic CT (Mir et al 1995) and FDG PET (Chicklore et al 2013) would therefore be of interest, especially in fat-induced hepatic inflammation, which currently can only be diagnosed by biopsy at a pre-fibrotic stage (Musso et al 2011). Texture analysis of the liver in hepatic steatosis is explored in the next chapter.

Chapter 11. Texture analysis of the liver in FDG PET and CT images

11.1. INTRODUCTION

There has been much work recently on the use of medical image texture analysis to improve clinical prediction and prognosis in a variety of tumours (Davnall et al 2012, Chicklore et al 2013, Willaime et al 2013). Images have included MRI, CT, US and PET. It has been shown that certain textural features may provide useful information that adds to standard image features, e.g. tumour size and SUV.

There are over 70 texture parameters described in the literature. They fall into several categories that can be conveniently divided into 2 groups: firstly, measures of central tendency (e.g. mean, median, mode, percentiles and quartiles of voxel values), measures of variability (e.g. range, standard deviation [SD], coefficient of variation [CV], kurtosis and skewness) and measures of texture (entropy and energy); and secondly, 6 categories of mathematically more complex texture matrices comprising fractal dimension, grey level co-occurrence matrices, grey level run length matrices, grey level size zone matrices, grey level difference methods and neighbourhood grey tone difference matrices. Within each of these 6 categories, the numbers of parameters ranges between 4 and 22.

There are limited data in the literature on texture analysis of the liver that aim to identify parenchymal hepatic disease, especially fatty liver disease, steatohepatitis and hepatic fibrosis. It is likely that normal hepatocytes, inflammatory cells and fat deposits in the liver show differences in glucose metabolism on a cellular scale and

my hypothesis for the study described in this chapter is that there are differences between normal and fatty livers in texture features based on the spatial distribution of FDG in PET images of the liver. The aim of the study reported in this chapter, therefore, was to see if texture analysis might be helpful to allow a better distinction between fatty and non-fatty livers using FDG PET and non-contrast CT and secondly, to detect progression of hepatic steatosis to steatohepatitis before the fibrotic, irreversible stage is reached.

11.2. METHODS

11.2.1. Patients

I analysed the data from 30 patients randomly selected from my prospective series of patients who had dynamic imaging for measurement of hepatic and splenic MRglu (Chapters 8 and 9). In addition to these, I analysed the PET/CT scans of a further 7 patients with severe hepatic steatosis (mean CT density 4-19 HU) and 7 patients with liver inflammation confirmed by liver biopsy. The patients were divided into 3 groups: firstly those without hepatic steatosis (group 1; HU >40 HU), secondly those with steatosis (group 2; mean CT density ≤40 HU; Boyce at al 2010) and thirdly a miscellaneous group of 7 patients with biopsy-proven hepatic inflammation (group 3). Only 3 patients in this group had steatosis by the above definition. Four of the 7 had biopsy evidence of fibrosis/cirrhosis, 2 of whom also had steatosis. Two of the patients in group 3 had 2 PET/CT scans. Biopsy data for group 3 patients and timings of PET/CT in relation to biopsy are summarised in Table 11.1.

Table 11.1. Mean CT density (CTD) and biopsy data of group 3 patients

Biopsy diagnosis	CTD (HU)	*PET timing
1. Marked steatosis with mildly active focal steatohepatitis.	16	+3 m
2A. Acute cholestatic hepatitis with early fibrosis and steatosis	47	-2 m
2B.	56	+11 m
3. Macro-vesicular steatosis with steatohepatitis, portal fibrosis.	13	+50 m
4. Steatohepatitis and advanced fibrosis (HIV infection/antiviral meds).	42	+38 m
5. Cirrhosis, minimal lobular inflammation and mild steatosis.	33	-74 m
6A. Micro and macrosteatosis with steatohepatitis	44	-2 m
6B.	48	+5 m
7. Mild chronic portal hepatitis with focal mixed steatosis.	45	-7 d

- Before biopsy; + after biopsy.
Patients 2 and 6 were studied on two separate occasions, 13 months and 7 months apart, respectively.

11.2.2. Image analysis

The 60 min post injection whole body FDG PET/CT scans were analysed. Regions of interest (ROI) were drawn around the liver, close to the periphery, at several axial levels from top to bottom. The ROI were added together to give a large, single VOI for the liver, with voxel numbers ranging between 160-1300. Calculation of the textural features was performed using in-house KCL software implemented under MATLAB (The MathWorks Inc.).

11.2.3. Texture parameters

Five measures of central tendency were examined (average SUV [SUV_{ave}], maximum SUV [SUV_{max}], peak SUV [SUV_{peak}], maximum CT density (CTD) and mean CTD), 6 measures of variability (ranges of SUV and CTD, CV of SUV, SD of CTD [note that CTD may be negative and so its variability cannot be expressed as CV (Fig 11.1)], kurtosis and skewness), 2 measures of texture (first order entropy and energy),

5 fractal based (FD) features, 22 grey level co-occurrence matrices (GLCM), 13 grey level run length matrices (GLRLM), 13 grey level size zone matrices (GLSZM), 4 grey level difference methods (GLDM) and 5 neighbourhood grey tone difference matrices (NGTM).

11.2.4. Statistical analysis

It turned out unexpectedly that the size of the VOI (metabolic active volume [MAV]) correlated with many texture parameters, some very strongly (see Results). Because livers of patients with steatosis tend to be enlarged, I ended up with MAV values in group 2 (steatosis) significantly higher than in group 1 (no steatosis). MAV in group 3 was also significantly higher than in group 1. Results were therefore expressed in terms of the numbers of conspicuous outliers, identified visually by consensus with my supervisor, in the regressions of each texture parameter on MAV, whether or not the correlations were significant. The relationships of SUV indices with mean CTD, weight and CV of SUV were examined using Pearson correlation analysis.

11.3. RESULTS

11.3.1. Relationships of SUV and CTD with their variabilities

Excluding group 3 patients with inflammation, the CV of CTD increased as mean CTD decreased and approached infinity as mean CTD approached zero (Fig 11.1). CV cannot therefore be used as a measure of CTD variability because CTD may become negative. The SD of CTD showed a less prominent but significant correlation with mean CTD, increasing as the liver became more steatotic. The SD of SUV correlated positively with SUV_{ave} but the CV of SUV showed no correlation with SUV_{ave} (Fig 11.1) and so is the appropriate way to express the variability of SUV.

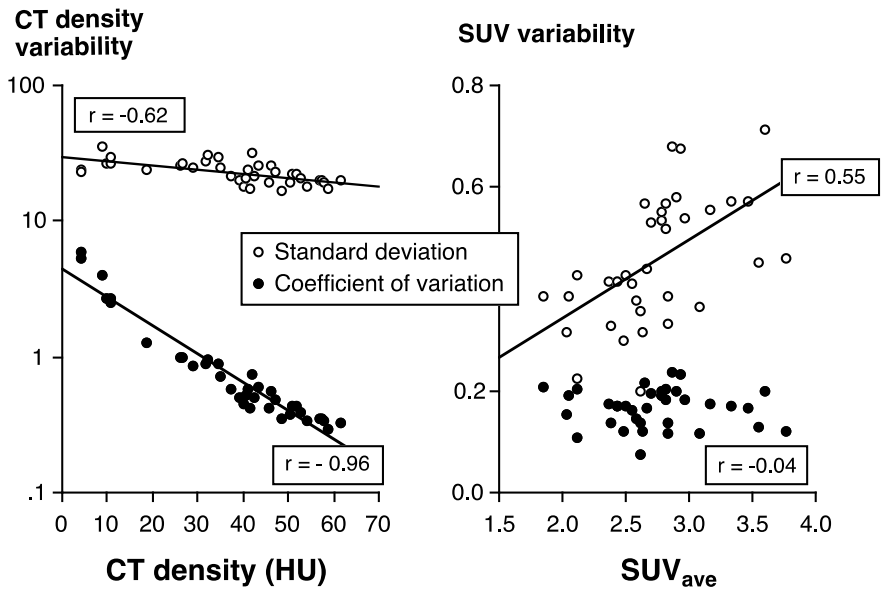

Fig 11.1. SD and CV of CTD density both correlate inversely with mean CTD (left panel); note logarithmic y-axis. The graph of CV of CTD is asymptotic to the y-axis. The SD of SUV correlates positively with SUV_{ave} but the CV of SUV shows no correlation with SUV_{ave}. This means that SD should be used to express variability of CTD while CV should be used to express variability of SUV.

11.3.2. Relationships of SUV indices with mean CTD and weight

Excluding group 3 patients, SUV_{max}, SUV_{peak} and SUV_{ave} all correlated strongly with weight, as would be expected as they were calculated using weight (Table 11.2). SUV_{max}/SUV_{ave} and SUV_{peak}/SUV_{ave} both correlated strongly with mean CTD (Table 11.2), which is consistent with 'dilution' of SUV_{ave} by hepatic fat. The CV of SUV showed a very strong correlation with SUV_{peak}/SUV_{ave} (r = 0.77), consistent with heterogeneity of hepatic fat distribution increasing in fatty liver.

Table 11.2. Correlation coefficients of relationships of SUV indices with mean CTD and weight (excluding group 3 patients; n = 37).

SUV index	mean CTD	weight
SUV_{max}	-0.34	0.74
SUV_{peak}	-0.32	0.67
SUV_{ave}	0.07	0.41
SUV_{max}/SUV_{ave}	-0.51	0.59
SUV_{peak}/SUV_{ave}	-0.60	0.51
Mean CTD	-	0.50

Significance at $p < 0.05$ is reached when $r = \geq 0.33$

11.3.3. Relationships of texture parameters with MAV and conspicuous outliers

The correlations of texture parameters with MAV were very strong, strong or weak, with outliers that were very conspicuous, conspicuous or non-conspicuous (Fig 11.2).

11.3.3.1. Central tendency

SUV_{ave}, SUV_{max}, SUV_{peak} and mean CTD showed no correlation with MAV and there were no outliers. Patients 6B and 7 from group 3 and patient 5 from group 2, however, were outliers with respect to maximum CTD. SUV_{max}/SUV_{ave} and SUV_{peak}/SUV_{ave} both correlated positively with MAV but there were no outliers.

11.3.3.2. Variability

SD of CTD showed no correlation with MAV and there were no outliers. CV of SUV correlated positively with MAV but there were no outliers. Ranges of SUV and CTD did not correlate with MAV but, with respect to CTD range, there were 3 obvious group 3 outliers (patients 2B, 6B and 7) and 2 group 2 outliers (patients 11 and 15). There were no outliers with respect to SUV range.

A (PET)

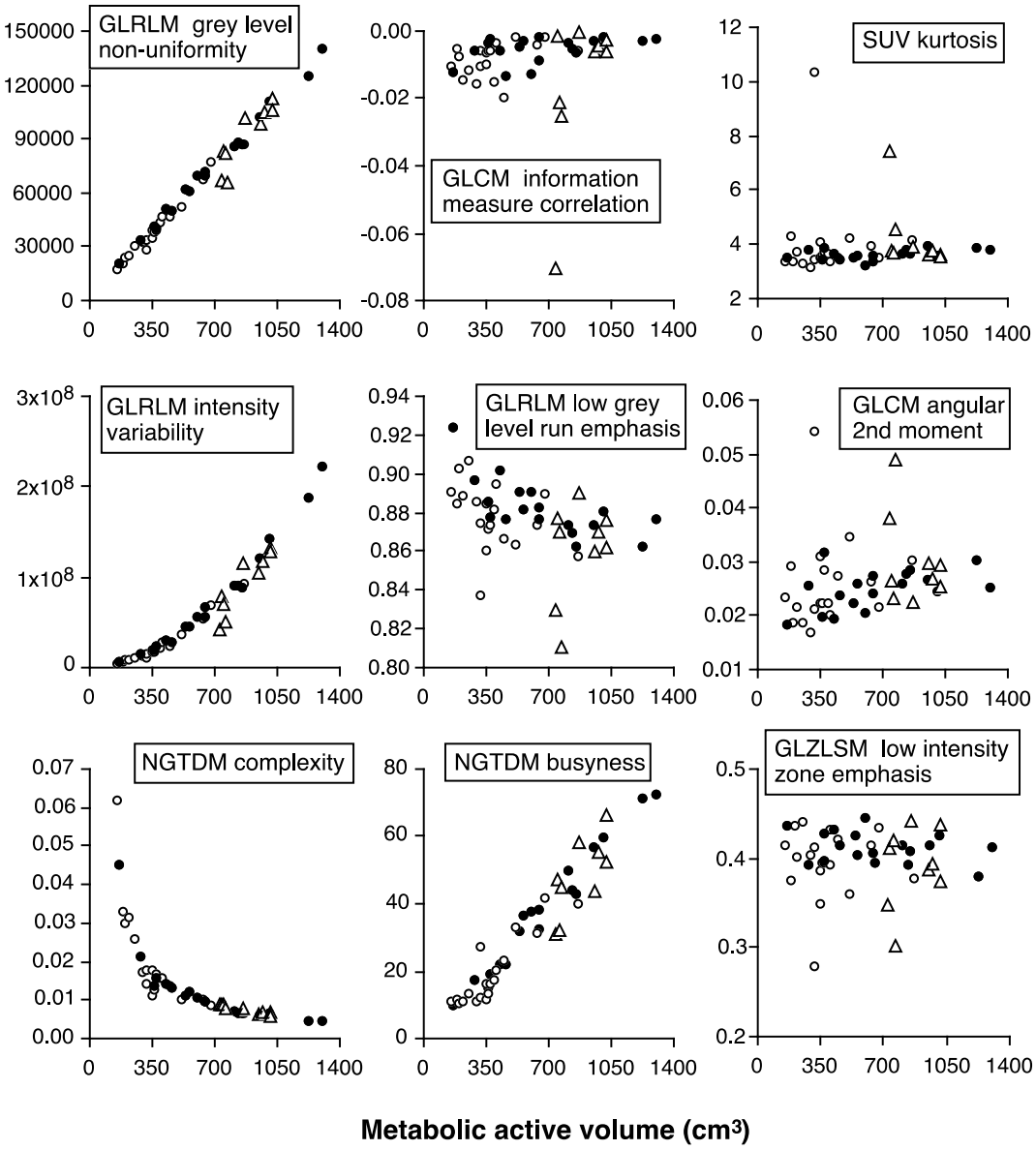
GLRLM grey level non-uniformity
GLCM information measure correlation
SUV kurtosis
GLRLM intensity variability
GLRLM low grey level run emphasis
GLCM angular 2nd moment
NGTDM complexity
NGTDM busyness
GLZLSM low intensity zone emphasis
Metabolic active volume (cm3)

B (CT)

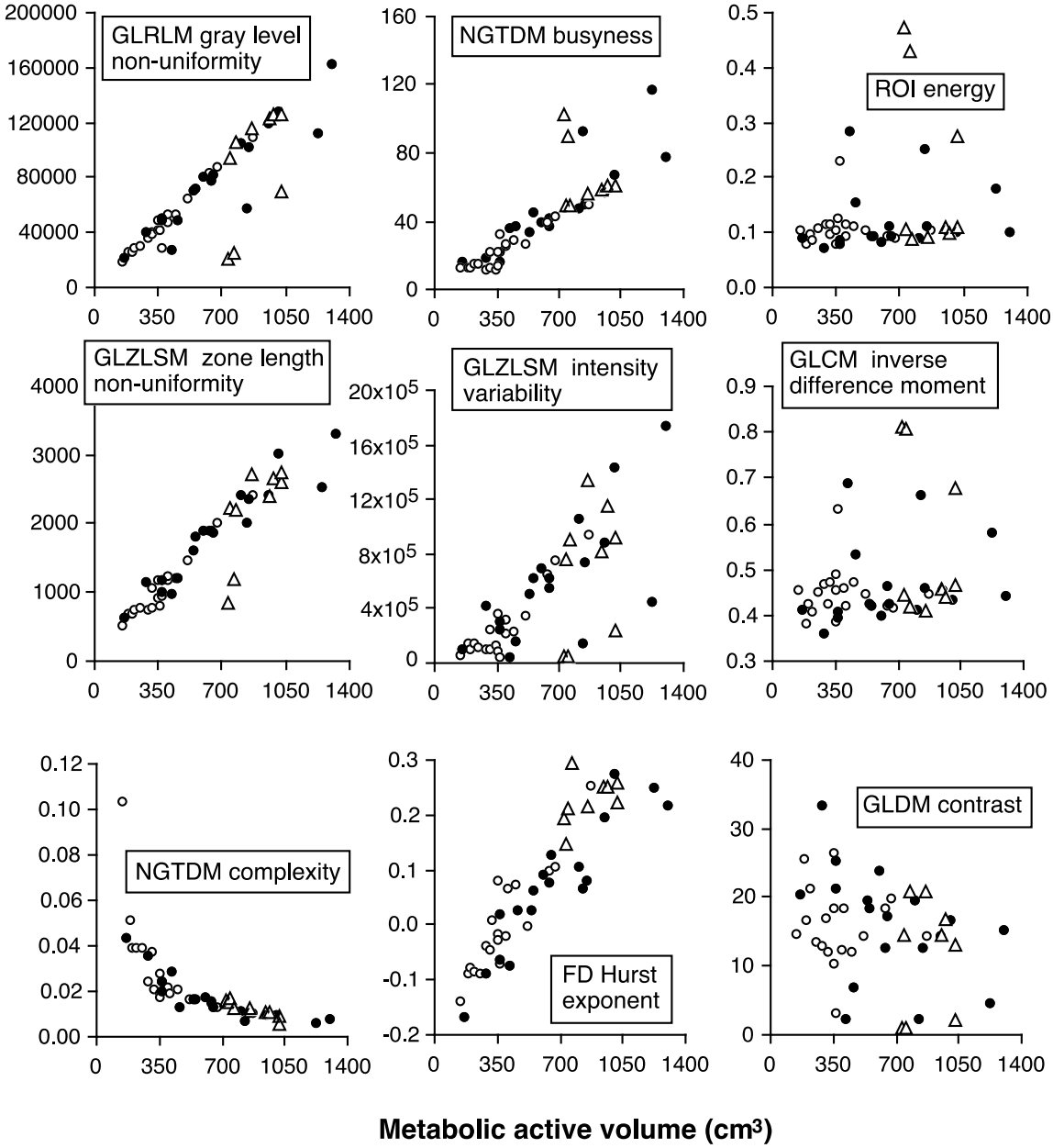

Fig 11.2. Examples of relationships between metabolic active volume and texture parameters from FDG PET (A) and CT (B). Outliers are very conspicuous in the top rows, conspicuous in the middle rows and absent in the bottom rows. Correlations are very strong in the left columns, strong in the middle columns and weak in the right columns. Open circles are patients without steatosis (group 1), filled circles are patients with steatosis (group 2) and open triangles are patients with evidence of hepatic inflammation on biopsy (group 3).

Kurtosis and skewness of SUV and CTD showed no correlation with MAV. For skewness of CTD, there were 2 obvious outliers from group 3 (patients 2B and 7), and one from group 2 (patient 11). For skewness of SUV, there 2 outliers (group 3 patient 7) and group 1 patient 12).

For kurtosis of CTD there were the same 3 outliers as for skewness (patients 2B and 7 from group 3 and patient 11 from group 2) and for SUV there were the same 2 outliers as for skewness (group 3 patient 7 and group 1 patient 12). So there was no difference between kurtosis and skewness.

11.3.3.3. First order entropy and energy

Entropy and Energy are essentially the inverse of each other and give the same information. Neither correlated with MAV (CT or PET). For CT, there were 3 group 3 outliers (2B, 6B and 7, none of whom had hepatic steatosis as defined by mean CTD) and 2 group 2 outliers (11 and 15). For PET, there were 2 outliers (group 3 patient 2A and group 1 patient 12 again).

11.3.3.4. Fractal dimension (FD)

Fractal dimensions of PET and CT revealed no correlations with MAV or group differences of interest apart from mean FD and Hurst exponent (mirror image of mean FD), which correlated strongly (negatively and positively, respectively) with MAV with respect to both PET and CT. The correlations were almost identical between PET and CT. However, there were no outliers.

11.3.3.5. Grey level co-occurrence matrices (GLCM)

PET

GLCM PET texture parameters in general showed weak or no correlations with MAV with the exception of run length variability, which showed a very strong positive non-linear relationship with MAV. In almost all GLCM correlations, group 3 patient 7 was an outlier and, in many, group 3 patient 2A also. One patient in group 1 (patient 12, mean CTD 46 HU) was also a frequent outlier.

CT

GLCM CT texture parameters, like PET, parameters in general showed weak or no correlations with MAV with the exception, as in PET, of run length variability, which also showed a very strong positive non-linear relationship with MAV. In several relationships, there were 3 prominent outliers in group 3 (patients 2B, 6B and 7) and 3 slightly less prominent, but nevertheless still obvious, outliers in group 2 (patients 11, 14 and 15), all of whom had severe steatosis (mean CTD <10 HU). The group 1 patient who was a frequent outlier in PET (patient 12) was not a frequent outlier in CT but patients 10 (mean CTD 58 HU) and 17 (mean CTD 42 HU) from group 1 were occasional outliers.

11.3.3.6. Grey level difference methods (GLDM)

PET

All 4 GLDM parameters showed non-significant correlations with MAV; however in all 4 relationships, 2 patients from group 3 (patients 2A and 7) and one from group 1 (patient 12) were consistent outliers.

CT

Correlations of GLDM CT parameters with MAV were also non-significant. In all 4 relationships the same outliers were again seen in groups 2 (patients 11, 14, 15) and 3 (patients 2A, 6B and 7), and also one from group 1 (patient 11). In contrast to PET, patient 2A in group 3 was not an outlier.

11.3.3.7. Grey level run length matrices (GLRLM)

PET

GLRLM **r**un length variability showed a very strong positive non-linear relationship with MAV. Patient 18 from group 2 was a conspicuous outlier. This patient was an outlier in several other GLRLM correlations with MAV. There were also very strong correlations between MAV and grey level non-uniformity and intensity variability in which patients 2A and 7 from group 3 were again obvious outliers. Other relationships with MAV were weak but, in most, patients 2A and 7 from group 3 were again outliers.

CT

As with PET, there were very strong correlations between MAV and intensity variability and grey level non-uniformity, in which patients 2B, 6B and 7 from group 3 were again obvious outliers. Three patients in group 2 (patients 11, 14, 15) were

also outliers with respect to grey level non-uniformity. These 6 patients were frequent and conspicuous outliers in several other weak or non-significant relationships between GLRLM parameters and MAV.

11.3.3.8. Grey level size zone matrices (GLZLSM)

PET

GLZLSM parameters in general showed weak and non-significant correlations with MAV, except for intensity non-uniformity, which showed a moderately strong correlation. As for GLCM parameters, patient 12 from group 1 (mean CTD 46 HU) was a frequent outlier. There was a tendency for group 3 patients 2A and 7 to be outliers but they were not strikingly conspicuous.

CT

As with PET, texture parameters correlated weakly or not at all with MAV except for intensity non-uniformity, which correlated quite strongly with MAV. Patients 2B and 7 from group 3 were frequent outliers in these relationships, along with the 3 group 2 patients with severe steatosis (patients 11, 14, 15) and one from group 1 (patient 10). Group 1 patient 12 (frequent PET outlier) was not an outlier in CT

11.3.3.9. Neighbourhood grey tone difference matrices (NGTDM)

PET

NGTDM coarseness and contrast revealed no features of interest. Texture strength, complexity and busyness correlated very strongly with MAV but there were no

obvious outliers. The relation of complexity with MAV appeared strikingly bi-exponential.

CT

As with PET, NGTDM coarseness and contrast revealed no features of interest, although with respect to coarseness, patients 11, 14, and 15 from group 2 and patients 2B, 6B and 7 from group 3 tended again to be outliers. NGTDM busyness correlated strongly with MAV. Group 3 patients 2B, 6B and 7, and group 2 patients 14 and 15 were again conspicuous outliers. NGTDM complexity, as with its PET counterpart, showed a strong bi-phasic correlation with MAV. NGTDM texture strength correlated negatively with MAV; 9 group 1 patients, one group 2 patient (patient 11) and 2 group 3 patients (patients 2B and 7) were clear outliers.

11.3.4. Summary and relationship to biopsy data

Three patients from group 3 (patients 2, 6 and 7) gave studies that were consistently abnormal and can therefore be regarded as having abnormal texture parameters. Two of them did not have evidence of fibrosis on biopsy, whilst the third had early fibrosis. Three of 4 group 3 patients with fibrosis/cirrhosis had unremarkable texture parameters that were not significantly different from group 1 livers. Three patients with steatosis from group 2 (patients 11, 14, and 15) were also consistently abnormal. They all had severe steatosis but there were 3 other patients from group 2 with severe steatosis who had normal texture parameters. No patient from group 1 was

consistently abnormal, although patient 12 (mean CTD 45 HU) was abnormal in PET first order entropy/energy, skewness, kurtosis, GLCM and GLZLSM.

The abnormalities in the 4 abnormal group 3 studies and 3 abnormal group 2 studies show striking consistency from one group of texture parameters to another and consistent differences between PET and CT (Tables 11.3 and 11.4). Abnormal texture parameters in group 2 were consistently seen on CT rather than PET, and also more frequently, though not exclusively, on CT in group 3 patients (Tables 11.3 and 11.4).

Table 11.3. Outlier frequency of patient studies in group 3. Studies 3 and 6 are from the same patient. Other patients were not outliers.

		Patient study			
		2A	2B	6B	7
CTD (HU)		47	56	48	45
range	PET	-	-	-	-
	CT	-	+	+	+
energy/	PET	+	-	-	-
entropy	CT	-	+	+	+
kurtosis	PET	-	-	-	+
/skewness	CT	-	+	-	+
FD	PET	-	-	-	-
	CT	-	-	-	-
GLCM	PET	+	-	-	+
	CT	-	+	+	+
GLDM	PET	+	-	-	+
	CT	-	+	+	+
GLRLM	PET	+	-	-	+
	CT	-	+	+	+
GLZLSM	PET	+	-	-	+

	CT	-	+	-	+
NGTDM	PET	-	-	-	-
	CT	-	+	+	+

Table 11.4. Outlier frequency of patients of group 2. Other patients were not outliers

		Patient			
		11	14	15	18
CTD (HU)		9	4	4	35
range	PET	-	-	-	-
	CT	+	-	+	-
energy/ entropy	PET	-	-	-	-
	CT	+	-	+	-
kurtosis/ skewness	PET	-	-	-	-
	CT	+	-	-	-
FD	PET	-	-	-	-
	CT	-	-	-	-
GLCM	PET	-	-	-	-
	CT	+	+	+	-
GLDM	PET	-	-	-	-
	CT	+	+	+	-
GLRLM	PET	-	-	-	+
	CT	+	+	+	-
GLZLSM	PET	-	-	-	-
	CT	+	+	+	-

NGTDM	PET	-	-	-	-
	CT	+	+	+	-

11.3.5. Reproducibility

Comparing the results between the 2 PET/CT scans in the 2 group 3 patients who had repeat scans (patients 2 and 6), it is noteworthy that one patient (patient 6) was a consistent outlier on the occasion of only one of his scans, while the other patient (patient 2) was a consistent outlier on both occasions. In this latter patient, however, the reproducibility of individual texture parameters was low; in other words, although both studies of this patient were consistent outliers they were not generally the same parameters. Moreover, whilst on one occasion they were all PET-related, on the other they were all CT-related.

11.3.6. Differences between groups 1 and 2 (steatosis versus non-steatosis)

Differences in texture parameters between group 1 and group 2 patients were frequent but could not be separated from a significant overall correlation of the parameter with MAV.

11.4. DISCUSSION

This study has shown that some patients with hepatic inflammation have abnormal texture features on both FDG PET and CT. One patient was reproducibly abnormal, although not in a consistent fashion. The results of this study justify more work to

characterise texture features of patients with hepatic inflammation and either early or no fibrosis. In particular, changes in texture parameters over time determined in sequential studies in the same patient may give useful results.

With the exception of abnormal parameters, CT and PET generally showed good correlation with each other, especially with respect to variability. However, CT performed somewhat better than PET in identifying abnormal texture parameters (Tables 11.3 and 11.4).

The strong correlation between SUV_{peak}/SUV_{ave} and CV of SUV is consistent with the notion that heterogeneity of hepatic fat distribution increases in fatty liver, although signal-to-noise ratio could also influence this relationship (see chapter 12). In any event, however, CV of SUV and SD of CTD were not obviously different in group 3 patients compared with groups 1 and 2, so there was no evidence to suggest increased hepatic fat distribution heterogeneity, or heterogeneity of inflammation, in this group. Therefore, the interpretation of the same 3 obvious group 3 outliers with respect to the range of CTD values is uncertain.

Several texture parameters correlated strongly with MAV. It has previously been recognised from texture analysis of tumours that when MAV is low (<40 cm^3), it correlates with many texture parameters (Orlhac et al 2014). The current work has revealed that MAV correlates with many texture parameters, some very strongly, over a much larger range of MAV values. The feasibility of a general technique for detecting abnormalities of texture would be limited if the MAV had to be held at a constant, agreed value.

It had been hoped that texture parameters might distinguish between normal and fatty livers and, moreover, do so better than CT density. However, because MAV was significantly different between steatosis and non-steatosis patients, when a texture parameter correlated with CT density, it inevitably also correlated with MAV.

MRI and MRS are probably the imaging gold standards for hepatic steatosis (Bohte et al 2011). Liver biopsy is the final gold standard but is subject to sampling error and to the heterogeneity of hepatic fat distribution, and indeed led to a diagnosis of steatohepatitis in several group 3 patients in whom mean CT density in contrast indicated no steatosis.

In conclusion, 3 of 7 patients with biopsy-proven hepatic inflammation and 3 of 18 patients with severe steatosis had consistently abnormal texture parameters on PET and CT. One patient with inflammation had abnormal parameters in two separate scans, although they were not the same parameters. No patient without steatosis or inflammation, with the possible exception of one, had any consistently abnormal texture parameters. Further work, preferably of a sequential nature, should be undertaken to establish if texture features are abnormal in patients with early hepatic inflammation and whether they change with the progression of simple fatty liver through steatohepatitis to early fibrosis. If texture parameters are to be used to diagnose hepatic steatosis, MAV will need to be standardised.

Chapter 12: Is the signal-to-noise ratio of hepatic FDG uptake affected by body habitus?

12.1. INTRODUCTION

Throughout this thesis, reference is made to the problem of spurious correlations arising from variations in signal-to-noise ratio and the inter-correlations that exist between hepatic steatosis, blood glucose level and body habitus. A concern is that signal-to-noise ratio may be reduced in overweight persons. It is thought that SUV_{max} is particularly susceptible to noise because it is based on a single voxel (Vanderhoek et al 2012, Bai et al 2013), which means that SUV_{max}/SUV_{ave}, which I have suggested in earlier chapters is a marker of hepatic fat, would also be susceptible to noise.

The aim of this study, therefore, was to examine the associations of body size indices, CT density and SUV indices with the signal-to-noise ratio determined from the Patlak-Rutland plots reported in chapter 8. One way of assessing signal-to-noise in a study is to look at the correlation coefficient of the Patlak-Rutland plot. However, in patients with low rates of hepatic FDG clearance, the plot is relatively flat and tends to have a low correlation coefficient even when there is not much scatter of the points around the regression line. Indeed, a plot could have no scatter at all yet it would have a correlation coefficient of zero if clearance rate was zero. I therefore measured the scatter of the points around the regression line by measuring the standard deviation of the residuals (the residual of a point is its 'distance' from the regression line).

12.2. METHODS

12.2.1. Patients

The patients were the 60 reported in chapter 8. They had dynamic imaging for 30 min over the upper abdomen at a frame rate of 1 per min with CT switched off. Lean body mass (LBM) and %body fat were estimated from height, weight and gender, and body mass index (BMI) as weight/height^2, as described previously. In 28 patients, texture analysis was also performed on 60 min post-injection whole body images, as described in chapter 11, with placement of large VOI enclosing the whole liver.

12.2.2. Analysis

Patlak-Rutland graphical analysis was undertaken as described in chapter 8. The standard deviation (SD) of the residuals of an individual Patlak-Rutland plot was calculated from the following equation.

$$SD = ([\Sigma \text{ residual}^2]/27)^{0.5} \quad (12.1)$$

where the residual is the y value at any time, t, minus the regression line y value at the same time (Fig 1). The SD was then normalised by dividing it by the intercept of the plot to give the 'normalised root mean standard deviation' (NRMSD) or 'noise'.

Using both weight and LBM in their calculations, SUV_{max} and SUV_{ave} were measured from a 3 cm diameter ROI placed over the centre of the right lobe of the liver, avoiding major vessels and any visible focal pathology, in the 60 min post-injection whole body image, as described previously. Mean CT density in the ROI was also

measured. The coefficient of variation (CV) of SUV and standard deviation (SD) of CT density were measured in the 28 patients who had texture analysis in addition to dynamic imaging.

12.3. RESULTS

Mean CT density correlated negatively with body weight ($r = -0.60$; $p < 0.0001$), LBM ($r = -0.52$; $p < 0.0001$), BMI ($r = -0.49$; $p < 0.0001$) and % body fat ($r = -0.36$; $p = 0.005$), consistent with large or obese individuals tending to have fatty liver.

Examples of Patlak-Rutland plots with high noise (upper panel) and low noise (lower panel) are shown in Fig 12.1.

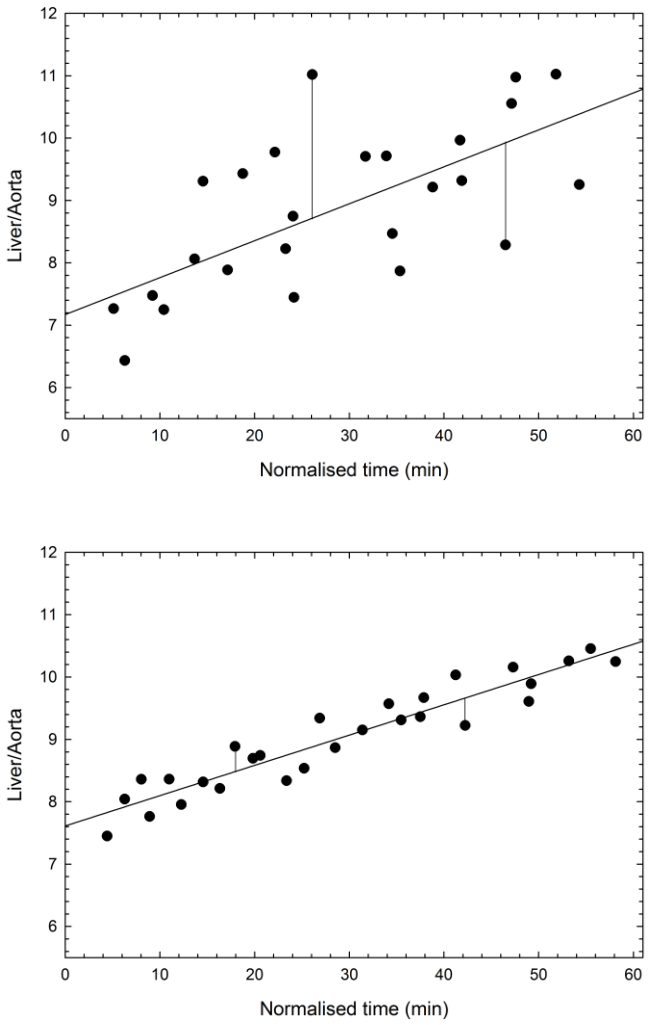

Fig 12.1. Examples of Patlak-Rutland plots showing low signal-to-noise ratio (upper panel, NRSMD = 0.224) and high signal-to-noise ratio (lower panel; NRSMD = 0.035). Vertical lines = residuals.

NRMSD showed significant correlations with body weight (r = 0.45; p = 0.0003), BMI (r = 0.44; p = 0.0004) LBM (r = 0.37; p = 0.004) and %body fat (r = 0.27; p = 0.037), but insignificant correlation with CT density (r = -0.21; p = 0.11) (Table 12.1). In contrast, the correlation coefficient, r_P, of the Patlak-Rutland plot correlated weakly with these indices of body size and mean CT density (Table 12.1). Surprisingly, NRMSD showed no significant correlation with r_P (r = 0.12; p = 0.36).

Table 12.1. Correlation coefficients (p values in brackets) of indices of body size, CT density and SUV indices with NRSMD and r_P.

	NRSMD (p)	r_P (p)
weight	0.45 (0.0003)	0.13 (0.32)
lean body mass	0.37 (0.004)	0.32 (0.013)
body mass index	0.44 (0.0004)	-0.08 (0.54)
%body fat	0.27 (0.037)	-0.23 (0.077)
mean CT density	-0.21 (0.11)	-0.26 (0.045)
SUV_{max} (weight)	0.27 (0.037)	0.08 (0.54)
SUV_{ave} (weight)	0.20 (0.13)	0.00 (1.00)
SUV_{max} (LBM)	0.16 (0.22)	0.27 (0.037)
SUV_{ave} (LBM)	0.00 (1.00)	0.21 (0,11)
SUV_{max}/SUV_{ave}	0.21 (0.11)	0.15 (0.25)
*CV of SUV	0.33 (0.086)	0.24 (0.22)
*SD of CT density	0.43 (0.022)	0.08 (0.69)

*Correlation coefficient of CV of SUV versus CT density = -0.49 (p = 0.008)

Correlation coefficient of NRSMD versus r_P = 0.12 (p = 0.36)

*Based on large VOI (n = 28); other values based on 3 cm ROI (n = 60).

SUV_{max} based on weight showed a weak but significant correlation with NRMSD but SUV_{ave} based on weight showed no significant correlation. Neither of the SUV indices based on LBM showed any correlation with NRMSD. SUV_{max}/SUV_{ave} (which is free of whole body metrics) showed no significant correlation with NRMSD. The only SUV index to correlate with r_P was SUV_{max} based on LBM ($r = 0.27$; $p = 0.037$).

SD of CT density ($r = 0.43$; $p = 0.022$), but not CV of SUV ($r = 0.33$; $p = 0.086$), correlated with NRMDS. Neither SD of CT density nor CV of SUV correlated with r_P (Table 12.1). However, CV of SUV correlated strongly with mean CT density ($r = -0.49$; $p = 0.008$), consistent with it being a marker of hepatic fat heterogeneity.

12.4. DISCUSSION

Body habitus has a prominent effect on the signal-to-noise ratio expressed in terms of the scatter of data points around the regression line of the Patlak-Rutland plot but not on the correlation coefficient of the plot. A critical assumption in this study is that if there is increased noise in the dynamic study, there will also be increased noise in the static study.

There are two possible ways that body size could influence signal-to-noise ratio. Firstly, the administered activity of FDG is not adjusted for body weight, so the tissue count density will be reduced in heavy persons, including lean ones. Secondly, mean path length of photons from the aorta and liver will be increased in large persons; in other words photon attenuation will be greater. The distance in water over which 511 keV photons lose 50% of counts by attenuation (‘half distance’, analogous to half life) is 7.3 cm. So increased abdominal girth could have a significant impact on the count

density. Any patient movement would also decrease signal-to-noise ratio but it would not be expected to correlate with body weight.

The weakness of the correlations of NRSMD with CV of SUV and SD of CT density are surprising because the variabilities of SUV and CT density, including those arising from patient movement, would be expected to increase with increasing noise. If the correlation between CV of SUV and mean CT density was the result of noise, then CV of SUV should have correlated more strongly with noise, but it correlated insignificantly with it. The correlation between CV of SUV and mean CT density is therefore likely, at least partly, to be the result of hepatic fat heterogeneity in hepatic steatosis, as I argued in chapter 10 in relation to the use of multiple ROI.

Although there was increased noise in large persons, noise had little or no effect on the SUV indices. Thus, although SUV_{max} based on weight correlated with NRSMD, SUV_{max} based on LBM showed no correlation with NRSMD. Moreover, SUV_{max}/SUV_{ave} also did not correlate with NRSMD, suggesting that the ratio does indeed reflect hepatic fat content and is not the result of a greater impact of noise on SUV_{max} compared with SUV_{ave}. Most of the scatter in the Patlak-Rutland plot is probably generated by noise in the signal from the abdominal aorta, over which a smaller ROI was drawn compared to that over the liver. If noise was generated in the aorta rather than the liver, then it would explain why noise was increased in large persons but had limited impact on the SUV indices.

In conclusion, I have shown how the Patlak-Rutland plot can be used to assess signal-to-noise ratio, which appears to be increased in heavy persons. SUV indices, however,

are affected minimally by noise, especially when calculated using LBM. The study supports the notion that SUV_{max}/SUV_{ave} is a marker of hepatic fat. Although CV of SUV and SD of CT density are probably susceptible to noise they are at least partly markers of hepatic fat distribution heterogeneity. Correcting them for the effects of noise would nevertheless be desirable if they are to be used as such markers.

Chapter 13: General discussion and future work

The conclusions of this thesis are as follows.

13.1. SUV as a measure of FDG uptake has serious limitations

Previous workers have used SUV to measure FDG uptake in the spleen. They measured SUV using weight as the whole body metric. This is not surprising as almost all departments use SUV based on weight to quantify the metabolic activity of tumours. However, as shown in chapters 3, 4, 5 and 6, SUV based on weight is affected by many different variables, including weight itself, blood glucose and, in the case of the liver, the diluting effect of hepatic fat. The inter-dependence of all these factors, which all correlate with each other, makes it difficult to obtain clear results with SUV, especially for the liver. Thus fat patients tend to have hepatic steatosis, tend to be overweight or obese, and tend to have high blood glucose levels. Dividing liver SUV by blood pool SUV does not entirely solve these problems because of the uncertainty of the differential effects of signal-to-noise ratio on SUV_{max} and SUV_{ave} with respect both to the liver and a blood pool region.

Whilst it is repeatedly shown in the thesis that SUV calculated using lean body mass is preferable to SUV calculated with weight, SUV scaled to lean body mass nevertheless also has problems. Firstly, it not clear how much FDG accumulates in fat and whether this varies with levels of obesity. Secondly, unlike weight, lean body

mass is difficult to measure or estimate and this is reflected by the numerous estimation formulae that have been published.

13.2. Hepatic FDG uptake and glucose utilisation are increased in steatosis

As far as I could tell from SUV measurements, the uptake of FDG is increased in hepatic steatosis. However, complex multi-variate statistical analysis would be required to prove this and is probably not worth the effort because a better approach that avoids the limitations of SUV is dynamic imaging and Patlak-Rutland analysis. I found this to show a clear increase in hepatic FDG clearance and glucose utilisation in hepatic steatosis but not in obese patients without hepatic steatosis. The limitations of SUV as a measure of FDG clearance are well illustrated in chapter 9, in which it is demonstrated that in general, the spleen is metabolically more active than the liver. Future research on glucose utilisation in the liver and spleen should not be based on SUV but instead on dynamic imaging, as described in chapters 8 and 9.

13.3. Texture analysis is complex and several parameters show such a high level of dependence on the volume of the region from which they are determined as to be unhelpful in the liver. I tried to make allowance for this but found that texture analysis failed to reveal any significant differences between patients with and without steatosis. However, 3 patients with severe steatosis and 3 with biopsy evidence of hepatic inflammation (who did not have steatosis), were frequent outliers in the relationships between texture parameters and metabolic volume and can therefore be regarded as having abnormal texture parameters.

13.4. Future work

1. Making an early diagnosis of steatohepatitis was one of my original aims but patient recruitment was difficult. I also aimed to study patients with acute alcoholic hepatitis but these are too sick to come to CISC. Future work should therefore focus on these conditions using dynamic imaging as described in chapter 8.

2. Another approach to imaging hepatic inflammation is to make use the presence of glucose-6-phosphatase in the liver and perform very delayed imaging. The enzyme is absent from inflammatory cells so in time all the FDG in hepatocytes should be cleared, leaving a signal exclusively from inflammatory cells and other cells in the liver that are not hepatocytes, especially Kupffer cells. The time required for a Patlak-Rutland plot to become horizontal as a result of equilibration between phosphorylation (k_3) and de-phosphorylation (k_4) depends on the sum of the two rate constants. k_3 has a value of about 0.005 min^{-1}. Literature values of k_4, are conflicting, but assuming it is 0.001 min^{-1}, then equilibration would be 90%complete in 383 min. Very delayed imaging with administered activity higher than the ARSAC reference level might permit imaging of inflammatory cells with effectively no signal from hepatocytes. Even better would be to perform this work using UltraPET, a novel PET scanner about to be built in the University of California Davis. This has a 2m length continuous tube of detectors that increases sensitivity 40-fold (Price et al 2014).

3. Pursuing texture analysis as a technique for making an early diagnosis of steatohepatitis should be further pursued, perhaps with contrast-enhanced CT or MRI as well as FDG PET. Metabolic volume needs be a standardised to get round the problem of the dependency on it of texture parameter values. Sequential studies examining the progression of texture may also give interesting results.

REFERENCES

Abele JT, Fung CI. Effect of hepatic steatosis on liver FDG uptake measured in mean standard uptake values. Radiology 2010;254:917-24.

Abikhzer G, Alabed YZ, Azoulay L, et al. Altered hepatic metabolic activity in patients with hepatic steatosis on FDGPET/CT. AJR Am J Roentgenol 2011;196:176-80.

Adams LA, Sanderson S, Lindor KD, et al. The histological course of nonalcoholic fatty liver disease: a longitudinal study of 103 patients with sequential liver biopsies. J Hepatol 2005;42:132–138.

Agopian VG, Kaldas FM, Hong JC, et al. Liver transplantation for nonalcoholic steatohepatitis: the new epidemic. Ann Surg 2012;256:624-633

Alberti KG, Eckel RH, Grundy SM, et al International Diabetes Federation Task Force on Epidemiology and Prevention; National Heart, Lung, and Blood Institute; American Heart Association; World Heart Federation; International Atherosclerosis Society; International Association for the Study of Obesity. Harmonizing the metabolic syndrome: a joint interim statement of the International Diabetes Federation Task Force on Epidemiology and Prevention; National Heart, Lung, and Blood Institute; American Heart Association; World Heart Federation; International Atherosclerosis Society; and International Association for the Study of Obesity. Circulation. 2009;120:1640-5

Altman DG. Practical statistics for medical research. Chapman and Hall, London, 1991.

Angulo P. Nonalcoholic fatty liver disease. N Engl J Med 2002;346:1221–31

Angus PW, Dixon RM, Rajagopalan B, et al. A study of patients with alcoholic liver disease by 31P nuclear magnetic resonance spectroscopy. Clin Sci 1990,78:33-8

Anstee QM, McPherson S, Day CP. How big a problem is non-alcoholic fatty liver disease? BMJ 2011; Jul 18;343:d389

Armstrong P, Wastie M, Rockall A. Diagnostic Imaging, 5th edition, Blackwell publishing, 2004

Arulanandan A, Ang B, Bettencourt R, et al. Association between quantity of liver fat and cardiovascular risk in patients with nonalcoholic fatty liver disease independent of nonalcoholic steatohepatitis. Clin Gastroenterol Hepatol 2015;8:1513-20

Atwell TD, Smith RL, Hesley GK, et al. Incidence of bleeding after 15,181 percutaneous biopsies and the role of aspirin. AJR 2010;194:784-9

Aulbert E, Gebherdt A, Schutz E, et al. Mechanism of gallium-67 accumulation in normal rat liver lysosomes. Nuklearmedizin (Stuttg) 1976;15:185-94

Bai B, Bading J, Conti PS. Tumor Quantification in Clinical Positron Emission Tomography Theranostics 2013; 3:787-801

Barrington SF, Mikhaeel NG, Kostakoglu L, et al. Role of imaging in the staging and response assessment of lymphoma: consensus of the International Conference on Malignant Lymphomas Imaging Working Group. J Clin Oncol 2014;32:3048-58.

Bedossa P, Dargère D, Paradis V. Sampling variability of liver fibrosis in chronic hepatitis C. Hepatology 2003;38:1449–57

Bellentani S, Saccoccio G, Masutti F, et al. Prevalence of and risk factors for hepatic steatosis in Northern Italy. Ann Intern Med 2000;132:112-7

Blockmans D, Knockaert D, Maes A, et al. Clinical value of [(18)F]fluoro-deoxyglucose positron emission tomography for patients with fever of unknown origin. Clin Infect Dis 2001;15;32:191-6

Boellaard R, O'Doherty MJ, Weber WA, et al. FDG PET and PET/CT: EANM procedure guidelines for tumour PET imaging: version 1.0. Eur J Nucl Med Mol Imaging 2010;37:181-200

Boer P. Estimated lean body mass as an index for normalization of body fluid volumes in man. Am J Physiol 1984;247:F632-5

Bohte AE , Jochem R, Werven V, et al. The diagnostic accuracy of US, CT, MRI and ^{1}H-MRS for the evaluation of hepatic steatosis compared with liver biopsy: a meta-analysis Eur Radiol 2011;21:87-97

Bohte AE, de Niet A, Jansen L, et al. Non-invasive evaluation of liver fibrosis: a comparison of ultrasound-based transient elastography and MR elastography in patients with viral hepatitis B and C. Eur Radiol 2014;24:638-48

Bohte AE, Koot BG, van der Baan-Slootweg OH, et al. US cannot be used to predict the presence or severity of hepatic steatosis in severely obese adolescents. Radiology 2012;262:327-34

Borra R, Lautamaki R, Parkkola R, et al. Inverse association between liver fat content and hepatic glucose uptake in patients with type 2 diabetes mellitus. Metabolism 2008;57:1445-51

Boyce CJ, Pickhardt PJ, Kim DH, et al. Hepatic steatosis (fatty liver disease) in asymptomatic adults identified by unenhanced low-dose CT. AJR 2010;194:623-8

Bravo AA, Sheth SG, Chopra S. Liver biopsy. N Engl J Med 2001;Feb 15;344(7):495-500

Brown MA, Semelka RC. MRI Basic Principles and Applications; 3rd edition, Willey-Liss, 2003

Brunt EM, Janney CG, Di Bisceglie AM, et al. Nonalcoholic steatohepatitis: a proposal for grading and staging the histological lesions. Am J Gastroenterol 1999;94:2467-74

Bucerius J, Mani V, Wong S, et al. Arterial and fat tissue inflammation are highly correlated: a prospective ^{18}F-FDG PET/CT study. Eur J Nucl Med Mol Imaging 2014;41:934-45

Buchert R, Santer R, Brenner W, et al. Computer simulations suggest that acute correction of hyperglycaemia with an insulin bolus protocol might be useful in brain FDG PET. Nuklearmedizin 2009;48:44-54

Bural GG, Torigian DA, Burke A, et al. Quantitative assessment of the hepatic metabolic volume product in patients with diffuse hepatic steatosis and normal controls through use of FDG-PET and MR imaging: a novel concept. Mol Imaging Biol 2010;12:233-9

Busing KA, Schonberg SO, Brade J, et al. Impact of blood glucose, diabetes, insulin, and obesity on standardized uptake values in tumors and healthy tissues. Nucl Med Biol 2013;40:206-13

Cadranel JF, Rufat P, Degos F. Practices of liver biopsy in France: results of a prospective nationwide survey. For the Group of Epidemiology of the French Association for the Study of the Liver (AFEF). Hepatology 2000;32:477-81

Chalasani N, Younossi Z, Lavine JE, et al. The diagnosis and management of non-alcoholic fatty liver disease: practice guideline by the American Association for the Study of Liver Diseases, American College of Gastroenterology, and the American Gastroenterological Association. Hepatology 2012;55:2005-23

Chicklore S, Goh V, Siddique M, et al. Quantifying tumour heterogeneity in ^{18}F-FDG PET/CT imaging by texture analysis. Eur J Nucl Med Mol Imaging 2013;40:133-40

Choi Y, Hawkins RA, Huang SC, et al. Evaluation of the effect of glucose ingestion and kinetic model configurations of FDG in the normal liver. J Nucl Med 1994;35:818-23

Claeys J, Mertens K, D'Asseler Y, et al. Normoglycemic plasma glucose levels affect F-18 FDG uptake in the brain. Ann Nucl Med 2010;24:501-505

Crippa F, Gavazzi C, Bozzetti F, et al. The influence of blood glucose levels on [^{18}F]fluorodeoxyglucose (FDG) uptake in cancer: a PET study in liver metastases from colorectal carcinomas. Tumori 1997;83:748-52

Dale BM, Brown MA, Semelka RC. MRI basic principles and applications, 5th edition 2015. Wiley Blackwell

Datz FL. In-111-labeled leukocytes for the detection of infection: current status. Semin Nucl Med 1994;24:92-109

Davnall F, Yip CS, Ljungqvist G, et al. Assessment of tumor heterogeneity: an emerging imaging tool for clinical practice? Insights Imaging 2012;3:573-89

Decarie PO, Lepanto L, Billiard JS, et al. Fatty liver deposition and sparing: a pictorial review. Insights Imaging 2011;2:533-8

de Geus-Oei LF, Visser EP, Krabbe PF, et al. Comparison of image-derived and arterial input functions for estimating the rate of glucose metabolism in therapy-monitoring ^{18}F-FDG PET studies. J Nucl Med 2006;47:945-9

Delbeke D, Coleman RE, Guiberteau MJ, et al. Procedure guideline for tumor imaging with ^{18}F-FDG PET/CT. J Nucl Med 2006; 47:885-95

de Lédinghen V, Le Bail B, Rebouissoux L, et al. Liver stiffness measurement in children using FibroScan: feasibility study and comparison with Fibrotest, aspartate transaminase to platelets ratio index, and liver biopsy. J Pediatr Gastroenterol Nutr 2007;45:443-50

Deurenberg P, Weststrate JA, Seidell JC. Body mass index as a measure of body fatness: age- and sex-specific prediction formulas. Br J Nutr 1991;65:105-14

Diederichs CG, Staib L, Glatting G, et al. FDG PET: Elevated plasma glucose reduces both uptake and detection rate of pancreatic malignancies. J Nucl Med 1998;39:1030-3

Dixon JB, Bhathal PS, O'Brien PE. Weight loss and non-alcoholic fatty liver disease: falls in gamma-glutamyl transferase concentrations are associated with histologic improvement. Obes Surg 2006;16:1278-86

Dutta P, Courties G, Wei Y, et al. Myocardial infarction accelerates atherosclerosis. Nature 2012;487(7407):325-9

Ekstedt M, Franzen LE, Mathiesen UL, et al. Long-term follow-up of patients with NAFLD and elevated liver enzymes. Hepatology 2006;44:865-73

El-Serag HB, Tran T, Everhart JE. Diabetes increases the risk of chronic liver disease and hepatocellular carcinoma. Gastroenterology 2004;126:460-8

El-Zayadi AR. Hepatic steatosis: a benign disease or a silent killer? World J Gastroenterol 2008;14: 4120-6

Emami H, Singh P, MacNabb M, et al. Splenic metabolic activity predicts risk of future cardiovascular events: demonstration of a cardiosplenic axis in humans. JACC Cardiovasc Imaging 2015;8:121-30

Erselcan T, Turgut B, Dogan D, et al. Lean body mass-based standardized uptake

value, derived from a predictive equation, might be misleading in PET studies. Eur J Nucl Med 2002;29:1630-8

Falchuk KR, Fiske SC, Haggitt RC, et al. Pericentral hepatic fibrosis and intracellular hyalin in diabetes mellitus. Gastroenterology 1980;78:535-41

Farrell GC, Larter CZ. Nonalcoholic fatty liver disease: from steatosis to cirrhosis. Hepatology 2006;43(2 Suppl 1):S99-112

Fink-Bennett D, Clarke K, Tsai D, et al. Indium-111-leukocyte imaging in acute cholecystitis.J Nucl Med. 1991;32:803-4

French SW. Biochemical basis for alcohol-induced liver injury. Clin Biochem 1989;22:41-9

Garg A, Misra A. Hepatic steatosis, insulin resistance, and adipose tissue disorders. J Clin Endocrinol Metab 2002;87:3019-22

Graham RC, Burke A, Stettler N. Ethnic and sex differences in the association between metabolic syndrome and suspected nonalcoholic fatty liver disease in a nationally representative sample of US adolescents. J Pediatr Gastroenterol Nutr 2009;49:442–9

Green LA, Gambhir SS, Srinivasan A, et al. Noninvasive methods for quantitating blood time-activity curves from mouse PET images obtained with fluorine-18-fluorodeoxyglucose. J Nucl Med 1998;39:729-34

Groheux D, Delord M, Rubello D, et al. Variation of liver SUV on ^{18}FDG-PET/CT studies in women with breast cancer. Clin Nucl Med 2013;38:422-5

Guido M, Rugge M. Liver biopsy sampling in chronic viral hepatitis. Semin Liver Dis 2004;24:89-97

Guiu B, Loffroy R, Petit JM, et al. Mapping of liver fat with triple-echo gradient echo imaging: validation against 3.0-T proton MR spectroscopy. Eur Radiol 2009;19:1786-93

Hallett WA, Marsden PK, Cronin BF, et al. Effect of corrections for blood glucose and body size on [^{18}F]FDG PET standardised uptake values in lung cancer. Eur J Nucl Med 2001;28:919-22

Hamer OW, Aguirre DA, Casola G, et al. Fatty liver: imaging patterns and pitfalls. Radiographics 2006;26:1637-53

Hasselbalch SG, Knudsen GM, Capaldo B, et al. Blood-brain barrier transport and brain metabolism of glucose during acute hyperglycemia in humans. J Clin Endocrinol Metab 2001;86:1986-90

Harris CC, Greer KL, Jaszczak RJ, et al. Tc-99m attenuation coefficients in water-filled phantoms determined with gamma cameras. Med Phys 1984;11:681-5

Haycock GB, Schwarz GJ, Wisotsky DH. Geometric method for measuring body surface area: a height-weight formula validated in infants, children and adults. J Pediatrics 1978;93:62-6

House MJ, Bangma SJ, Thomas M, et al. Texture-based classification of liver fibrosis using MRI. J Mag Res Imaging 2015;41:322-8

Hughes RD, Mitry RR, Dhawan A. Current Status of Hepatocyte Transplantation. Transplantation 2012;93:342-7

Hui JM, Kench JG, Chitturi S, et al. Long-term outcomes of cirrhosis in nonalcoholic steatohepatitis compared with hepatitis C. Hepatology 2003;38:420-7

Iozzo P, Geisler F, Oikonen V, et al. Insulin stimulates liver glucose uptake in humans: an ^{18}F-FDG PET Study. J Nucl Med 2003;44:682-9

Iozzo P, Jarvisalo MJ, Kiss J, et al. Quantification of liver glucose metabolism by positron emission tomography: validation study in pigs. Gastroenterology 2007;132:531-42

Ishizu K, Nishizawa S, Yonekura Y, et al. Effects of hyperglycemia on FDG uptake in human brain and glioma. J Nucl Med 1994;35:1104-9

Joshi NV, Toor I, Shah AS, et al. Systemic atherosclerotic inflammation following acute myocardial infarction: myocardial infarction begets myocardial infarction. J Am Heart Assoc 2015; Aug 27;4(9):e001956

Kamimura K, Nagamachi S, Wakamatsu H, et al. Associations between liver (18)F fluoro-2-deoxy-D-glucose accumulation and various clinical parameters in a Japanese population: influence of the metabolic syndrome. Ann Nucl Med 2010;24:157-61

Keramida G , Shur J, Bush J, et al. Contrasting relations with blood glucose level of FDG accumulation in the brain and liver: potential clinical impact. Nucl Med Comm 2013;34:376 (abstract)

Keramida G, Potts J, Bush J, et al. Hepatic steatosis is associated with increased hepatic FDG uptake. Eur J Radiol 2014;83:751-5

Keramida G, Potts J, Bush J, et al. Accumulation of ^{18}F-FDG in the liver in hepatic steatosis. Am J Roentgenol. 2014;203:643-8

Keramida G Hunter J, Dizdarevic S, et al. The appropriate whole body index on which to base standard uptake value in 2-deoxy-2-[^{18}F]fluoro-d-glucose PET. Br J Radiol (in press)

Keramida G, Peters AM. FDG accumulation is increased in hepatic steatosis. J Nucl Med 2015; 56 (suppl 3):412P (abstract)

Khandani AH, Wahl RL. Applications of PET in liver imaging. Radiol Clin North Am 2005;43:849-60

Kim CG, Kim WH, Kim MH, et al. Direct determination of lean body mass by CT in F-18 FDG/CT studies: comparison with estimates using predictive equations. Nucl Med Mol Imaging 2013;47:98-103

Kim EJ, Kim S, Kang DO, et al. Metabolic activity of the spleen and bone marrow in patients with acute myocardial infarction evaluated by ^{18}F-fluorodeoxyglucose positron emission tomographic imaging. Circ Cardiovasc Imaging 2014;7:454-60

Kim K, Kim SJ, Kim IJ, et al. Factors associated with diffusely increased splenic F-18 FDG uptake in patients with cholangio-carcinoma. Nucl Med Mol Imaging 2014;48:137-43

Kim H, Taksali SE, Dufour S, et al, Comparative MR study of hepatic fat quantification using single-voxel proton spectroscopy, two-point dixon and three-point IDEAL. Magn Reson Med 2008; 59:521-7

Kim SH, Jeong ML, Jong HK et al. Appropriateness of a donor liver with respect to macrosteatosis: Application of artificial neural networks to US images - Initial experience. Radiology 2005;234:793-803

Kleiner DE, Brunt EM, Van Natta M, et al. Design and validation of a histological scoring system for nonalcoholic fatty liver disease. Hepatology 2005;41:1313–21

Koo S-H. Non alcoholic fatty liver disease; molecular mechanisms for the hepatic steatosis. Clin Mol Hepatol 2013;19:210-5

Krishnamurthy GT, Krishnamurthy S. Nuclear hepatology, a textbook of hepatobiliary diseases; 2nd edition. Springer, Berlin 2009

Krssak M, Hofer H, Wrba F, et al. Non-invasive assessment of hepatic fat accumulation in chronic hepatitis C by (1)H magnetic resonance spectroscopy. Eur J Radiol 2010;74:60-6

Kubota K, Watanabe H, Murata Y, et al. Effects of blood glucose level on FDG uptake by liver: a FDG-PET/CT study. Nucl Med Biol 2011;38:347-51

Kudo M, Ikekubo K, Yamamoto K, et al. Focal fatty infiltration of the liver in acute alcoholic liver injury: hot spots with radiocolloid SPECT scan. Am J Gastroenterol 1989;84:948-52

Kumar R, Xiu Y, Yu JQ, et al. ^{18}F-FDG PET in evaluation of adrenal lesions in patients with lung cancer. J Nucl Med 2004;45:2058-62

Kwee TC, Basu S, Torigian DA, et al. FDG PET imaging for diagnosing prosthetic joint infection: discussing the facts, rectifying the unsupported claims and call for evidence-based and scientific approach. Eur J Nucl Med Mol Imaging 2013;40:464-6

Lantto EH, Lantto TJ, Vorne M. Fast diagnosis of abdominal infections and inflammations with technetium-99m -HMPAO labelled leukocytes . J Nucl Med 1991;32:2029-34

Layer G, Zuna I, Lorenz A, et al. Computerized ultrasound B-scan texture analysis of experimental diffuse parenchymal liver disease: correlation with histopathology and tissue composition. J Clin Ultrasound 1991;19:193-201

Lee RG. Nonalcoholic steatohepatitis: tightening the morphological screws on a hepatic rambler. Hepatology 1995;21:1742-3

Lee SM, Kim TS, Lee JW, et al. Improved prognostic value of standardized uptake value corrected for blood glucose level in pancreatic cancer using F-^{18}FDG PET. Clin Nucl Med 2011;36:331-6

Lee SS, Park SH, Kim HJ, et al. Non-invasive assessment of hepatic steatosis: prospective comparison of the accuracy of imaging examinations. J Hepatol 2010;52:579-85

Lee JY, Kim KM, Lee SG, et al. Prevalence and risk factors of non-alcoholic fatty liver disease in potential living liver donors in Korea: a review of 589 consecutive liver biopsies in a single center. J Hepatol 2007;47:239-44

Lewin M, Poujol-Robert A, Boelle P, et al. Diffusion-weighted magnetic resonance imaging for the assessment of fibrosis in chronic hepatitis C. Hepatology 2007;46:658-65

Li G, Hu H, Shi W, et al. Elevated hematocrit in nonalcoholic fatty liver disease: a potential cause for the increased risk of cardiovascular disease? Clin Hemorheol Microcirc 2012;51:59-68

Ligabue G, Besutti G, Scaglioni R, et al. MR quantitative biomarkers of non-alcoholic fatty liver disease: technical evolutions and future trends. Quant Imaging Med Surg 2013;3:192-5

Lin M. Molecular imaging using positron emission tomography in colorectal cancer, Discovery medicine 2011;11:435-47

Lin CY, Lin WY, Lin CC, et al. The negative impact of fatty liver on maximum standard uptake value of liver on FDG PET. Clin Imaging 2011;35:437-41

Lindholm P, Minn H, Leskinen-Kallio S, et al. Influence of the blood glucose concentration on FDG uptake in cancer - a PET study. J Nucl Med 1993;34:1-6

Liu G, Li Y, Hu P, et al. The combined effects of serum lipids, BMI, and fatty liver on 18F-FDG uptake in the liver in a large population from China: an ^{18}F-FDG-PET/CT study. Nucl Med Commun 2015;36:709-16

Liu Y. Clinical significance of diffusely increased splenic uptake on FDG-PET. Nucl Med Commun 2009;30:763-9

Lomas F, Dibos PE, Wagner HN Jr. Increased specificity of liver scanning with the use of 67-gallium citrate. New Engl J Med 1972;286:1323-9

Long C. Studies involving enzymatic phosphorylation 1. The hexokinase activity of rat tissue .Biochem J 1952;50:407-15

Longo R, Pollesello P, Ricci C et al. Proton MR spectroscopy in quantitative in vivo determination of fat content in human liver steatosis. J Magn Reson Imaging 1995;5:281-5

Lucey MR, Mathurin P, Morgan TR. Alcoholic hepatitis. N Engl J Med 2009;360(26):2758-69

Lubberink M, Boellaard R, van der Weerdt AP, et al. Quantitative comparison of analytic and iterative reconstruction methods in 2- and 3-dimensional dynamic cardiac ^{18}F-FDG PET. J Nucl Med 2004;45:2008-15

Ma X, Holalkere NS, Kambadakone R A, et al. Imaging-based quantification of hepatic fat: methods and clinical applications. Radiographics 2009;29:1253-77.

McCullough AJ, O'Shea RS, Dasarathy S. Diagnosis and management of alcoholic liver disease. J Dig Dis 2011;12:257-62

McPherson S, Jonsson JR, Cowin GJ et al: Magnetic resonance imaging and spectroscopy accurately estimate the severity of steatosis provided the stage of fibrosis is considered. J.Hepatol 2009;51:389-97

Mejia AA , Nakamura T , Masatoshi I, et al. Estimation of absorbed doses in humans due to intravenous administration of fluorine-18-fluorodeoxyglucose in PET studies. J Nucl Med 1991;32:699-706

Mehta AK, Lyon GM 3rd. Infectious diseases in end-stage liver disease patients. Crit Care Nurs Clin North Am 2010;22:291-30

Miette V, Abdennour M, Sandrin L, et al. Metabolic steatosis and fibrosis: Review of the non-invasive tools for diagnosis and screening, liver biopsy in modern medicine.

Mizuguchi Y (Ed.), 2011; ISBN: 978-953-307-883-0, InTech, Available from:http://www.intechopen.com/books/liver-biopsy-in-modern-medicine/metabolic-steatosis-fibrosis-review-of-the-non-invasive-tools-for-diagnosis-and-screening

Mir AH, Hanmandlu M, Tandon SN. Texture analysis of CT-images for early detection of liver malignancy. Biomed Sci Instrum 1995;31:213-7

Munk OL, Bass L, Roelsgaard K, et al. Liver kinetics of glucose analogs measured in pigs by PET: importance of dual-input blood sampling. J Nucl Med 2001;42:795-801

Musso G, Gambino R, Cassader M, et al. Meta-analysis: natural history of non-alcoholic fatty liver disease (NAFLD) and diagnostic accuracy of non-invasive tests for liver disease severity. Ann Med 2011;43:617-49

Nagore N, Scheuer PJ. The pathology of diabetic hepatitis. J Pathol 1988;156:155-60

Nam HY, Kim SJ, Kim IJ, et al. The clinical implication and prediction of diffuse splenic FDG uptake during cancer surveillance. Clin Nucl Med 2010;35:759-63

Namba H, Nakagawa K, Iyo M, et al. A simple method for measuring glucose utilization of insulin-sensitive tissues by using the brain as a reference. Eur J Nucl Med 1994;21:228-31

Nozawa A, Rivandi AH, Kesari S, et al. Glucose corrected standardized uptake value (SUV_{gluc}) in the evaluation of brain lesions with ^{18}F-FDG PET. Eur J Nucl Med Mol Imaging 2013;40:997-1004

Nugent C, Younossi ZM. Evaluation and management of obesity-related nonalcoholic fatty liver disease. Nat Clin Pract Gastroenterol Hepatol 2007;4:432-41

Núñez R, Rini JN, Tronco GG, et al. Correlation of hematologic parameters with bone marrow and spleen uptake in FDG PET. Rev Esp Med Nucl 2005;24:107-12

Oehr P, Biersack HJ, Coleman RE (eds). Radiopharmaceutical Production and Safety of [^{18}F] FDG PET and PET-CT in: Oncology. Springer, Berlin, 2004

Orlhac F, Soussan M, Maisonobe JA, et al. Tumor texture analysis in ^{18}F-FDG PET: relationships between texture parameters, histogram indices, standardized uptake values, metabolic volumes, and total lesion glycolysis. J Nucl Med 2014;55:414-22

Oudry J, Chen J, Glaser KJ, et al. Cross-validation of magnetic resonance elastography and ultrasound-based transient elastography: a preliminary phantom study. J Magn Reson Imaging 2009;30:1145-50

Oya N, Nagata Y, Ishigaki T, et al. Evaluation of experimental liver tumors using fluorine-18-2-fluoro-2-deoxy-d-glucose PET. J Nucl Med 1993;34:2124-9

Paquet N, Albert A, Foidert J, et al. Within-patient variability of ^{18}F-FDG: standardized uptake values in normal tissues. J Nucl Med 2004;45:784-8

Paschos P, Paletas K. Non alcoholic fatty liver disease and metabolic syndrome. Hippokratia. 2009;13:9-19.

Patlak CS, Blasberg RG, Fenstermacher JD. Graphical evaluation of blood-to brain transfer constants from multiple-time uptake data. J Cereb Blood Flow Metab 1983;3:1–7

Peters AM, White JF, Chilvers ER. Physiological granulocyte destruction in vivo by apoptosis. J Nucl Med 2004;45:526

Petersen KF, Dufour S, Befroy D, et al. Reversal of nonalcoholic hepatic steatosis, hepatic insulin resistance, and hyperglycemia by moderate weight reduction in patients with type-2 diabetes. Diabetes 2005;54:603-60

Price PM, Badawi RD, Cherry SR, Jones T. Ultra staging to unmask the prescribing of adjuvant therapy in cancer patients: the future opportunity to image micro-metastases using total-body 18F-FDG PET scanning. J Nucl Med 2014;55:696-7

Purohit V, Russo D, Coates PM. Role of fatty liver, dietary fatty acid supplements, and obesity in the progression of alcoholic liver disease: introduction and summary of the symposium. Alcohol 2004;34:3-8

Ramos CD, Erdi YE, Gonen M, et al. FDG-PET standardized uptake values in normal anatomic structures using iterative reconstructed segmented attenuation cor- rection and filtered back-projection. Eur J Nucl Med 2001;28:155-64

Ratziu V, Charlotte F, Heurtier A, et al. Sampling variability of liver biopsy in nonalcoholic fatty liver disease. Gastroenterology 2005;128:1898–1906

Ricci C, Longo R, Gioulis E, et al. Noninvasive in vivo quantitative assessment of fat content in human liver. J Hepatol 1997;27:108-113

Rinella ME. Nonalcoholic fatty liver disease: a systematic review. JAMA 2015;9;313:2263-73

Rini JN, Leonidas JC, Tomas MB, et al. ^{18}F-FDG PET versus CT for evaluating the spleen during initial staging of lymphoma. J Nucl Med 2003;44:1072-4

Rouviere O, Meng Y, Dresner A, et al. MR elastography of the liver: preliminary results. Radiology 2006;240:440-8

Rudd JH, Narula J, Strauss HW, et al. Imaging atherosclerotic plaque inflammation by fluorodeoxyglucose with positron emission tomography: ready for prime time? J Am Coll Cardiol. 2010 Jun 8;55(23):2527-35

Runge JH, Bohte AE, Verheij J, et al. Comparison of interobserver agreement of magnetic resonance elastography with histopathological staging of liver fibrosis. Abdom Imaging 2014;39:283-90

Rutland MD. A single injection technique for subtraction of blood background in ^{131}I-hippuran renograms. Br J Radiol 1979;52:134-7

Saadeh S, Younossi ZM, Remer EM, et al. The utility of radiologic imaging in non-alcoholic fatty liver disease. Gastroenterology 2002;123:745-50

Salaun PY, Gastinne T, Bodet-Milin C, et al. Analysis of ^{18}F-FDG PET diffuse bone marrow uptake and splenic uptake in staging of Hodgkin's lymphoma: a reflection of disease infiltration or just inflammation? Eur J Nucl Med Mol Imaging 2009;36:1813-21

Sandrin L, Fourquet B, Hasquenoph JM, et al. Transient elastography: a new noninvasive method for assessment of hepatic fibrosis. Ultrasound Med Biol 2003;29:1705-13

Saverymuttu SH, Peters AM, Keshavarzian A, et al. The kinetics of 111-indium distribution following injection of 111-indium labelled autologous granulocytes in man. Br J Haematol 1985;61:675-85

Saverymuttu SH, Joseph a E, Maxwell JD Ultrasound scanning in the detection of hepatic fibrosis and steatosis. Br Med J (Clin Res Ed) 1986;292:13–5

Sebastiani G, Halfon P, Castera L, et al. SAFE biopsy: a validated method for large-scale staging of liver fibrosis in chronic hepatitis C. Hepatology 2009;49:1821-7

Sevastianova K, Hakkarainen A, Kotronen A, et al. Nonalcoholic fatty liver disease: detection of elevated nicotinamide adenine dinucleotide phosphate with in vivo 3.0-T 31P MR spectroscopy with proton decoupling. Radiology 2010;256:466-73

Soloway RD, Baggenstoss a H, Schoenfield LJ, et al. Observer error and sampling variability tested in evaluation of hepatitis and cirrhosis by liver biopsy. Am J Dig Dis 1971;16:1082–6

Sugawara Y, Zasadny KR, Neuhoff AW, et al. Reevaluation of the standardized uptake value for FDG: variations with body weight and methods for correction. Radiology 1999;213:521-5

Tahari AK, Chien D, Azadi JR, et al. Optimum lean body formulation for correction of standardized uptake value in PET imaging. J Nucl Med (in press)

Tezuka D, Terashima M, Kato Y, et al. Clinical characteristics of definite or suspected isolated cardiac sarcoidosis: application of cardiac magnetic resonance imaging and 18F-Fluoro-2-deoxyglucose positron-emission tomography/computerized tomography. J Card Fail 2015;21:313-22

Thakur ML, Segal AW, Louis L , et al. Indium-111-labeled cellular blood components: mechanism of labelling, and intracellular location in human neutrophils. J Nucl Med 1977;18:1022-6

Tsan MF. Mechanism of gallium-67 accumulation in inflammatory lesions. J Nucl Med 1985;26:88-92

Tsochatzis EA, Gurusamy KS, Ntaoula S, et al. Elastography for the diagnosis of severity of fibrosis in chronic liver disease: a meta-analysis of diagnostic accuracy. J Hepatol 2011;54:650–9

Tsoulfas G, Goulis I, Giakoustidis D, et al. Hepatitis C and liver transplantation. Hippokratia 2009;13:211-5

Torizuka T, Tamaki N, Inokuma T, et al. In vivo assessment of glucose metabolism in hepatocellular carcinoma with FDG PET. J NucI Med 1995;36:1811-7

Vaidyanathan S, Patel CN, Scarsbrook AF, et al. FDG PET/CT in infection and inflammation--current and emerging clinical applications. Clin Radiol 2015;70:787-800

Vanderhoek M, Perlman SB, Jeraj R. Impact of the definition of peak standardized uptake value on quantification of treatment response. J Nucl Med 2012;53:4-11

van der Weerdt AP, Klein LJ, Boellaard R, et al. Image-derived input functions for determination of MRGlu in cardiac (18)F-FDG PET scans. J Nucl Med 2001;42:1622-9

van Kouwen MC, Jansen JB, van Goor H, et al. FDG-PET is able to detect pancreatic carcinoma in chronic pancreatitis. Eur J Nucl Med Mol Imaging 2005;32:399-404

Valour F, Sénéchal A, Chidiac C, Ferry T. Chronic HIV-1 infection mimicking splenic malignant lymphoma on F-18 FDG-PET/CT. BMJ Case Rep. 2012 Jan 18

VanWagner LB, Lapin B, Skaro AI, et al. Impact of renal impairment on cardiovascular disease mortality after liver transplantation for nonalcoholic steatohepatitis cirrhosis. Liver Int 2015;35:2575-83

VanWagner LB, Wilcox JE, Colangelo LA, et al. Association of nonalcoholic fatty liver disease with subclinical myocardial remodeling and dysfunction: A population-based study. Hepatology 2015;62:773-83

Vernon G, Baranova A, Younossi ZM. Systematic review: the epidemiology and natural history of non-alcoholic fatty liver disease and non-alcoholic steatohepatitis in adults. Aliment Pharmacol Ther 2011;34:274-85

Willaime JM, Turkheimer FE, Kenny LM, et al. Quantification of intra-tumour cell proliferation heterogeneity using imaging descriptors of ^{18}F fluorothymidine-positron emission tomography. Phys Med Biol 2013;58:187-203

Williams CD, Stengel J, Asike MI, et al. Prevalence of nonalcoholic fatty liver disease and nonalcoholic steatohepatitis among a largely middle-aged population utilizing ultrasound and liver biopsy: a prospective study. Gastroenterology 2011;140:124-31

Wollenweber T, Roentgen P, Schafer A, et al. Characterizing the inflammatory tissue response to acute myocardial infarction by clinical multimodality noninvasive imaging. Circ Cardiovasc Imaging 2014;7:811-8

Wong VW, Vergniol J, Wong GL, et al. Diagnosis of fibrosis and cirrhosis using liver stiffness measurement in nonalcoholic fatty liver disease. Hepatology 2010;51: 454-62

You J, Liu L, Zhang M, et al. Diagnostic value of the signal intensity on T1-weighted images of MRI and 1H MRS for neonatal hypoxic-ischemic encephalopathy Zhongguo Dang Dai Er Ke Za Zhi. 2011;13:107-10

Zeb I, Li D, Nasir K, et al. Computed Tomography Scans in the Evaluation of Fatty Liver Disease in a population based study: the multi-ethnic study of atherosclerosis. Acad Radiol 2012;19:811-818

Zhuang HM, Cortes-Blanco A, Pourdehnad M, et al. Do high glucose levels have differential effect on FDG uptake in inflammatory and malignant disorders? Nucl Med Commun 2001;22:1123-8